MARTIN MARIETTA ENERGY SYSTEMS LIBRARIES
3 4456 0064252 5

ornl

ORNL/TM-10098

OAK RIDGE NATIONAL LABORATORY

MARTIN MARIETTA

R-Matrix Analysis of the ^{239}Pu Cross Sections up to 1 keV

H. Derrien [1]
G. de Saussure
R. B. Perez [2]
N. M. Larson
Roger L. Macklin [3]

OAK RIDGE NATIONAL LABORATORY
CENTRAL RESEARCH LIBRARY
CIRCULATION SECTION
4500N ROOM 175
LIBRARY LOAN COPY
DO NOT TRANSFER TO ANOTHER PERSON
If you wish someone else to see this report, send in name with report and the library will arrange a loan.

OPERATED BY
MARTIN MARIETTA ENERGY SYSTEMS, INC.
FOR THE UNITED STATES
DEPARTMENT OF ENERGY

Printed in the United States of America. Available from
National Technical Information Service
U.S. Department of Commerce
5285 Port Royal Road, Springfield, Virginia 22161
NTIS price codes—Printed Copy: A05 Microfiche A01

This report was prepared as an account of work sponsored by an agency of the United States Government. Neither the United States Government nor any agency thereof, nor any of their employees, makes any warranty, express or implied, or assumes any legal liability or responsibility for the accuracy, completeness, or usefulness of any information, apparatus, product, or process disclosed, or represents that its use would not infringe privately owned rights. Reference herein to any specific commercial product, process, or service by trade name, trademark, manufacturer, or otherwise, does not necessarily constitute or imply its endorsement, recommendation, or favoring by the United States Government or any agency thereof. The views and opinions of authors expressed herein do not necessarily state or reflect those of the United States Government or any agency thereof.

ORNL/TM-10098

Engineering Physics and Mathematics Division

R-MATRIX ANALYSIS OF THE ^{239}Pu CROSS SECTIONS UP TO 1 keV

H. Derrien,* G. de Saussure, R. B. Perez†
N. M. Larson, and Roger L. Macklin**

Date Published: June 1986

*Centre D'Etudes Nucleaires de Cadarache, France

†Engineering Physics and Mathematics Division and Nuclear Engineering Department, University of Tennessee.

**Nuclear Engineering Department, University of Tennessee.

This Work Sponsored by
U.S. Department of Energy
Office of Basic Energy Sciences

Prepared by the
Oak Ridge National Laboratory
Oak Ridge, Tennessee 37831
operated by
Martin Marietta Energy Systems, Inc.
for the
U.S. DEPARTMENT OF ENERGY
under Contract No. DE-AC05-840R21400

MARTIN MARIETTA ENERGY SYSTEMS LIBRARIES
3 4456 0064252 5

TABLE OF CONTENTS

ABSTRACT 1
1. INTRODUCTION 1
2. PREVIOUS RESONANCE ANALYSES OF THE ^{239}Pu NEUTRON CROSS SECTIONS 2
3. THE RESONANCE ANALYSIS CODE SAMMY 4
4. SELECTION OF ^{239}Pu NEUTRON CROSS-SECTION MEASUREMENTS 4
5. ASSUMPTIONS OF THE ANALYSIS 6
6. RESULTS OF THE ANALYSIS 7
SUMMARY AND CONCLUSIONS 70
REFERENCES 71

ABSTRACT

We report here the results of an R-matrix resonance analysis of the ^{239}Pu neutron cross sections up to 1 keV. After a description of the method of analysis we list the nearly 1600 resonance parameters obtained and present extensive graphical and numerical comparisons between calculated and measured cross-section and transmission data.

1. INTRODUCTION

The representation of the ^{239}Pu neutron cross sections in the resonance region in the most important national or international evaluations is unsatisfactory; the single-level formalism is used, necessitating a structured "smooth cross-section" contribution.[1,2] Furthermore, M. Salvatores[3] and R. N. Hwang,[4] among others, have stressed the need to extend the resolved resonance region above the present limit of energy for the calculation of self-shielded group cross sections and Doppler effect. The resolved resonance region extends to 300 eV in ENDF/B-V[5] and to 660 eV in JEF,[6] JENDL,[7] KEDAK,[8] and SOKRATOR.[9]

In their recent "evaluation and testing of n + ^{239}Pu nuclear data for revision 2 of ENDF/B-V," Arthur *et al.*[10] summarize the improvements that should be considered in any future revisions of the ENDF/B ^{239}Pu evaluation. The second item of that list is:

> "a new analysis of the resolved and unresolved resonance regions that extends the resolved resonance region to as high an energy as feasible, that utilizes a multilevel formulation, and that includes the most recent experimental results."

The purpose of the analysis reported here is to address this item.

In order to improve the representation of the ^{239}Pu cross sections by using a multilevel formalism (which avoids the need for the file-3 contributions) and to extend the resolved resonance range from 300 eV up to 1 keV, ^{239}Pu neutron cross section measurements were analyzed with the resonance analysis Bayesian code SAMMY[12] using the Reich-Moore multilevel formalism.[13]

The purpose of the present report is to outline the selection of experimental data which were analyzed, the method of analysis, and the assumptions made; to list the nearly 1600 resonance parameters obtained; and to present detailed graphical and tabular comparisons between the cross sections obtained from the resonance analysis and several recent and older sets of experimental data and the ENDF/B-V evaluation.

A summary of the extensive results collected in this report, and a discussion of their significance will be submitted for a journal publication.

2. PREVIOUS RESONANCE ANALYSES OF THE ^{239}Pu NEUTRON CROSS SECTIONS

The resonance analyses of the ^{239}Pu neutron cross sections have been reviewed by Moore,[14] Derrien,[15] and more recently by Antsipov *et al.*[9] Characteristics of some of these analyses are summarized in Table 1.

Vogt's early R-matrix multilevel analysis extended over a very small energy range.[16] Single-level analyses have been performed up to above 600 eV[17] but, as is well known, the single-level formalism cannot properly represent the resonance asymmetries due to multilevel interference in the fission channels.[18] Some analyses are based on the Adler-Adler multilevel formalism.[19-22] However, the Reich-Moore R-matrix formalism is preferable because it has less flexibility than the Adler-Adler formalism, and hence it constrains tighter consistency between the different partial cross sections. Furthermore, Reich-Moore type resonance parameters can be converted into equivalent Adler-Adler type parameters,[23] whereas the converse is not generally true.[24]

R-matrix analyses of the ^{239}Pu cross sections, covering a wide energy range, were performed by Farrell[25] and by Derrien.[26] Farrell's analysis extends from 14 to 90 eV, but it is based only on the fission measurement of Shunk *et al.*,[27] and an unambiguous determination of all the partial widths cannot be made by analyzing a single partial cross section.[24] Derrien's analysis extends from 4 to 205 eV and is based on the high resolution, liquid-nitrogen temperature transmission measurement of Derrien[26] and the fission measurement of Blons.[28] The resonance parameters from Derrien's analysis were used as prior information in the present analysis in the region up to 210 eV.

The ENDF/B-V evaluation is based on a single-level analysis done in 1971 by Simpson and Simpson[29] for ENDF/B-III. Derrien[30] pointed out that the analysis could not correctly describe the cross sections because it did not contain the information about the spin of the resonances and hence the spin-dependence of the statistical factors. Later attempts by Smith *et al.* (see discussion in Ref. 31) to include the spin information were not successful in removing the inconsistency between partial cross-section measurements and transmission measurements. In the end, the low-energy cross sections in the ENDF/B-V evaluation were generated by adding to some parametric representation a "smooth" contribution forcing a fit to some selected measurements of Gwin *et al.* This evaluation was left undocumented.[31]

The recent JEF evaluation[6] is based on the multilevel resonance parameters of Derrien[15] up to 200 eV and on the single-level resonance parameters evaluated by Ribon and LeCoq[17] in the energy range from 200 to 600 eV. In the JENDL, KEDAK, and SOKRATOR evaluations the single-level resonance parameters of Ribon and LeCoq are used up to 660 eV.

A previous analysis[32] of the ^{239}Pu neutron cross sections up to 30 eV by some of the same authors using also the computer program SAMMY, and some of the same experimental data, is now superseded by the analysis presented here which extends over a much greater energy range.

Table 1. Selected resonance analyses of the ^{239}Pu cross sections

Reference	Formalism	Energy Range	Comment
Vogt (1960)[16]	Vogt R-matrix	0.01 – 10 eV	Consistent analysis of σ_{nT} and σ_{nf}
Ignatev *et al.* (1964)[44]	Multilevel	0.02 – 110 eV	Consistent analysis of η and σ_{nf}
Adler and Adler (1967)[19]	Adler-Adler	0.4 – 40 eV	Consistent analysis of σ_{nf}, σ_{nT}, and η
Gwin *et al.* (1971)[20]	Adler-Adler	0.02 – 100 eV	Simultaneous fit of σ_{nf} and $\sigma_{n\gamma}$
Ribon and LeCoq (1971)[17]	Breit-Wigner	0 – 660 eV	Consistent analysis of σ_{nT} and σ_{nf}
Simpson and Simpson (1971)[29]	Breit-Wigner	1 – 300 eV	Consistent σ_{nT}, σ_{nf}, and $\sigma_{n\gamma}$
Farrell (1971)[25]	Reich-Moore	14 – 90 eV	Analysis of σ_{nf} only
Derrien (1973)[26]	Reich-Moore	4 – 214 eV	Consistent σ_{nT} and σ_{nf}
	Briet-Wigner	200 – 660 eV	Consistent σ_{nT} and σ_{nf}
Kolesov and Luk'yanov (1982)[21]	Adler-Adler	0 – 160 eV	Consistent σ_{nT} and σ_{nf}

3. THE RESONANCE ANALYSIS CODE SAMMY

The computer code SAMMY[12] was used to perform a consistent resonance-parameter analysis of several ^{239}Pu neutron fission and capture cross-section and transmission measurements. The program SAMMY uses the multilevel R-matrix Reich-Moore formalism[13,33] and leads to a physically sound representation of the neutron cross sections in the resonance region. The Bayesian approach, which includes the direct introduction of experimental uncertainties such as on sample thicknesses, broadening parameters etc., allows the successive incorporation of new data in a consistent manner. The option to search on sample thicknesses, effective sample temperature, and the parameters of the instrumental resolution function all consistent with predetermined uncertainty limits, leads to realistic parameter uncertainities and covariance matrices.[12]

4. SELECTION OF ^{239}Pu NEUTRON CROSS-SECTION MEASUREMENTS

Most of the ^{239}Pu neutron cross-section measurements on the CSISRS file[34] or listed in CINDA[35] were examined for possible inclusion in the consistent SAMMY analysis. Six sets of measurements[20,28,36-39] were selected as listed in Table 2. These measurements were chosen because they had good energy resolution and relatively low background and because detailed information on the experimental conditions and on the uncertainties were readily accessible to the authors. Data from other measurements, evaluations, and analyses were compared on a differential and integral basis with the data from the six selected measurements in order to assess the consistency of the data and to study the nature of discrepancies, as will be discussed below.

The measurement of Blons[28] is the only fission measurement done on a sample at liquid nitrogen temperature (77 K) and covering an extensive energy range. Blons' data were used in the range from 40 to 1000 eV. The reduced Doppler broadening is very helpful in resolving the structure of closely spaced resonances. The recent fission measurement of Weston and Todd[37] was used between 9 and 1000 eV. This measurement has a poorer resolution but a much better statistical accuracy and lower background than that of Blons. The recent fission measurement of Gwin *et al.*[36] is particularly useful from 0.01 to 10 eV: it has high accuracy and low background. In the overlap region between 9 and 100 eV the measurements of Gwin *et al.*[36] and Weston and Todd[37] are consistent to within 2 to 4%.

Two series of transmission measurements with samples of several thicknesses cooled at liquid nitrogen temperature were done by Harvey *et al.*[39] in conjunction with the present resonance analysis. The high resolution measurements done on a flight path of 80 m were used in the range 30 to 1000 eV. The low energy measurements done on a 18 m flight path were used from 1.5 to 30 eV. The transmission measurements of Spencer *et al.*[38] were done with relatively thin samples, mostly to determine the resonance parameters of the 1.056 eV level in ^{240}Pu. These measurements were used below 30 eV and proved particularly helpful in the range from 0.01 to 0.5 eV.

Table 2. Selected measurements of the ^{239}Pu neutron cross sections

Reference	Energy range used in the analysis	Measurement characteristics
Blons (1973)	40 to 1000 eV	Fission at 50 m; sample cooled to 77 K
Gwin *et al.* (1971)	0.01 to 0.5 eV	Fission and absorption at 25.6 m
Gwin *et al.* (1984)	0.01 to 100 eV	Fission at 21.65 m
Weston and Todd (1984)	9 to 1000 eV	Fission at 18.9 m
Spencer *et al.* (1984)	0.01 to 30 eV	Transmission at 18 m. Samples of 0.00180, 0.00117, 0.00062, 0.00058, and 0.00029 atom/b
Harvey *et al.* (1985)	0.7 to 30 eV	Transmission at 18 m. Samples cooled to 97 K. Samples of 0.07375, 0.01802, 0.00638, 0.001815, 0.00058 atom/b
	30 to 1000 eV	Transmission at 80 m. Samples cooled at 97 K. Samples of 0.07375, 0.01802, 0.00058 atom/b

Direct capture cross-section measurements have relatively large normalization uncertainties and large backgrounds. These measurements are also contaminated with spurious resonances due to impurities in the sample or detector. The single capture measurement[20] weighted in our resonance analysis was used only in the range 0.01 to 0.5 eV.

The selected measurements and other data sets used in comparisons, as stated above, were first all precisely aligned on a common energy scale. The energy scale of the high resolution transmission measurement of Harvey *et al.*[39] was chosen as a standard since that measurement was done on the longest flight path, and since the length of that flight path has recently been measured with great accuracy.[40] Other energy scales were transformed by the relation:

$$E' = aE - bE^{3/2} ,$$

where E' is the new and E the old energy of a channel. The relation is appropriate for time-of-flight measurements;[41] the parameter a, nearly equal to unity, and b, very small relative to unity, were obtained by a least-square fit of resonance centroids.

The partial cross-section measurements extending over the thermal region were also renormalized to the latest 2200-m/s values evaluated by Divadeenam and Stehn[11] of 1017.3 ± 2.0 b, 748.1 ± 2.0 b, and 269.3 ± 2.2 b for the absorption, fission and capture cross sections, respectively. These values are consistent with the values recently evaluated by Axton[47] of 1018.9667 ± 2.8747 b, 747.6263 ± 2.0105 b, and 271.343 ± 2.1340 b, respectively. Typical energy rescaling and renormalization factors are given in Table 3.

5. ASSUMPTIONS OF THE ANALYSIS

The neutron cross sections in the energy range considered, 0 to 1000 eV, are described with 376 levels (see Table 4). Four of these levels are bound. The contribution of bound levels was found to be necessary to properly describe the neutron cross sections at low energy and in between resonances; however, the energy and widths of these levels were adjusted somewhat arbitrarily and are by no means determined uniquely by the measurements. In fact, the four bound levels are included to simulate the contributions of a very large number of bound levels; the parameters of these levels should not be given any physical interpretation.

Two levels with energies greater than 1000 eV are also included in the analysis. These correspond in energy to resonances which are observed in the ^{239}Pu neutron cross-section measurements, but again these levels are intended to simulate the contribution of the infinite number of levels above 1000 eV to the cross sections in the interval 0 to 1000 eV. The parameters of the levels above 1000 eV were adjusted to optimize the cross-section representation in the 0- to 1000-eV interval and hence should not be given further physical interpretation; in particular, these parameters are not necessarily adequate to represent the results of measurements above 1000 eV.

It is hoped that the parameters of these six fictitious outside resonances represent correctly the contributions of the truncated external levels to the range of interest, 0 to 1000 eV. If these contributions are properly described, the cross sections in the range of interest can be represented without the need of a "smooth-file" contribution, and using a constant effective radius a. An effective radius $a = 0.946$ f was used in the analysis; this radius was obtained essentially from a fit in the 30 to 40 eV region of the thick sample (0.0737 atom/b) transmission measurement of Harvey *et al.*

All the levels of Table 4 were treated as s-wave levels. The p-wave penetration factor $\frac{\rho^2}{1+\rho^2}$ is approximately 5×10^{-3} at 1 keV so that some of the smaller levels, at the energies near 1 keV, could in fact be p-wave levels. However, existing data do not allow to distinguish between the smaller s-wave levels and large p-wave levels. The levels must be partitioned between the two spin states accessible to the compound nucleus: $J=0^+$ and $J=1^+$. Up to 205 eV the spin assignment used here was mostly that of Derrien,[15,26] which is mainly based on the work of Trochon,[42] who determined the spin statistical factors g from neutron-scattering and transmission measurements.

Table 3. Energy rescaling and renormalization factors

Measurement	Energy alignment $E' = aE - bE^{3/2}$		Renormalization $(\sigma'_x = R_x\sigma_x)$
	a	$b(eV^{-1/2})$	R_x[a]
Gwin *et al.* (1971)	Not realigned		$R_f = 1.0086$, $R_\gamma = 0.963$
Blons (1973)	0.9963736	−0.000141	Not renormalized
Gwin *et al.* (1976)	Not realigned		1.0086
Wagemans *et al.* (1980)	Not realigned		1.0084
Gwin *et al.* (1984)	1.001650	+0.00048	1.0047
Weston and Todd (1984)	0.9988759	−0.000051	1.0086

[a]The ratio of the 2200 m/s fission cross section of Stehn *et al.* to that of ENDF/B-V is 1.0086.

For the level near 0.3 eV the original spin assignment 0^+ of Derrien was changed to 1^+ on the basis of the work of Weinstein *et al.*[43] Two 0^+ levels, at 74.9 and 190.1 eV were added to the Derrien set because this gave a better fit to the data. The two levels at 74.9 and 75.0 eV are poorly resolved, so that the direct experimental evidence concerning the spin of these levels is ambiguous. Between 200 and 300 eV the spin attribution of Trochon was followed except for two narrow resonances at 279.9 and 292.7 eV which were changed from the original 0^+ attribution of Trochon to 1^+.

Above 300 eV there are many differences in the spin attribution of the resonances, between the present analysis and Trochon's work. As the energy increases the energy resolution becomes broader and there is a greater proportion of unresolved multiplets. The resonance parameters provide a good representation of the available cross-section data, but this representation cannot be considered unique.

Again, following the work of Derrien,[26] two fission channels were assumed to contribute to the $J=0^+$ states and one fission channel to the $J=1^+$ states.

6. RESULTS OF THE ANALYSIS

The best resonance parameters obtained by a Bayesian analysis of the selected measurements discussed in Section 4 are given in Table 4. The extent to which the resonance parameters of Table 4 represent the experimental data is illustrated in the figures and tables below. These resonance parameters are however not unique and are strongly correlated. A description of the covariance matrix of these nearly 1600 parameters must await the implementation of more extensive computing facilities now under development.

Table 4. ^{239}Pu resonance parameters

	E_0 (eV)	Γ_γ (meV)	Γ_n (meV)	Γ_{f1} (meV)	Γ_{f2} (meV)	J
1	−150.0	42.00	700.6	226.2		1
2	−15.46	24.30	23.93	−0.2428E–02		1
3	−7.067	45.65	25.06	−419.7	344.5	0
4	−0.1156	28.13	0.1737E–01	−73.33	−466.0	0
5	0.2956	39.39	0.7962E–01	56.87		1
6	7.817	39.42	0.7945	−44.30		1
7	10.93	43.12	1.783	−143.9		1
8	11.90	38.99	0.9826	20.81		1
9	14.33	48.07	0.6506	63.05		1
10	14.68	44.85	1.961	33.32		1
11	15.44	63.75	1.840	−0.1957E–01	645.9	0
12	17.66	37.28	1.797	−34.91		1
13	22.27	42.74	2.612	−61.16		1
14	23.93	29.13	0.7311E–01	19.01		1
15	26.27	40.13	1.539	41.91		1
16	27.27	33.65	0.1337	3.437		1
17	32.32	42.87	0.8337	14.85	−111.1	0
18	35.48	41.04	0.2683	3.646		1
19	41.46	45.09	3.609	−4.957		1
20	41.73	40.28	0.9264	53.90		1
21	44.53	36.78	6.403	−3.383		1
22	47.54	36.38	4.955	491.5	−0.1274E–03	0
23	49.59	42.00	3.957	−985.9	8.563	0
24	50.14	42.03	2.563	−10.94		1
25	52.65	37.21	10.78	−6.371		1
26	55.70	36.96	1.607	17.83		1
27	56.94	42.00	10.90	−2105.	48.03	0
28	59.28	36.65	4.501	84.50		1
29	61.40	42.00	28.53	7143.	7.661	0
30	63.16	47.98	0.7065	99.63		1
31	65.44	51.00	3.726	506.5	−0.2117E–12	0
32	65.79	61.67	9.707	113.3		1
33	74.16	37.87	3.173	−34.54		1
34	74.88	42.00	8.022	1.264	−266.2	0
35	75.05	38.63	17.61	−88.88		1
36	79.08	42.00	0.4238E–01	6.000		1
37	80.96	42.00	5.513	1828.	−1.512	0
38	82.77	47.00	0.3260	5.000		1
39	85.59	51.00	46.96	−1792.	2.226	0
40	85.61	27.22	8.284	5.603		1
41	90.84	38.20	11.77	6.852		1
42	93.07	40.51	0.6657	−2.518		1

Table 4. Continued

	E_0 (eV)	Γ_γ (meV)	Γ_n (meV)	Γ_{f1} (meV)	Γ_{f2} (meV)	J
43	95.51	61.19	2.062	−27.43		1
44	96.61	42.00	8.611	1337.	−59.06	0
45	99.74	42.00	25.33	−27.37	9719.	0
46	103.1	35.31	1.612	6.480		1
47	105.4	44.75	4.637	4.529		1
48	106.8	39.49	9.749	−22.53		1
49	110.5	50.95	0.4882	21.17		1
50	114.6	42.00	2.505	−1227.	416.1	0
51	115.3	42.00	0.2143	160.0		1
52	116.2	34.15	10.45	−160.2	−23.83	0
53	119.0	42.27	17.52	−39.19		1
54	121.2	42.72	2.526	31.35		1
55	123.6	67.02	0.5822	−63.18		1
56	126.4	49.64	1.737	−10.93		1
57	127.7	42.58	0.5442	13.70		1
58	131.8	42.00	35.55	3909.	−16.32	0
59	134.0	40.11	5.603	−3.719		1
60	136.9	32.16	11.04		−85.27	0
61	139.4	42.00	0.8361E–01	−19.30		1
62	143.2	36.16	3.334	78.92		1
63	143.7	33.64	4.502	18.44		1
64	146.5	38.10	7.287	7.025		1
65	147.4	42.00	4.987	2309.	2.037	0
66	148.4	47.00	0.3405	34.27		1
67	149.6	32.12	1.546	18.75		1
68	157.2	42.00	30.18	181.3	581.2	0
69	157.2	42.00	1.200	3.000		1
70	162.1	35.60	0.9590E–01	15.40		1
71	164.7	42.54	28.54	−7.024		1
72	167.3	41.91	6.091	64.08		1
73	170.1	42.00	0.1201	3.000		1
74	170.7	38.00	0.4393	80.00		1
75	170.9	42.00	3.549	−32.72	1846.	0
76	171.3	42.00	0.2500E–01	3.000		1
77	176.2	43.68	2.142	29.42		1
78	177.4	39.62	3.576	5.510		1
79	179.1	31.98	1.213	7.439		1
80	183.8	48.00	1.623	22.00		1
81	184.9	42.00	18.60	−1913.	376.9	0
82	188.5	39.50	0.6267	12.50		1
83	190.1	42.00	1.239	60.01	4165.	0

Table 4. Continued

	E_0 (eV)	Γ_γ (meV)	Γ_n (meV)	Γ_{f1} (meV)	Γ_{f2} (meV)	J
84	190.8	42.82	1.687	−11.45		1
85	195.4	22.49	52.05	−597.8	0.3931	0
86	196.9	53.70	4.001	24.30		1
87	199.6	52.33	9.072	76.52		1
88	203.6	42.00	1.789	36.00		1
89	204.1	57.66	61.06	29.02	431.4	0
90	207.6	43.93	7.160	4.842		1
91	211.1	42.00	4.064	−104.1	1246.	0
92	213.5	35.00	0.3607	27.70		1
93	215.5	42.00	0.4600E–01	34.00		1
94	216.0	42.00	7.479	8989.	−172.4	0
95	216.8	37.25	6.104	4.447		1
96	219.7	39.90	3.608	17.60		1
97	220.5	35.55	7.743	−8.373		1
98	223.4	32.81	3.326	4.189		1
99	225.1	52.42	1.725	17.81		1
100	227.4	42.00	13.69	−1185.	−4400.	0
101	228.1	39.71	1.756	−14.06		1
102	230.3	42.00	4.144	3692.	−30.59	0
103	231.6	35.78	12.69	5.228		1
104	232.8	42.00	0.3859	27.00		1
105	233.8	42.00	11.18	5639.	−532.1	0
106	234.6	35.49	10.24	6.038		1
107	239.3	37.82	5.566	−9.109		1
108	240.8	42.00	0.3330E–01	34.00		1
109	243.1	39.16	6.487	−51.62		1
110	247.7	45.09	0.8267	179.3		1
111	249.1	33.06	15.48	−3.107		1
112	251.5	35.86	29.72	8.903		1
113	254.8	38.92	3.011	28.89		1
114	256.3	41.50	1.164	1069.	9.975	0
115	256.4	55.61	6.005	−15.04		1
116	259.3	41.50	0.2640	−200.0		1
117	262.1	42.00	79.01	−2665.	2561.	0
118	263.0	46.00	2.415	−10.00		1
119	264.5	41.50	0.1650	21.00		1
120	269.4	42.00	1.271	−86.00		1
121	269.8	40.00	4.165	23.65		1
122	272.9	41.43	25.45	−45.32		1
123	275.1	42.00	30.58	0.4886	886.6	0
124	275.9	39.26	21.15	49.19		1
125	277.7	42.00	40.07	8970.	−795.9	0

Table 4. Continued

	E_0 (eV)	Γ_γ (meV)	Γ_n (meV)	Γ_{f1} (meV)	Γ_{f2} (meV)	J
126	279.9	32.58	7.742	−19.87		1
127	283.2	37.07	27.74	4.716		1
128	286.0	41.50	0.2000	10.00		1
129	288.3	41.50	0.9330E–01	−34.00		1
130	291.9	42.00	20.73	−5829.	592.3	0
131	292.7	29.06	3.692	19.63		1
132	292.9	42.00	0.4500	−10.87	−793.0	0
133	296.8	44.96	3.382	−29.85		1
134	298.9	36.87	10.89	15.63		1
135	302.2	38.40	18.89	−35.39		1
136	308.6	32.40	3.316	118.1		1
137	309.4	46.69	14.16	18.47		1
138	311.6	43.97	0.3632	−24.90		1
139	314.0	40.53	14.74	−9.532		1
140	317.0	36.54	5.713	17.39		1
141	323.7	77.83	19.48	−25.22		1
142	324.6	42.00	21.01	−444.3	−6349.	0
143	325.7	35.68	8.114	−16.78		1
144	329.4	42.00	5.065	1308.	−680.0	0
145	334.3	36.29	5.621	6.163		1
146	336.3	38.17	15.55	−11.41		1
147	338.3	35.83	8.153	6.068		1
148	339.6	37.56	3.487	−15.42		1
149	343.6	34.65	16.72	17.33		1
150	346.8	42.00	11.63	−17.80	−1522.	0
151	350.7	32.82	22.52	21.15		1
152	353.2	29.45	3.667	10.79		1
153	355.3	25.58	0.2711	15.20		1
154	360.4	50.00	1.120	−26.92		1
155	361.7	35.00	0.2047	−0.6864		1
156	364.6	42.00	53.37	−0.2643E+05	1188.	0
157	369.1	41.50	1.383	−1945.		1
158	370.8	49.13	2.819	18.73		1
159	373.1	42.00	8.149	681.1	2049.	0
160	375.5	29.00	2.448	0.3047E–01		1
161	377.5	18.04	1.590	−7.314		1
162	378.5	54.00	0.9528	7.627		1
163	382.8	43.00	0.3694	12.12		1
164	384.7	28.00	6.002	−23.15		1
165	388.1	42.00	3.192	6012.	−2311.	0
166	390.0	51.00	1.554	−19.39		1
167	392.0	55.00	1.053	46.74		1
168	394.9	51.96	7.153	−38.60		1

Table 4. Continued

	E_0 (eV)	Γ_γ (meV)	Γ_n (meV)	Γ_{f1} (meV)	Γ_{f2} (meV)	J
169	397.4	44.00	2.044	51.08		1
170	402.1	46.00	18.95	−174.5		1
171	404.7	56.00	22.07	−74.87		1
172	406.5	41.50	1.205	−21.14		1
173	407.5	30.00	0.9290	148.1		1
174	409.2	55.00	1.169	−42.34		1
175	412.8	46.00	8.777	38.69		1
176	416.2	50.00	2.994	−7.044		1
177	418.1	50.00	1.241	−19.32		1
178	419.8	42.00	3.444	226.6	3042.	0
179	420.4	45.00	6.110	−29.43		1
180	426.1	41.50	0.5164	22.72		1
181	426.1	42.00	9.727	164.1	8535.	0
182	430.0	41.50	3.345	725.1		1
183	433.4	41.50	0.6071	−4.309		1
184	433.4	41.50	23.08	3616.	−2815.	0
185	438.3	49.00	2.935	−8.552		1
186	439.3	55.00	3.229	3.849		1
187	440.9	46.00	0.2565	−133.1		1
188	443.0	44.00	20.40	−87.40	274.9	0
189	450.4	46.00	0.9535	−35.48		1
190	451.9	20.01	14.05	1.419		1
191	455.4	20.75	0.6306	−70.18		1
192	456.3	46.00	78.22	202.6	−56.73	0
193	457.9	46.00	8.047	−204.2		1
194	459.4	25.25	5.155	20.49		1
195	461.9	46.00	2.447	−103.4		1
196	463.1	24.00	0.5778	35.36		1
197	466.1	24.00	0.5442E–01	36.13		1
198	469.1	46.00	10.10	−3366.		1
199	473.7	25.00	4.424	−2.157		1
200	475.1	46.00	2.476	1759.	3355.	0
201	476.1	46.00	25.68	3.689	2810.	0
202	478.9	46.00	0.2392E–01	−4390.	−507.1	0
203	479.6	46.00	0.1087	20.85		1
204	484.7	26.24	2.477	−5.334		1
205	488.0	46.00	5.243	688.0		1
206	489.0	46.00	0.7143	−473.3		1
207	491.7	46.00	39.96	614.7	1853.	0
208	494.7	35.57	5.683	−45.64		1
209	496.2	39.49	0.6675	16.62		1

Table 4. Continued

	E_0 (eV)	Γ_γ (meV)	Γ_n (meV)	Γ_{f1} (meV)	Γ_{f2} (meV)	J
210	501.1	46.00	4.117	42.36		1
211	503.5	56.09	12.39	48.49		1
212	506.4	46.00	0.3426	−123.2		1
213	510.3	46.00	38.69	−130.1		1
214	510.5	46.00	0.5942E–01	508.6	3945.	0
215	510.5	46.00	131.4	479.0	2657.	0
216	515.7	46.00	0.4109	−12.26		1
217	517.2	46.00	0.6346E–01	59.30		1
218	518.7	46.00	0.6430	−110.8		1
219	520.9	46.00	15.80	−28.16		1
220	524.6	46.00	231.2	9807.	−1641.	0
221	524.9	27.93	37.46	−8.743		1
222	526.7	46.00	0.7444	2.485		1
223	528.1	46.00	0.8335	19.86		1
224	531.2	23.13	59.66	−21.18		1
225	531.4	46.00	0.1255	−1829.	43.09	0
226	539.9	46.00	12.00	3.507		1
227	541.3	46.00	1.777	−37.62		1
228	542.2	46.00	4.778	426.8		1
229	543.8	46.00	11.69	−7.543		1
230	546.5	46.00	35.77	−25.94	1239.	0
231	550.4	46.00	11.48	6.401		1
232	554.3	46.00	16.62	10.84		1
233	554.8	46.00	101.2	796.3	−823.3	0
234	556.1	46.00	0.7124	−20.78		1
235	559.9	46.00	29.16	8.394		1
236	563.5	46.00	29.75	−512.7		1
237	564.7	46.00	9.080	−0.1287E–01		1
238	566.5	46.00	8.794	−0.8242		1
239	571.8	46.00	9.207	−31.04		1
240	574.7	46.00	157.0	60.04	82.85	0
241	576.6	46.00	39.06	8.023		1
242	578.6	46.00	1.489	0.3941		1
243	579.8	46.00	7.101	4.656		1
244	585.4	46.00	0.4516	−29.79		1
245	588.8	46.00	11.21	6.866		1
246	594.4	46.00	1.938	12.37		1
247	596.0	46.00	21.21	−7283.	2107.	0
248	598.1	46.00	8.071	−1.890		1
249	604.8	24.17	22.87	−2.472		1
250	608.4	21.30	9.072	−4.589		1
251	610.0	17.19	14.69	−2.696		1
252	613.6	31.93	5.183	−7.501		1

Table 4. Continued

	E_0 (eV)	Γ_γ (meV)	Γ_n (meV)	Γ_{f1} (meV)	Γ_{f2} (meV)	J
253	616.0	46.00	13.90	0.4844E+05	−2737.	0
254	621.6	25.70	10.47	−3.532		1
255	623.3	35.50	8.534	5.485		1
256	625.9	23.98	7.102	−5.316		1
257	629.0	40.30	1.578	9.277		1
258	634.6	46.00	78.71	2177.	−4050.	0
259	637.3	52.19	4.664	14.43		1
260	640.0	24.46	8.438	15.89		1
261	641.6	46.35	1.770	3000.		1
262	645.7	32.39	5.047	1.720		1
263	647.5	47.74	1.416	2132.		1
264	658.6	46.00	32.39	−30.63	31.04	0
265	659.3	73.37	57.62	−12.78		1
266	662.4	45.92	0.3722	2.431		1
267	667.2	42.78	1.819	−5.419		1
268	669.9	35.90	3.334	4.519		1
269	672.1	29.10	15.87	3.304		1
270	675.1	49.17	2.155	25.54		1
271	676.4	43.16	0.8599	161.0		1
272	681.3	46.00	5.323	0.6470E−01	−798.0	0
273	682.1	49.93	3.078	−116.4		1
274	684.1	46.00	38.71	4.991	−3072.	0
275	684.7	40.26	7.414	2.951		1
276	686.5	40.26	0.4759	1.173		1
277	688.5	24.46	13.05	5.448		1
278	692.7	48.01	5.080	53.63		1
279	693.7	49.87	3.676	742.0		1
280	701.4	46.00	10.45	14.85	−5269.	0
281	707.6	81.93	12.47	19.70		1
282	713.2	36.02	9.033	11.61		1
283	714.0	46.00	6.818	13.06		1
284	717.5	26.77	10.31	3.937		1
285	718.9	46.00	7.833	1.900		1
286	720.9	45.96	0.2273E−01	0.1643		1
287	727.8	42.30	2.676	−12.57		1
288	733.3	52.21	9.616	13.52		1
289	734.7	49.48	22.47	−221.3	−2353.	0
290	738.1	46.00	8.201	665.7		1
291	739.5	76.67	6.027	73.36		1
292	744.7	27.02	11.06	10.65		1
293	747.1	26.33	13.22	4.121		1
294	749.4	47.41	1.221	10.23		1

Table 4. Continued

	E_0 (eV)	Γ_γ (meV)	Γ_n (meV)	Γ_{f1} (meV)	Γ_{f2} (meV)	J
295	750.9	48.38	2.527	15.32		1
296	753.5	31.08	45.64	6.567		1
297	758.0	46.00	70.05	−164.3	1707.	0
298	764.8	49.77	7.040	−7.268		1
299	767.1	42.62	2.937	19.68		1
300	773.8	46.00	6.400	9.727		1
301	777.6	48.97	10.57	42.67		1
302	781.6	60.00	6.896	260.0		1
303	782.0	60.00	10.60	21.66		1
304	784.8	48.54	2.606	9.901		1
305	787.1	45.43	9.798	15.15		1
306	790.5	49.44	1.491	83.38		1
307	795.8	49.44	9.375	27.88		1
308	798.3	46.00	99.95	−5220.	2384.	0
309	800.9	60.00	3.957	31.46		1
310	805.2	46.00	16.24	−628.9	0.1340E+05	0
311	807.0	60.00	7.893	24.11		1
312	811.1	46.00	3.474	321.6	169.1	0
313	816.7	28.00	12.10	6.916		1
314	820.7	28.16	5.164	4.918		1
315	823.9	46.00	2.621	−391.4		1
316	825.2	46.00	7.266	−64.00		1
317	829.3	46.00	1.968	1179.	1111.	0
318	829.8	53.09	29.46	40.32		1
319	833.1	46.00	1.203	163.0		1
320	836.2	46.00	2.078	−0.9384E–02		1
321	843.3	46.00	110.0	1984.	6013.	0
322	843.8	46.00	1.414	48.75		1
323	845.6	46.00	5.679	−39.90		1
324	848.3	46.00	6.063	32.54		1
325	854.0	46.00	1.727	91.37		1
326	856.0	46.00	4.902	838.3		1
327	858.7	46.00	5.857	1095.		1
328	861.5	46.00	4.263	616.7		1
329	865.8	46.00	1.727	86.01		1
330	867.5	46.00	4.487	68.26		1
331	870.2	28.55	4.283	10.98		1
332	874.4	46.00	17.68	16.30		1
333	875.7	46.00	13.90	17.88		1
334	878.2	46.00	3.704	9131.	−0.6275	0
335	878.6	46.00	3.583	0.5440		1
336	885.6	46.00	11.34	8.920		1
337	892.0	46.00	69.14	4.937		1

Table 4. Continued

	E_0 (eV)	Γ_γ (meV)	Γ_n (meV)	Γ_{f1} (meV)	Γ_{f2} (meV)	J
338	895.8	46.00	7.007	252.5		1
339	896.0	46.00	1.507	1863.	−42.06	0
340	897.1	46.00	6.827	53.79		1
341	903.8	46.00	10.38	−19.31		1
342	905.9	46.00	20.55	−3364.	716.1	0
343	906.1	46.00	4.706	−10.30		1
344	908.5	46.00	10.03	−917.4		1
345	913.1	46.00	29.89	−909.3	1385.	0
346	916.2	46.00	6.733	604.2		1
347	920.3	46.00	16.45	−194.4		1
348	923.2	46.00	23.74	4.765		1
349	926.0	46.00	2.825	184.2		1
350	928.0	46.00	3.730	36.26		1
351	929.8	46.00	8.379	969.3	907.5	0
352	933.0	46.00	11.96	−8.703		1
353	937.5	46.00	0.2961	16.73		1
354	937.7	46.00	27.31	1621.	−828.8	0
355	939.8	46.00	12.31	179.3		1
356	941.2	46.00	9.165	20.69		1
357	944.1	46.00	7.870	16.34		1
358	946.4	46.00	6.942	−3.440		1
359	951.7	46.00	5.280	13.39		1
360	955.0	46.00	8.049	49.34		1
361	958.9	46.00	41.65	24.17		1
362	966.4	46.00	30.55	47.90		1
363	972.0	46.00	18.77	636.7		1
364	974.4	46.00	56.44	35.38		1
365	978.0	46.00	2.072	4.950		1
366	980.7	46.00	80.81	−1664.	225.5	0
367	985.4	46.00	82.33	−20.29		1
368	987.1	46.00	0.2530E–02	827.3	756.9	0
369	989.7	46.00	1.753	5.009		1
370	990.8	46.00	6.234	118.1		1
371	994.3	46.00	19.92	28.44		1
372	997.9	46.00	36.25	−204.2		1
373	998.7	46.00	37.22	−26.14		1
374	1005.	46.00	160.4	1.179		1
375	1010.	46.00	97.90	−4884.	20.85	0

Figures 1 to 43 provide a detailed graphical comparison between the results of several measurements and the corresponding quantities as computed from the resonance parameters of Table 4. In Tables 5 to 8 we give numerical comparisons of measured cross sections, integrated or averaged over selected energy intervals, with cross sections computed from our analysis and from the ENDF/B-V evaluation. In Figs. 1 to 3 the fission and capture cross sections obtained from the parameters of Table 4 are compared with ENDF/B-V and with available low energy data for energies up to 0.5 eV.

In Fig. 4 the capture cross section obtained from the parameters of Table 4 is compared to the capture data from the 1971 Oak Ridge National Laboratory/Rensselaer Polytechnic Institute measurement.[20] Note that the experimental data are not corrected for the contributions of the ^{240}Pu isotopic contaminant at 1.056 eV and of tungsten, a chemical impurity with large resonances at 18.84, 21.2, and 27.05 eV. In Fig. 5 the fission cross section obtained from our parameters is compared with the data from the measurements of Gwin *et al.* (1984)[36] and of Wagemans *et al.* (1980).[45] For clarity of display the data of Wagemans *et al.*, and the corresponding calculation have been multiplied by a factor of 10. In the valleys between resonances our calculation is more consistent with the data of Gwin *et al.*, suggesting a residual background of approximately 15 b in the data of Wagemans *et al.* In Fig. 6 the fission cross section is compared with the high accuracy data of Weston and Todd[37] in the range 10 to 50 eV.

In Figs. 7 to 18 we compare measured and computed cross sections between 30 and 1000 eV. The measurement of Blons[28] was done on a 50 m flight path with a sample effective temperature of 101 K, and hence has a better resolution than the measurement of Weston and Todd done on a 19 m flight path with a room temperature sample. Note that for clarity of display the data of Blons and the corresponding calculation were multiplied by a factor of 10. In some energy ranges the data of Blons have large statistical uncertainties and, again for clarity, have been averaged over three successive channels to reduce these uncertainties.

In Figs. 19 to 24 we compare the measured fission cross section of Weston and Todd with both the calculation made with our resonance parameters and ENDF/B-V. The ENDF/B-V calculation and corresponding data set have been multiplied by a factor of 10 for clarity of display. Note that our parameters provide a better representation of the experiment than does ENDF/B-V, particularly in the valley between resonances, and at the higher energies.

In Fig. 25 we compare transmission ratios computed with our resonance parameters, with measurements of Spencer *et al.*, in the region 0.01 to 0.7 eV. In Figs. 26 to 28 we compare transmission ratios computed with our resonance parameters with measurements for eight sample thicknesses, over the range 0.7 to 30 eV. These measurements were done on a flight path of 18 m. The three samples of Spencer *et al.*, Fig. 26, were at room temperature; the five samples of Harvey *et al.*, Figs. 27 and 28 were at liquid nitrogen temperature. The data of the thinner samples were displaced by 0.25 and 0.5, respectively, for clarity of display.

ORNL-DWG 86-11910

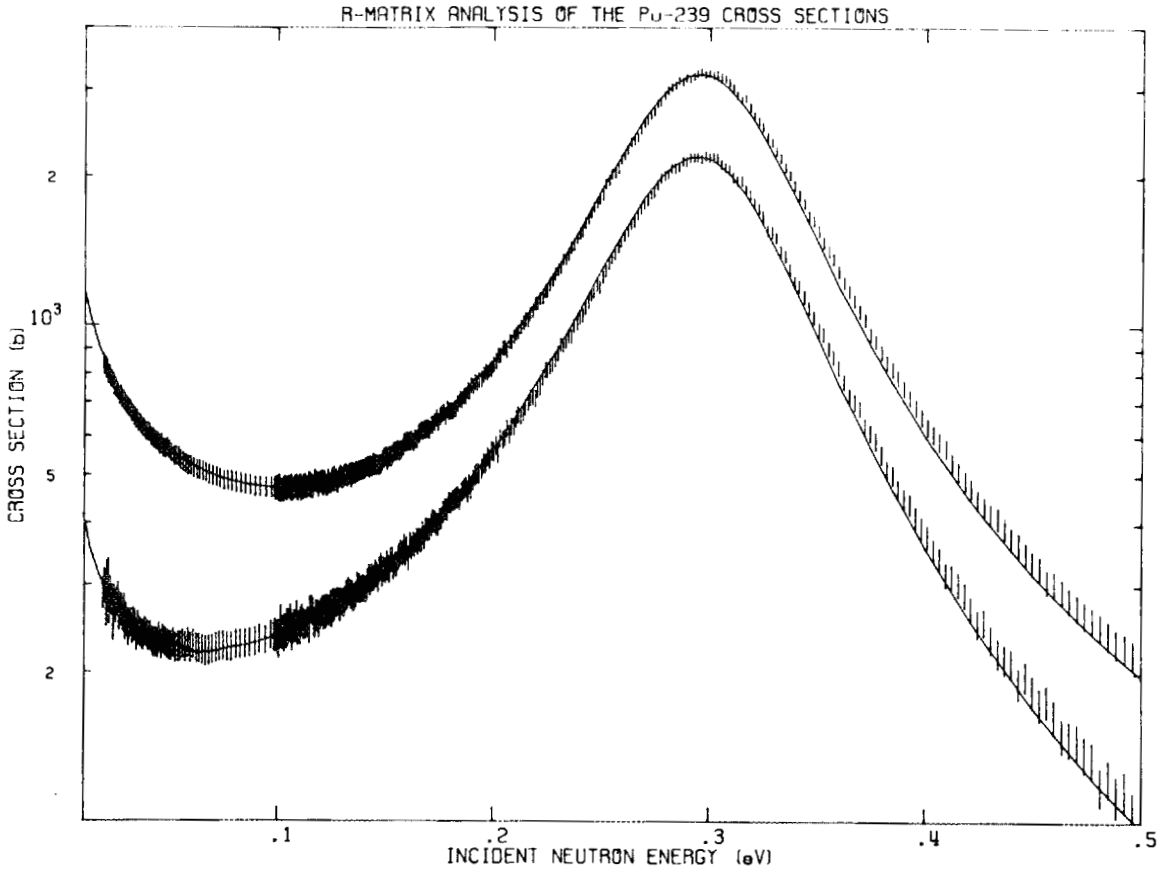

Fig. 1. Comparison of cross sections computed with our resonance parameters (solid line) with data from the measurement of Gwin *et al.* (1971) (error bars), over the incident neutron energy range from 0.01 to 0.5 eV. The upper curves represent the fission cross sections, the lower curves the capture cross section. The experimental data were renormalized to the current 0.0253 eV values of 748.1 and 269.3 b, respectively.

ORNL-DWG 86-11911

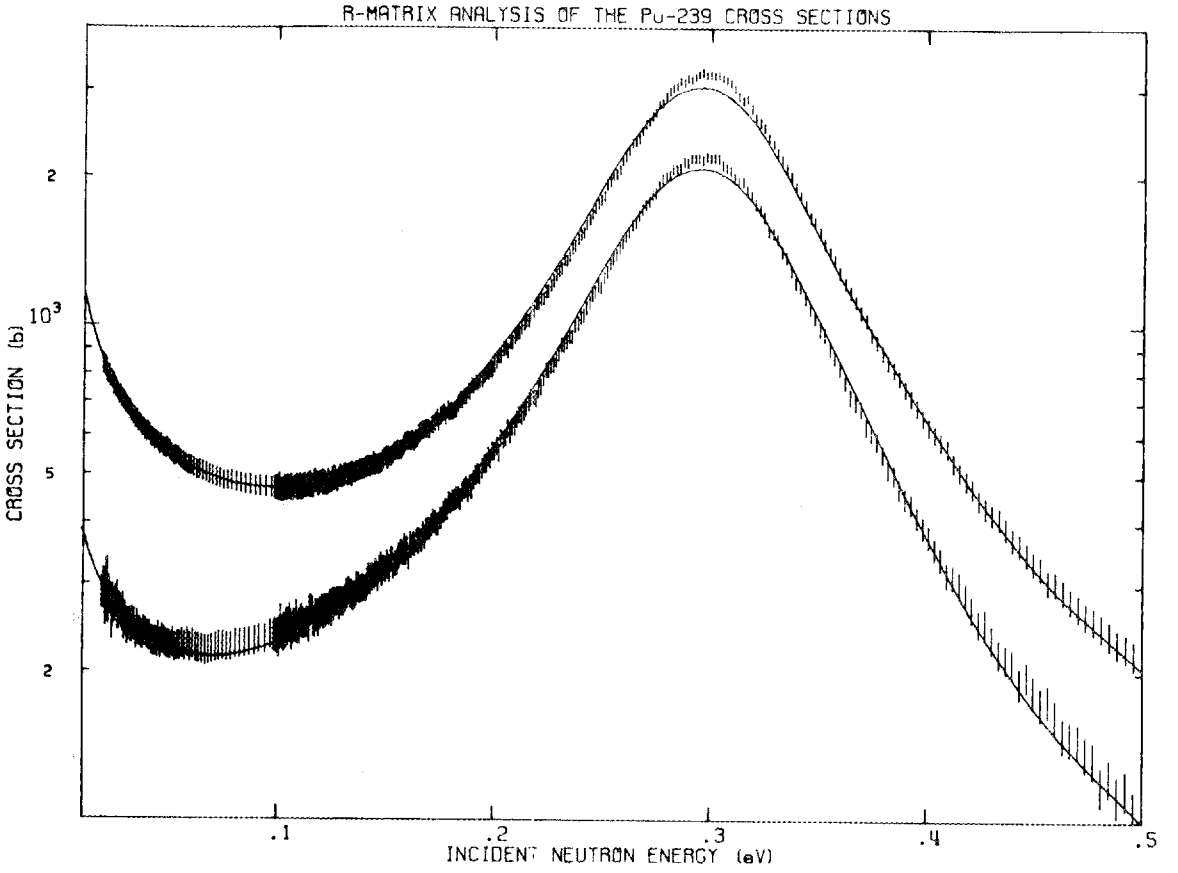

Fig. 2. Comparison of the cross sections computed with ENDF/B-V (solid line) with the data of Gwin *et al.* (1971) also shown on Fig. 1.

ORNL-DWG 86-11912

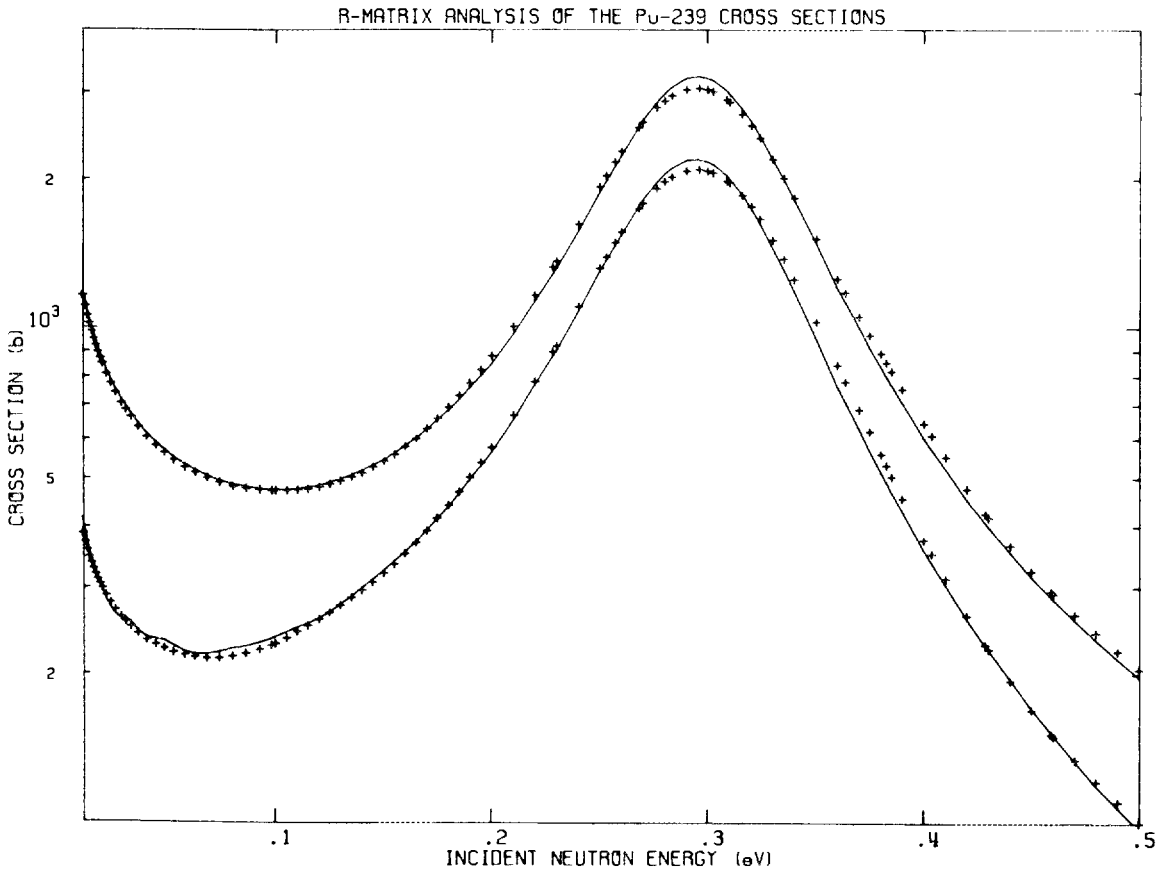

Fig. 3. Comparison of the cross sections computed with our resonance parameters (solid line) with ENDF/B-V (crosses) over the incident energy range from 0.01 to 0.5 eV. The upper curves represent the fission cross sections, the lower curves the capture cross sections.

ORNL-DWG 86-11913

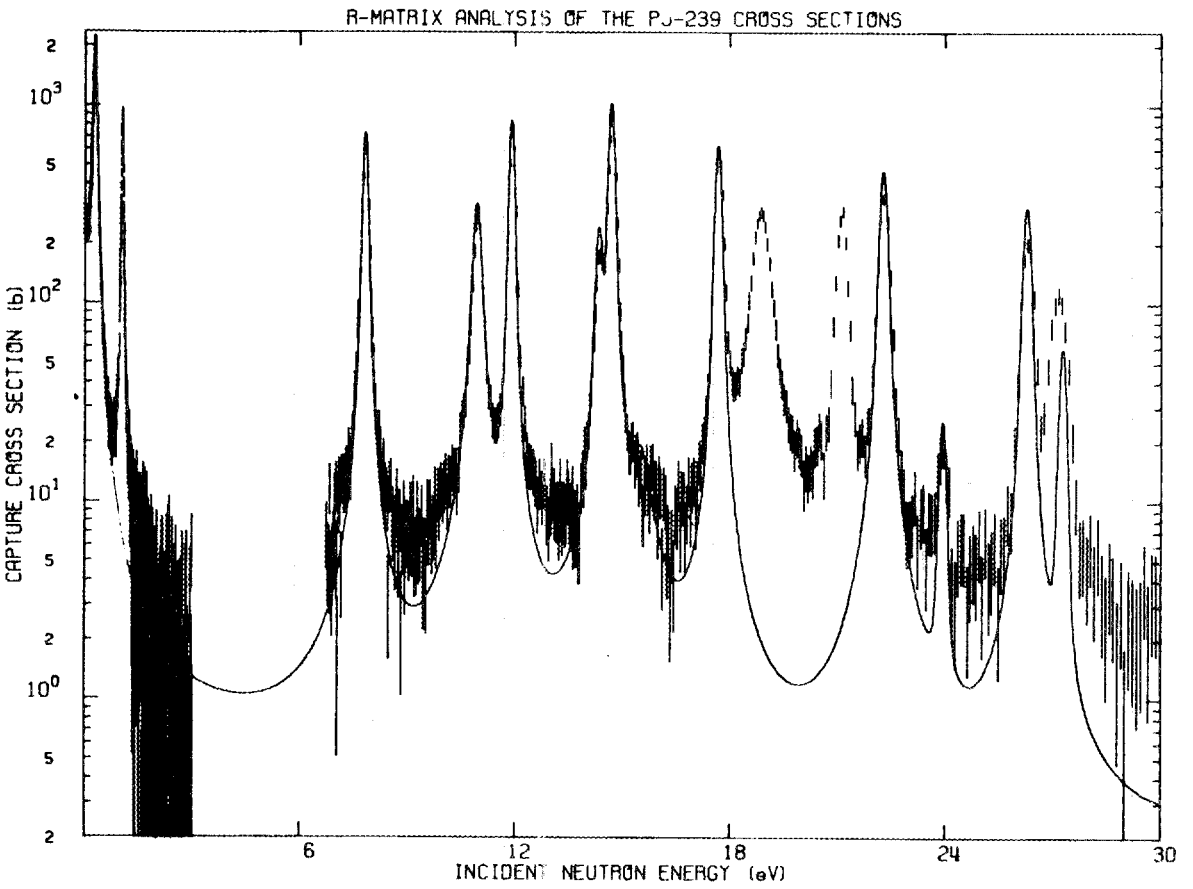

Fig. 4. Comparison of the capture cross sections computed from our resonance parameters (solid line) with the data from the measurement of Gwin *et al.* (1971) (error bars), over the incident neutron energy range from 0.01 to 30 eV. The resonance at 1.056 eV is a ^{240}Pu resonance from an isotopic impurity. No data were taken in the interval 5 to 7 eV where a ^{198}Au background filter distorted the incident neutron spectrum. The experimental data were renormalized as in Fig. 1.

ORNL-DWG 86-11914

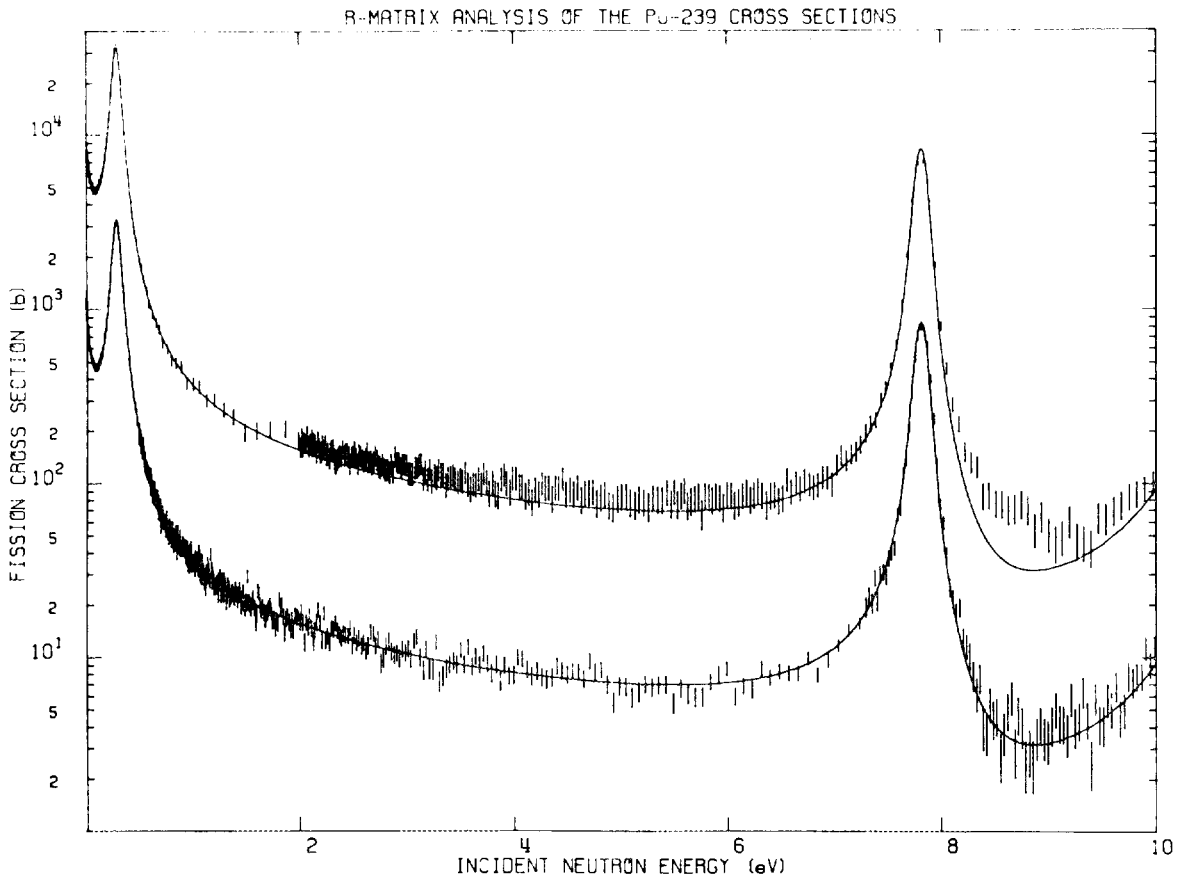

Fig. 5. Comparison of the fission cross sections computed with our resonance parameters (solid line) with the data from the measurement of Gwin *et al.* (1976) and Wagemans *et al.* over the incident neutron energy range from 0.01 to 10 eV. The data of Wagemans *et al.* and the corresponding fit have been displaced up by a factor of ten for clarity.

ORNL-DWG 86-11915

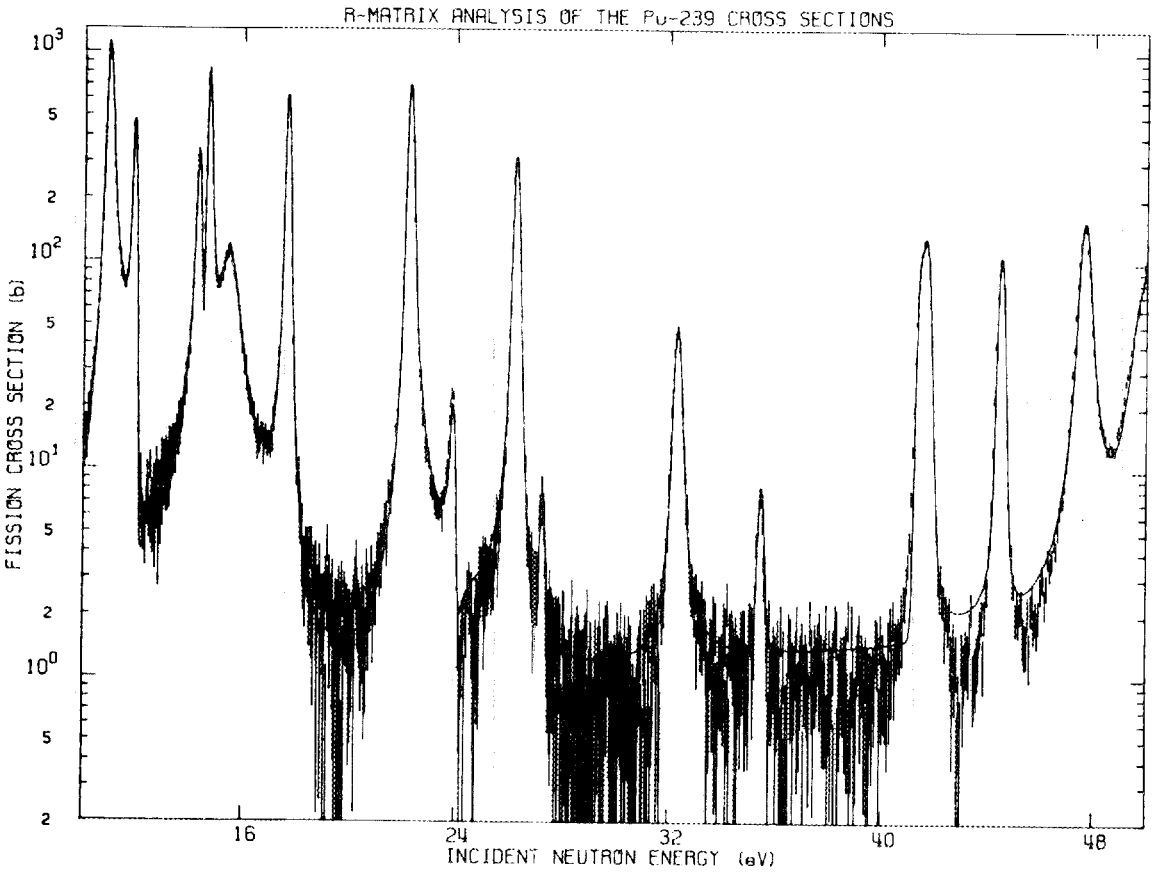

Fig. 6. Comparison of the fission cross sections computed with our resonance parameters (solid line) with the data from the measurements of Weston and Todd (1984), error bars, over the incident neutron energy range from 10 to 50 eV.

ORNL-DWG 86-11916

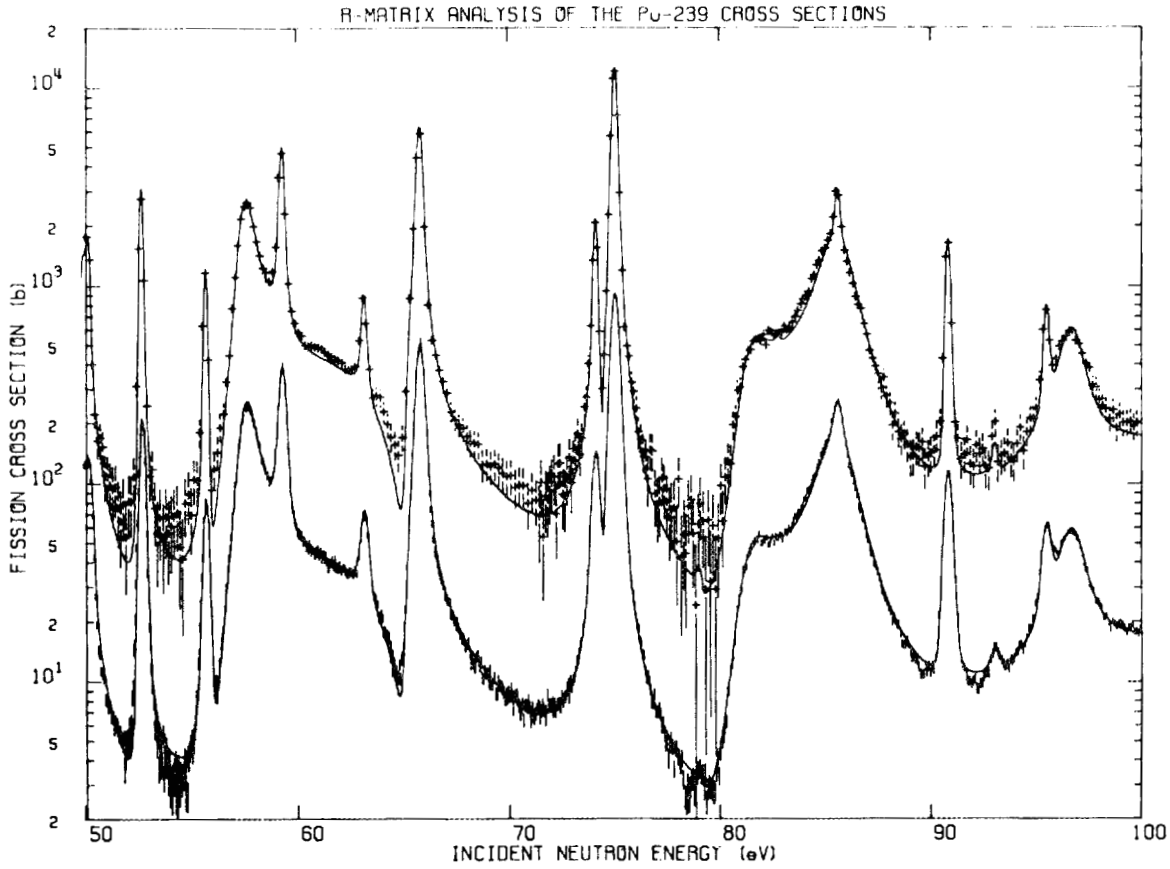

Fig. 7. Comparison of the fission cross sections computed with our resonance parameters (solid lines) with the data from the measurements of Weston and Todd (1984), error bars, and Blons (1973), error bars with cross, over the incident neutron energy range from 50 to 100 eV. The measurements of Weston and Todd, and calculation, correspond to a temperature of 300 K and a flight path of 19 m. The measurements of Blons and calculation, correspond to a sample temperature of 77 K and a flight path of 50 m. The data of Blons and corresponding calculation are displaced up by one decade, for clarity.

ORNL-DWG 86-11917

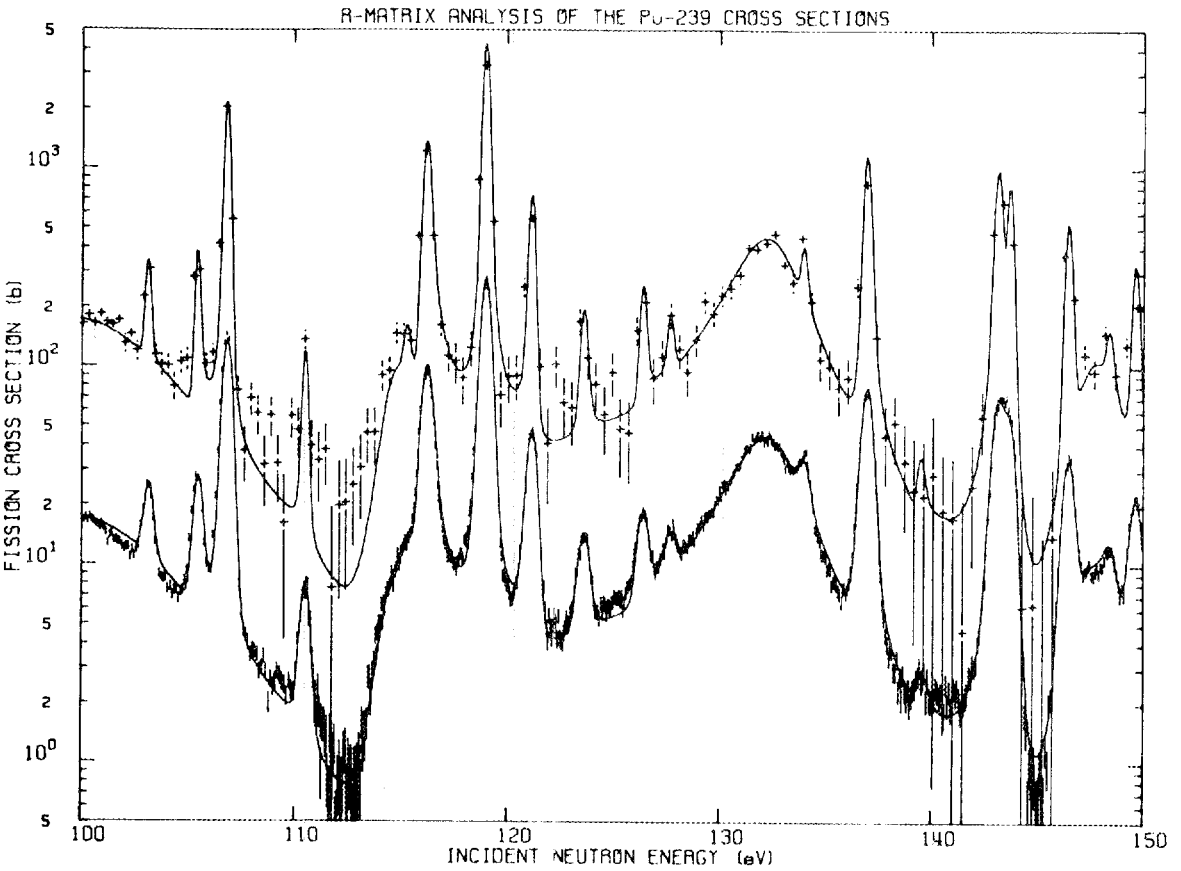

Fig. 8. Comparison of the fission cross sections computed with our resonance parameters (solid lines) with the data from the measurements of Weston and Todd (1984), error bars, and Blons (1973), error bars with cross, over the incident neutron energy range from 100 to 150 eV. The measurements of Weston and Todd, and calculation, correspond to a temperature of 300 K and a flight path of 19 m. The measurements of Blons and calculation, correspond to a sample temperature of 77 K and a flight path of 50 m. The data of Blons and corresponding calculation are displaced up by one decade, for clarity.

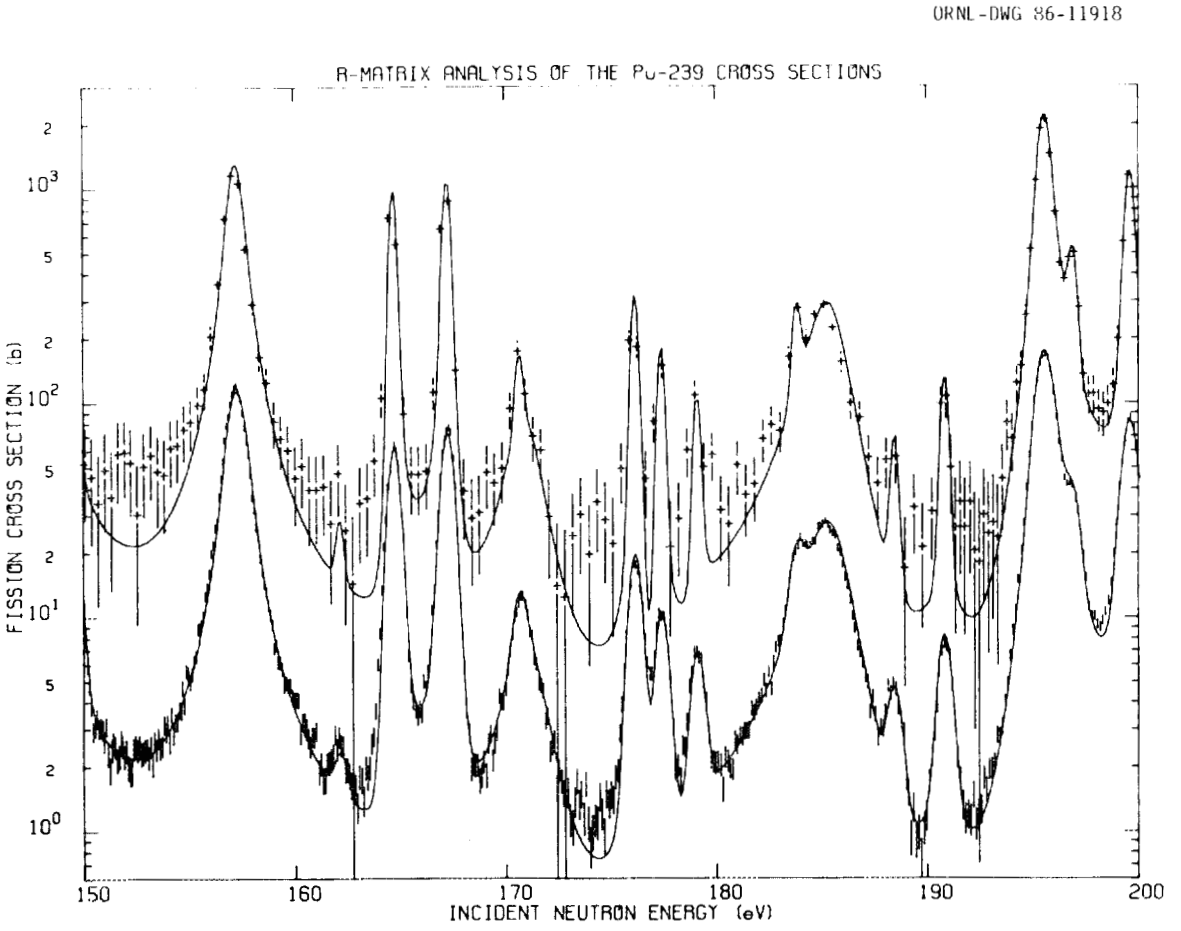

Fig. 9. Comparison of the fission cross sections computed with our resonance parameters (solid lines) with the data from the measurements of Weston and Todd (1984), error bars, and Blons (1973), error bars with cross, over the incident neutron energy range from 150 to 200 eV. The measurements of Weston and Todd, and calculation, correspond to a temperature of 300 K and a flight path of 19 m. The measurements of Blons and calculation, correspond to a sample temperature of 77 K and a flight path of 50 m. The data of Blons and corresponding calculation are displaced up by one decade, for clarity.

ORNL-DWG 86-11919

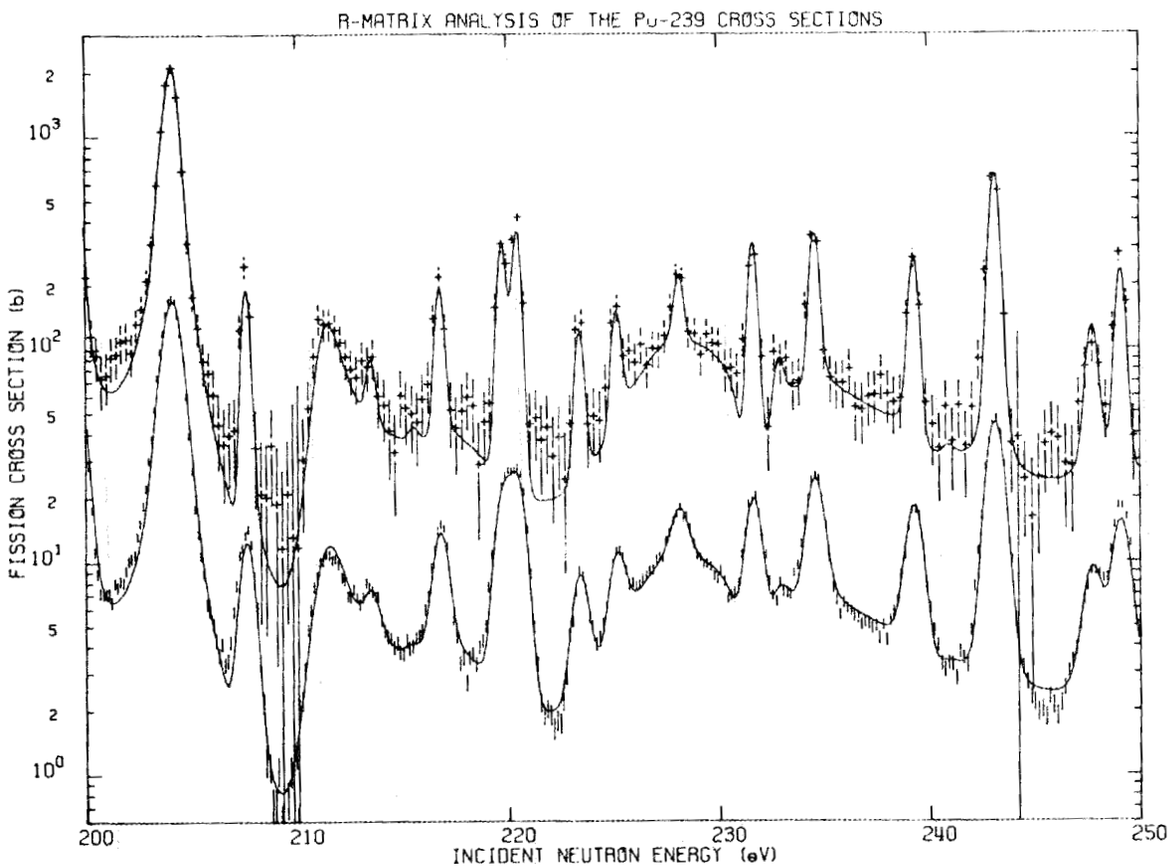

Fig. 10 Comparison of the fission cross sections computed with our resonance parameters (solid lines) with the data from the measurements of Weston and Todd (1984), error bars, and Blons (1973), error bars with cross, over the incident neutron energy range from 200 to 250 eV. The measurements of Weston and Todd, and calculation, correspond to a temperature of 300K and a flight path of 19 m. The measurements of Blons and calculation, correspond to a sample temperature of 77 K and a flight path of 50 m. The data of Blons and corresponding calculation are displaced up by one decade, for clarity.

ORNL-DWG 86-11920

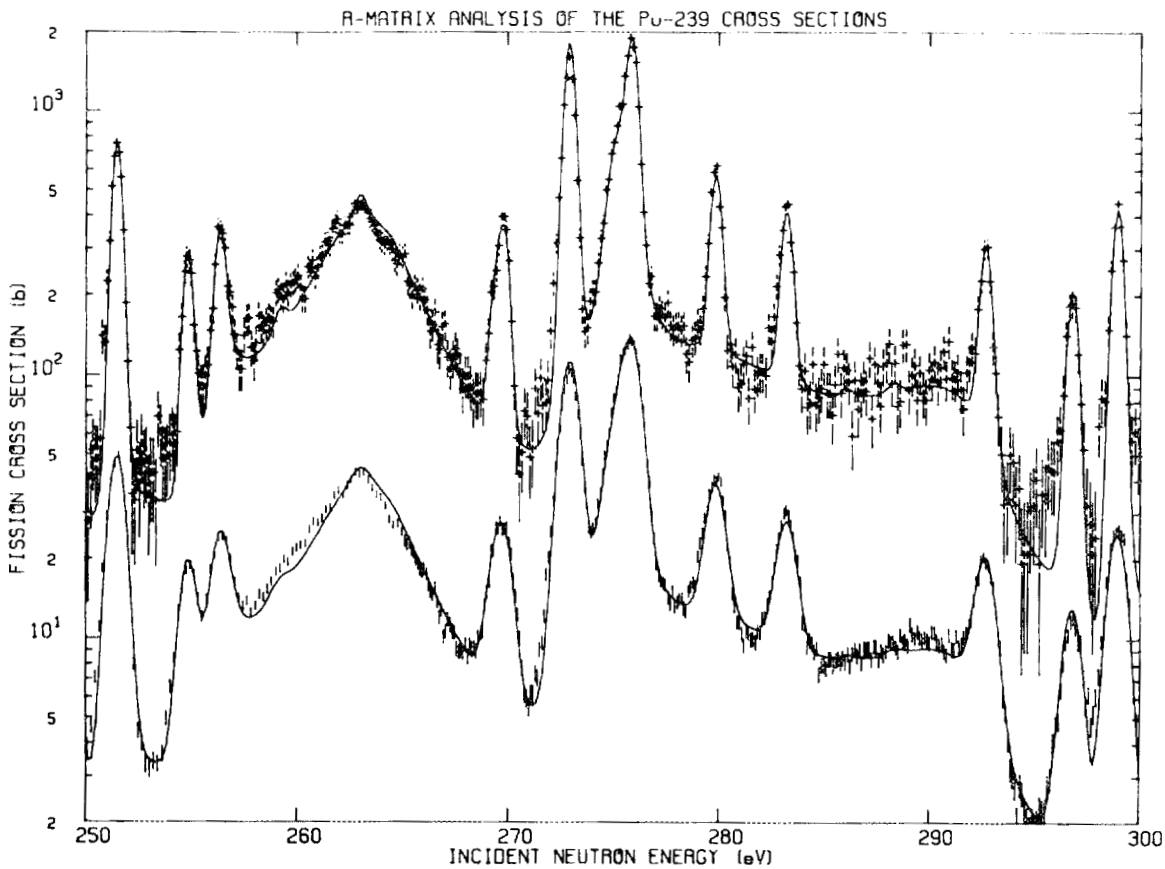

Fig. 11. Comparison of the fission cross sections computed with our resonance parameters (solid lines) with the data from the measurements of Weston and Todd (1984), error bars, and Blons (1973), error bars with cross, over the incident neutron energy range from 250 to 300 eV. The measurements of Weston and Todd, and calculation, correspond to a temperature of 300 K and a flight path of 19 m. The measurements of Blons and calculation, correspond to a sample temperature of 77 K and a flight path of 50 m. The data of Blons and corresponding calculation are displaced up by one decade, for clarity.

ORNL-DWG 86-11921

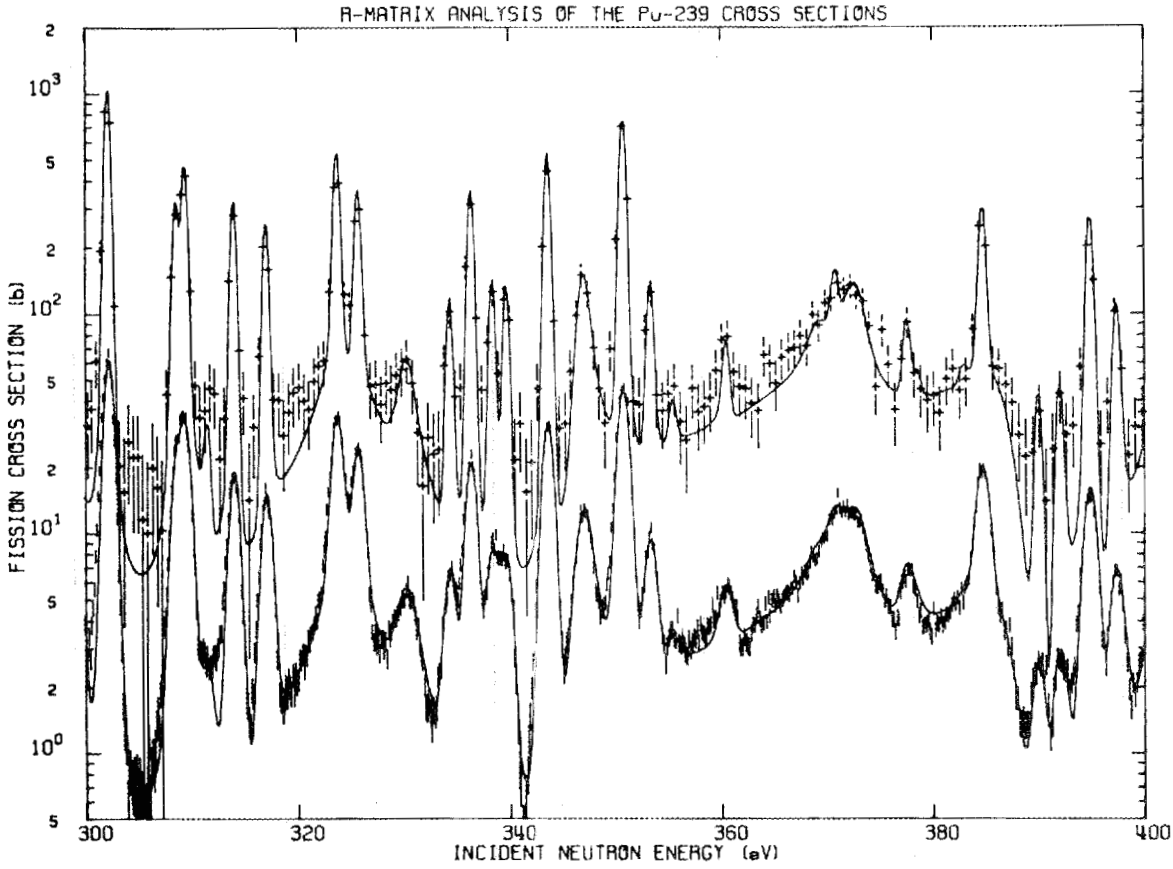

Fig. 12. Comparison of the fission cross sections computed with our resonance parameters (solid lines) with the data from the measurements of Weston and Todd (1984), error bars, and Blons (1973), error bars with cross, over the incident neutron energy range from 300 to 400 eV. The measurements of Weston and Todd, and calculation, correspond to a temperature of 300 K and a flight path of 19 m. The measurements of Blons and calculation, correspond to a sample temperature of 77 K and a flight path of 50 m. The data of Blons and corresponding calculation are displaced up by one decade, for clarity.

ORNL-DWG 86-11922

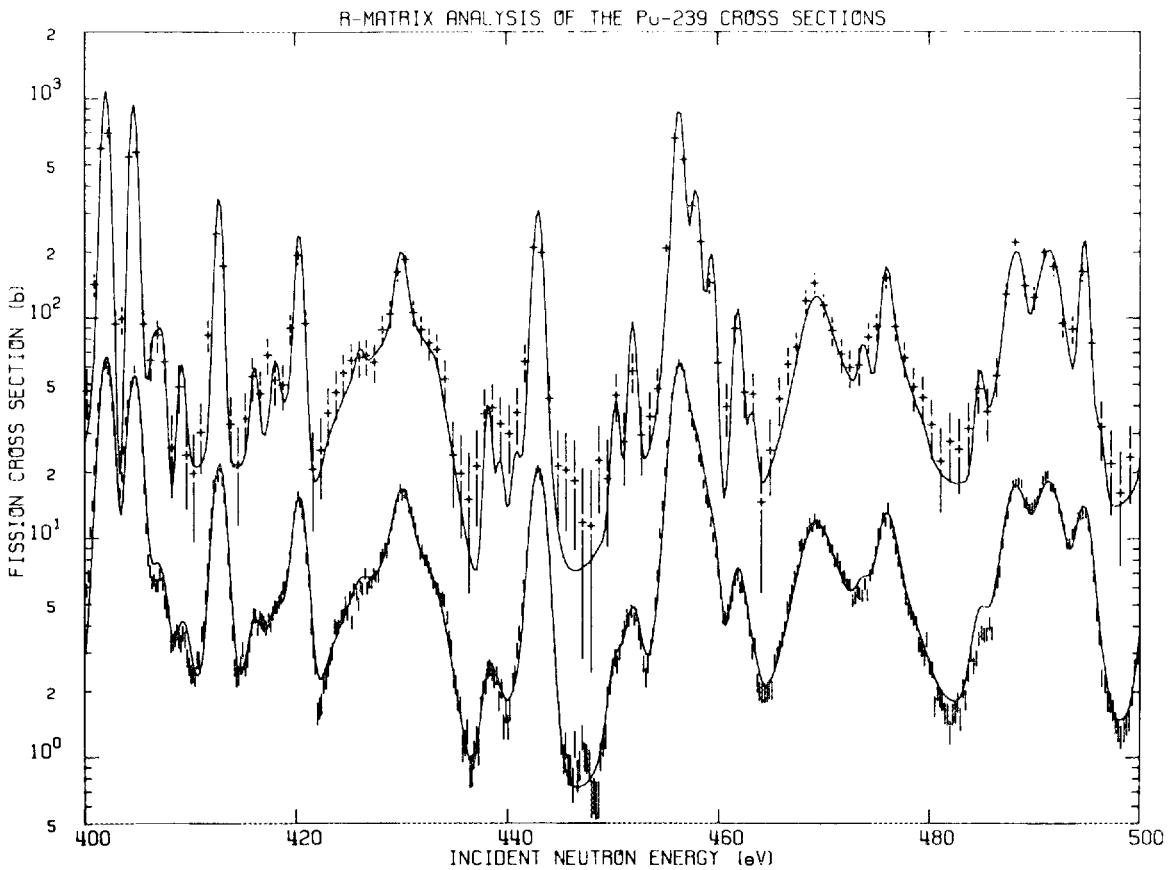

Fig. 13. Comparison of the fission cross sections computed with our resonance parameters (solid lines) with the data from the measurements of Weston and Todd (1984), error bars, and Blons (1973), error bars with cross, over the incident neutron energy range from 400 to 500 eV. The measurements of Weston and Todd, and calculation, correspond to a temperature of 300 K and a flight path of 19 m. The measurements of Blons and calculation, correspond to a sample temperature of 77 K and a flight path of 50 m. The data of Blons and corresponding calculation are displaced up by one decade, for clarity.

ORNL-DWG 86-11923

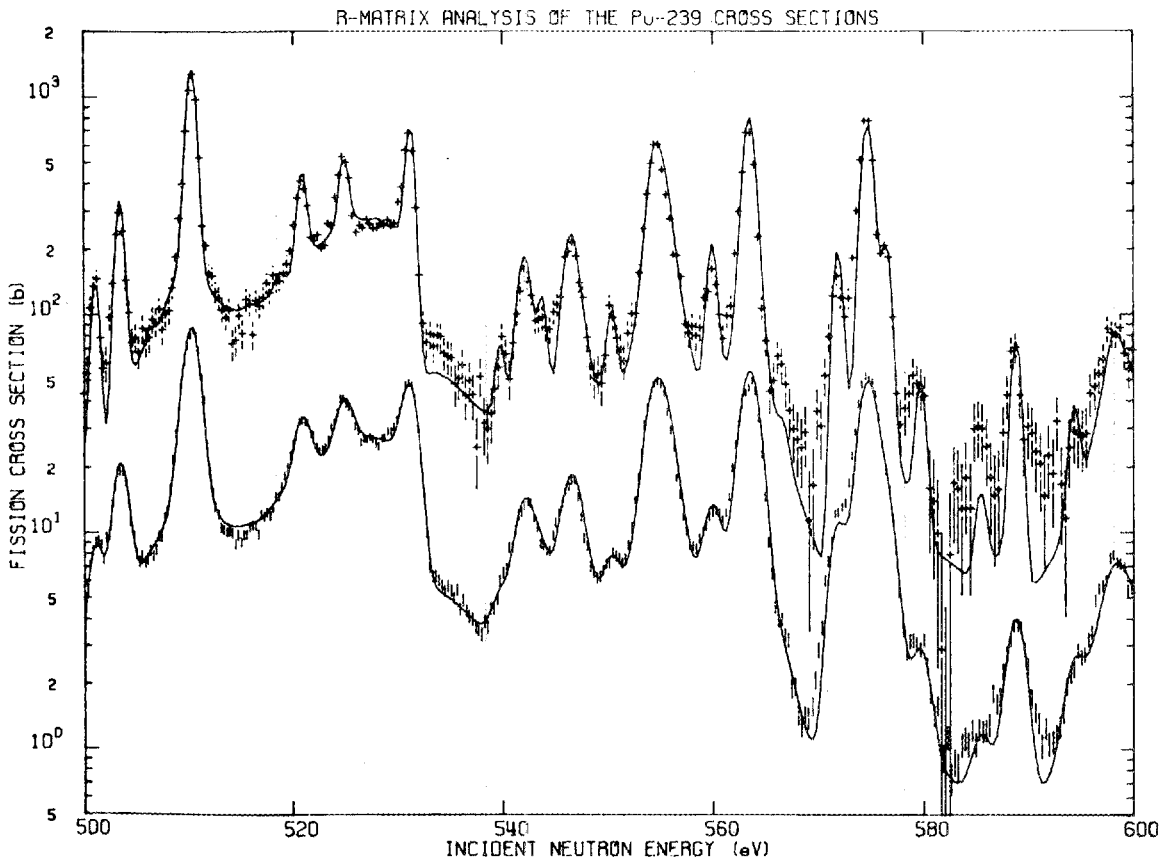

Fig. 14. Comparison of the fission cross sections computed with our resonance parameters (solid lines) with the data from the measurements of Weston and Todd (1984), error bars, and Blons (1973), error bars with cross, over the incident neutron energy range from 500 to 600 eV. The measurements of Weston and Todd, and calculation, correspond to a temperature of 300 K and a flight path of 19 m. The measurements of Blons and calculation, correspond to a sample temperature of 77 K and a flight path of 50 m. The data of Blons and corresponding calculation are displaced up by one decade, for clarity.

ORNL-DWG 86-11924

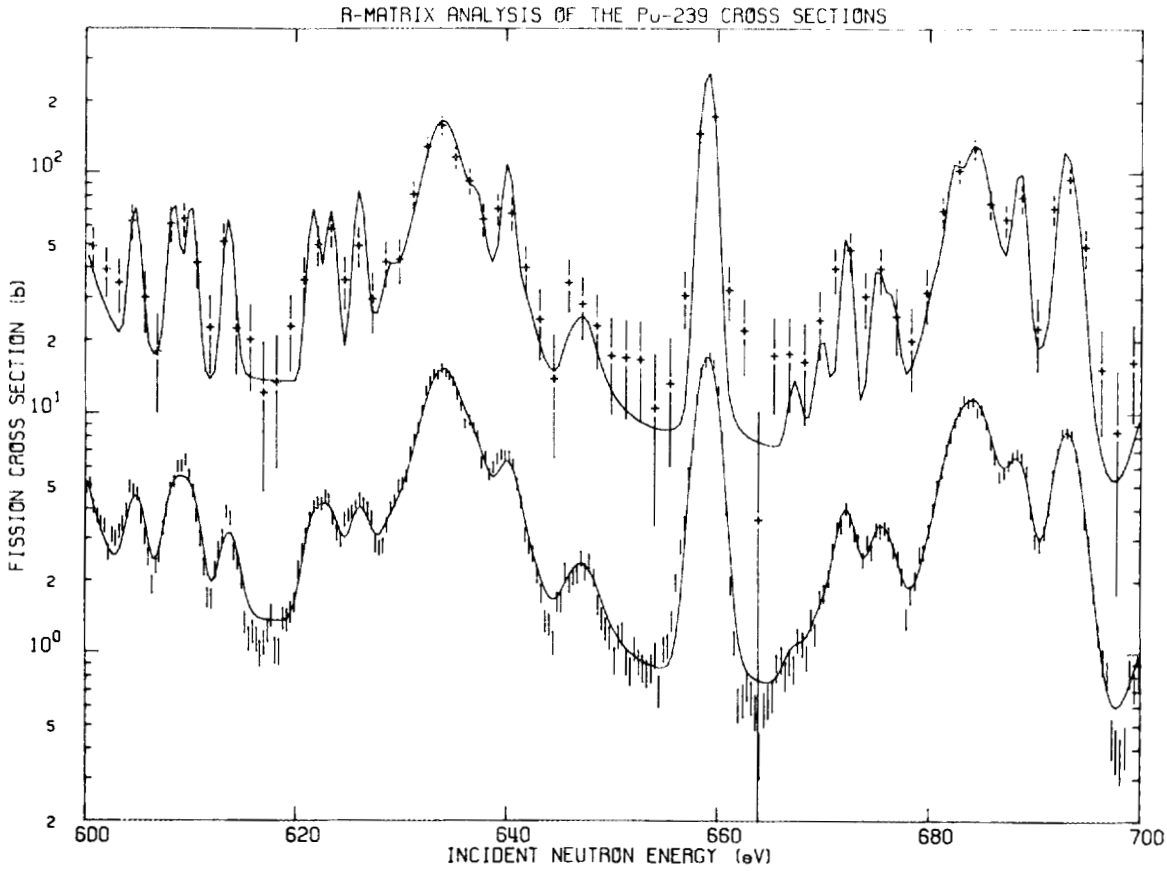

Fig. 15. Comparison of the fission cross sections computed with our resonance parameters (solid lines) with the data from the measurements of Weston and Todd (1984), error bars, and Blons (1973), error bars with cross, over the incident neutron energy range from 600 to 700 eV. The measurements of Weston and Todd, and calculation, correspond to a temperature of 300 K and a flight path of 19 m. The measurements of Blons and calculation, correspond to a sample temperature of 77 K and a flight path of 50 m. The data of Blons and corresponding calculation are displaced up by one decade, for clarity.

ORNL-DWG 86-11925

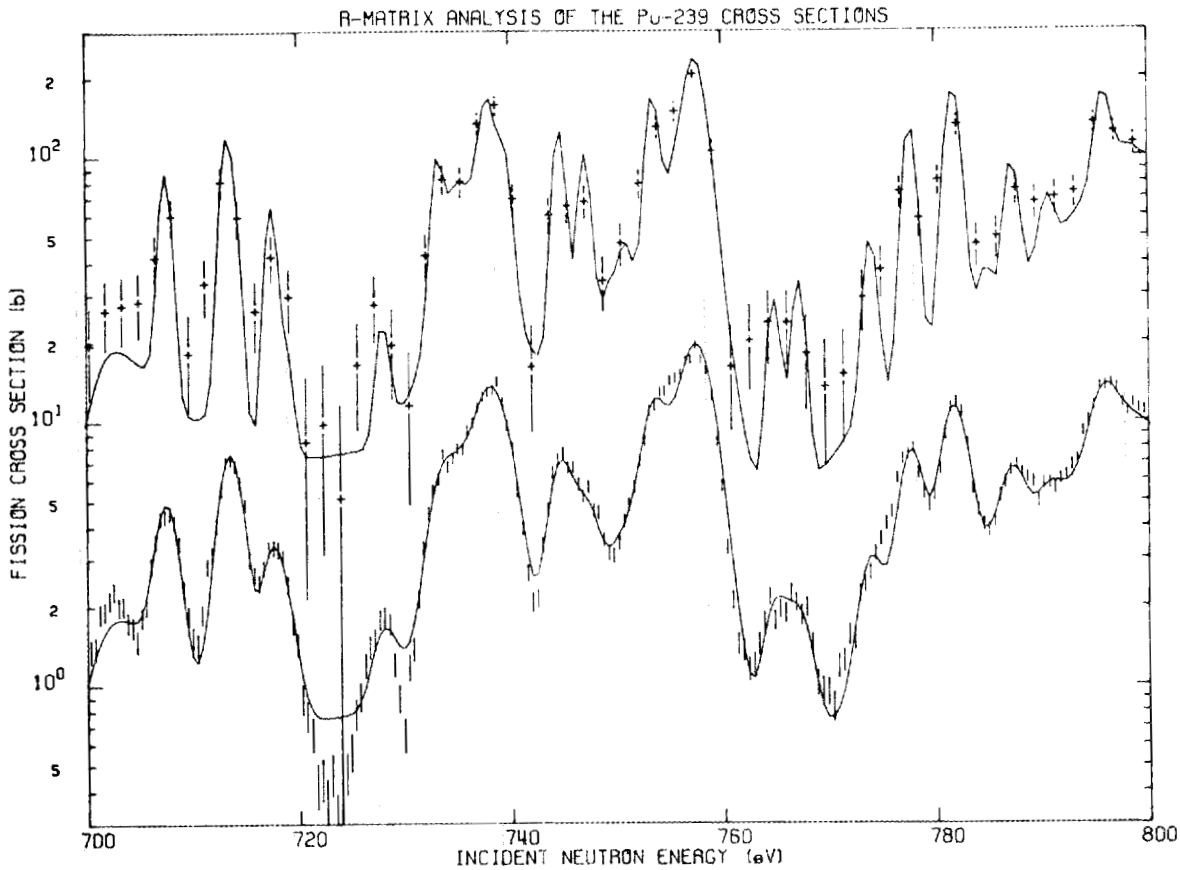

Fig. 16. Comparison of the fission cross sections computed with our resonance parameters (solid lines) with the data from the measurements of Weston and Todd (1984), error bars, and Blons (1973), error bars with cross, over the incident neutron energy range from 700 to 800 eV. The measurements of Weston and Todd, and calculation, correspond to a temperature of 300 K and a flight path of 19 m. The measurements of Blons and calculation, correspond to a sample temperature of 77 K and a flight path of 50 m. The data of Blons and corresponding calculation are displaced up by one decade, for clarity.

ORNL-DWG 86-11926

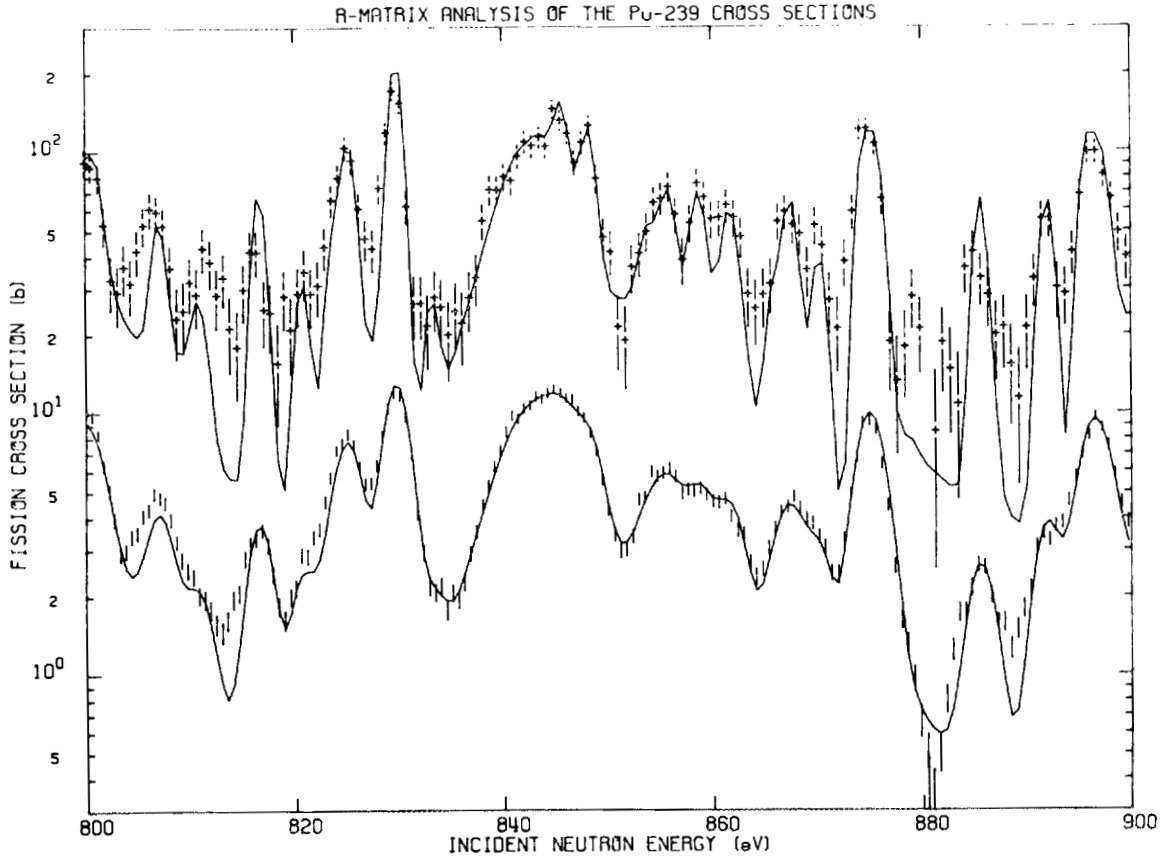

Fig. 17. Comparison of the fission cross sections computed with our resonance parameters (solid lines) with the data from the measurements of Weston and Todd (1984), error bars, and Blons (1973), error bars with cross, over the incident neutron energy range from 800 to 900 eV. The measurements of Weston and Todd, and calculation, correspond to a temperature of 300 K and a flight path of 19 m. The measurements of Blons and calculation, correspond to a sample temperature of 77 K and a flight path of 50 m. The data of Blons and corresponding calculation are displaced up by one decade, for clarity.

ORNL-DWG 86-11927

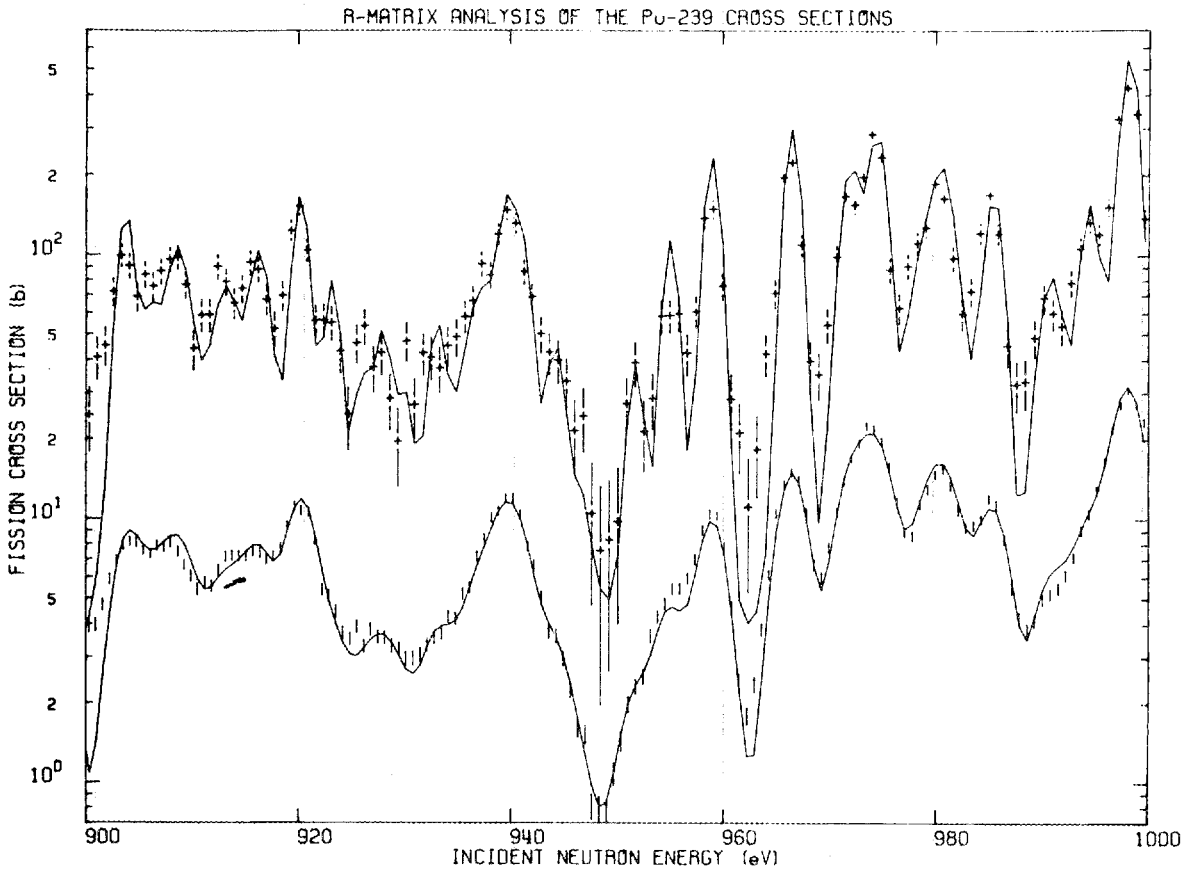

Fig. 18. Comparison of the fission cross sections computed with our resonance parameters (solid lines) with the data from the measurements of Weston and Todd (1984), error bars, and Blons (1973), error bars with cross, over the incident neutron energy range from 900 to 1000 eV. The measurements of Weston and Todd, and calculation, correspond to a temperature of 300 K and a flight path of 19 m. The measurements of Blons and calculation, correspond to a sample temperature of 77 K and a flight path of 50 m. The data of Blons and corresponding calculation are displaced up by one decade, for clarity.

ORNL-DWG 86-11928

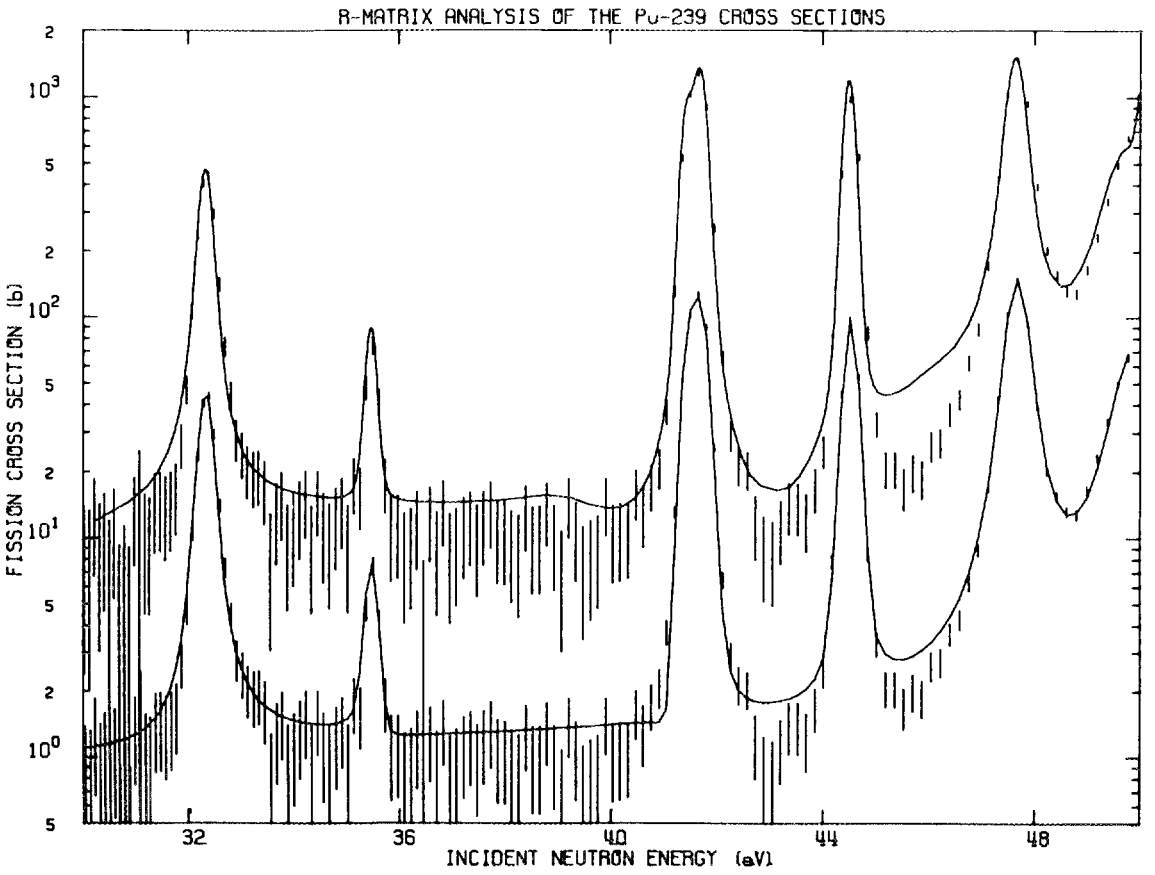

Fig. 19. Comparison of the fission cross sections computed with our resonance parameters, lower solid line, and with ENDF/B-V, upper solid line, with the data from Weston and Todd (1984), over the incident neutron energy range from 30 to 50 eV. The ENDF/B-V calculation and corresponding set of data were displaced up by one decade for clarity. Both calculations are Doppler broadened to 300 K the ENDF/B-V calculation is not resolution broadened.

ORNL-DWG 86-11929

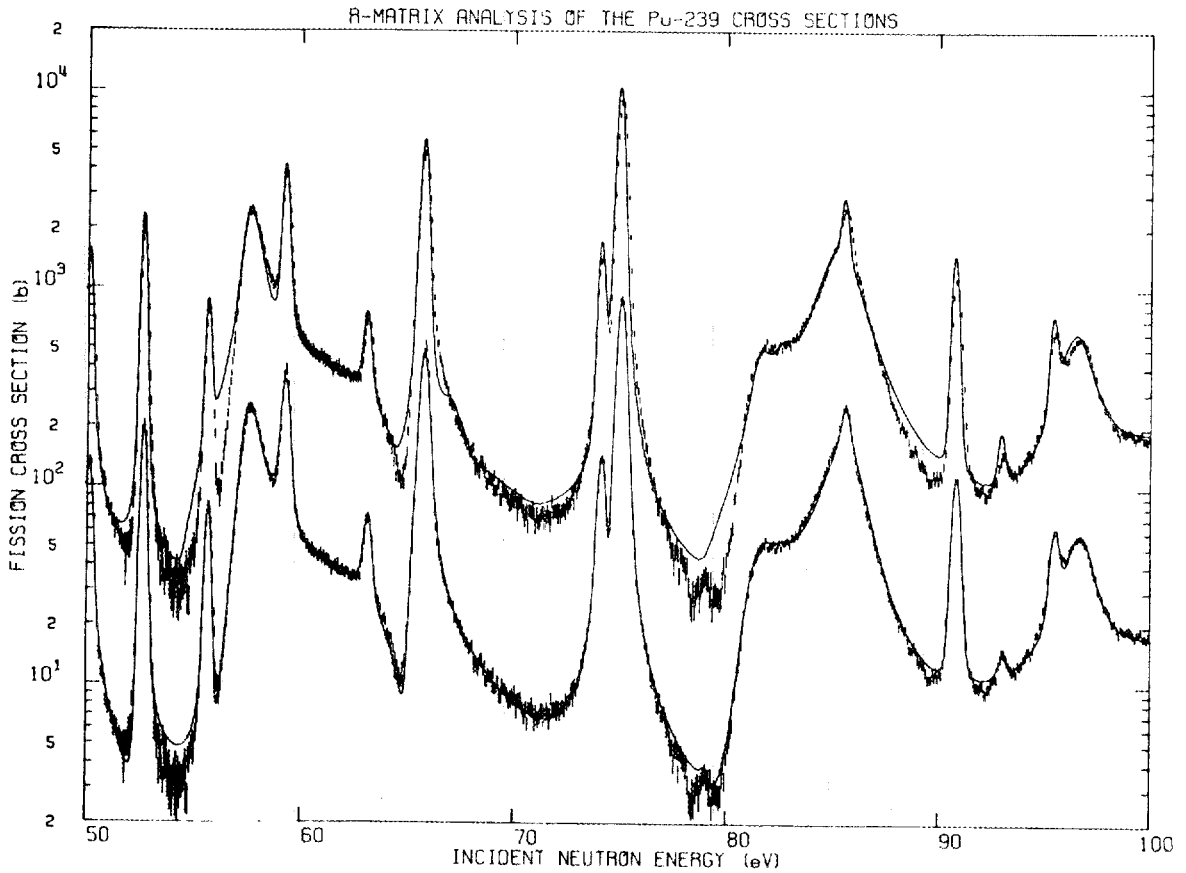

Fig. 20. Comparison of the fission cross sections computed with our resonance parameters, lower solid line, and with ENDF/B-V, upper solid line, with the data from Weston and Todd (1984), over the incident neutron energy range from 50 to 100 eV. The ENDF/B-V calculation and corresponding set of data were displaced up by one decade for clarity.

ORNL-DWG 86-11930

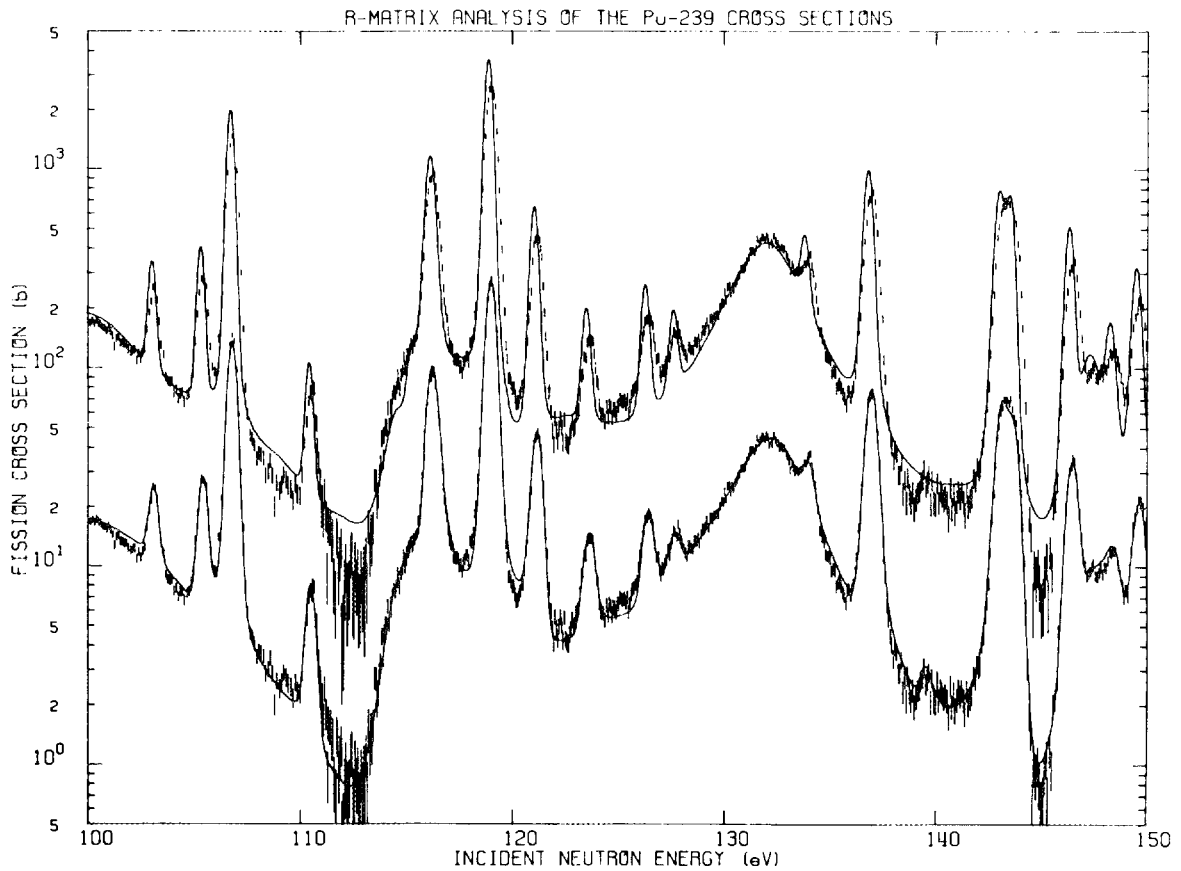

Fig. 21. Comparison of the fission cross sections computed with our resonance parameters, lower solid line, and with ENDF/B-V, upper solid line, with the data from Weston and Todd (1984), over the incident neutron energy range from 100 to 150 eV. The ENDF/B-V calculation and corresponding set of data were displaced up by one decade for clarity.

ORNL-DWG 86-11931

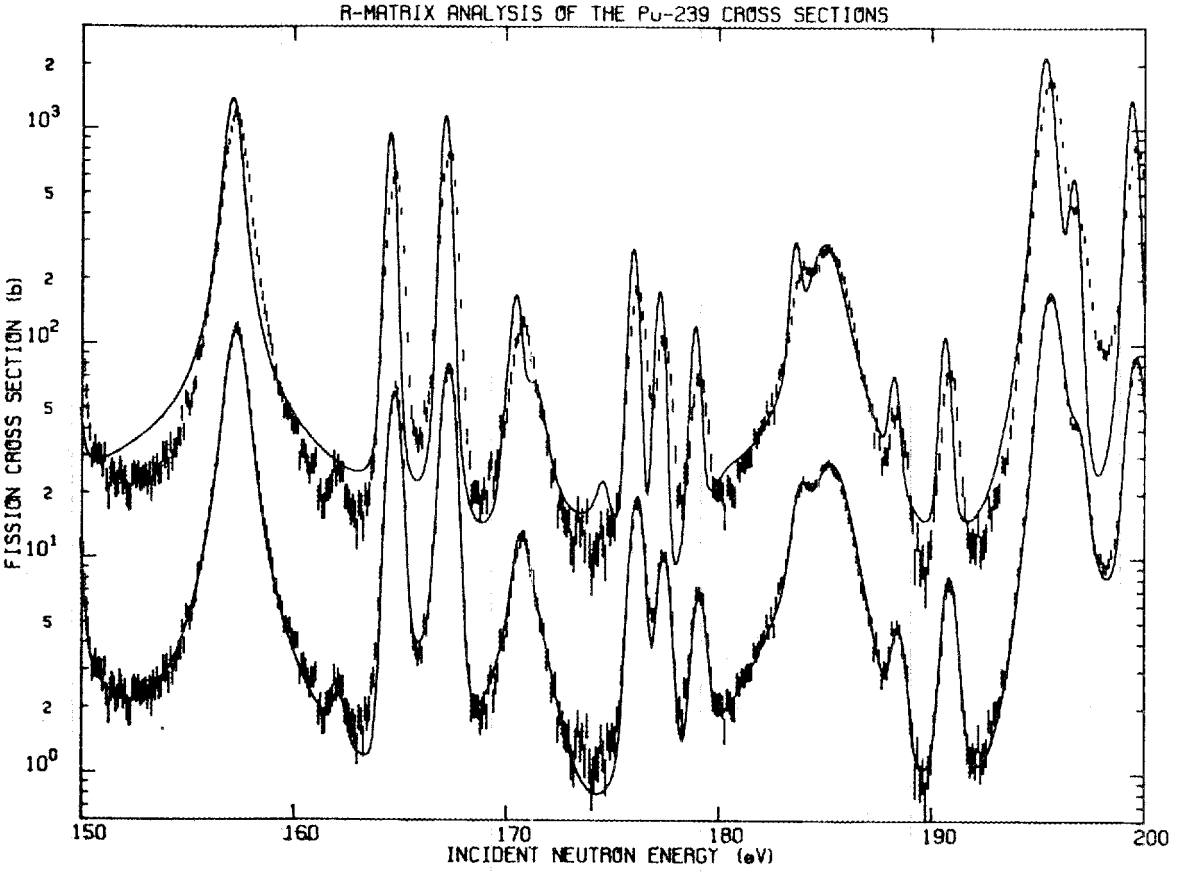

Fig. 22. Comparison of the fission cross sections computed with our resonance parameters, lower solid line, and with ENDF/B-V, upper solid line, with the data from Weston and Todd (1984), over the incident neutron energy range from 150 to 200 eV. The ENDF/B-V calculation and corresponding set of data were displaced up by one decade for clarity.

ORNL-DWG 86-11932

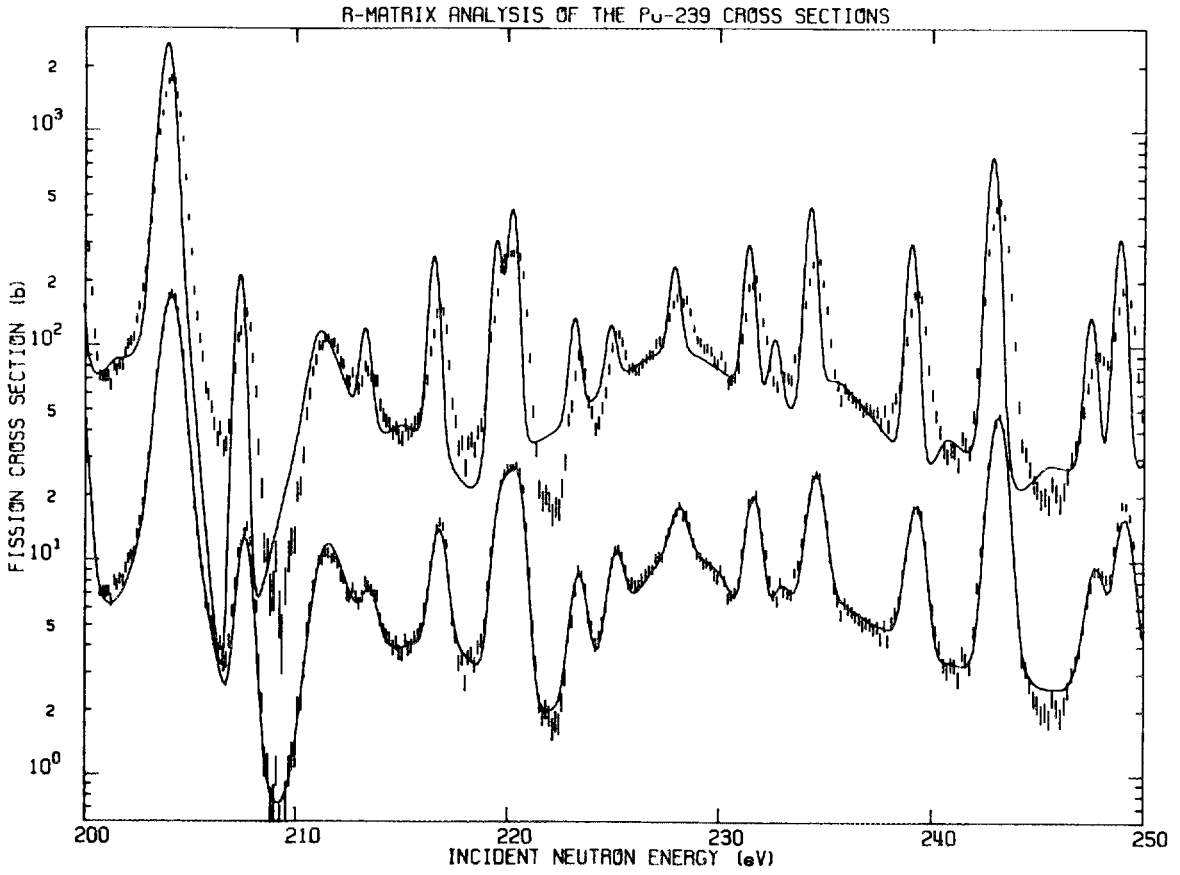

Fig. 23. Comparison of the fission cross sections computed with our resonance parameters, lower solid line, and with ENDF/B-V, upper solid line, with the data from Weston and Todd (1984), over the incident neutron energy range from 200 to 250 eV. The ENDF/B-V calculation and corresponding set of data were displaced up by one decade for clarity.

ORNL-DWG 86-11933

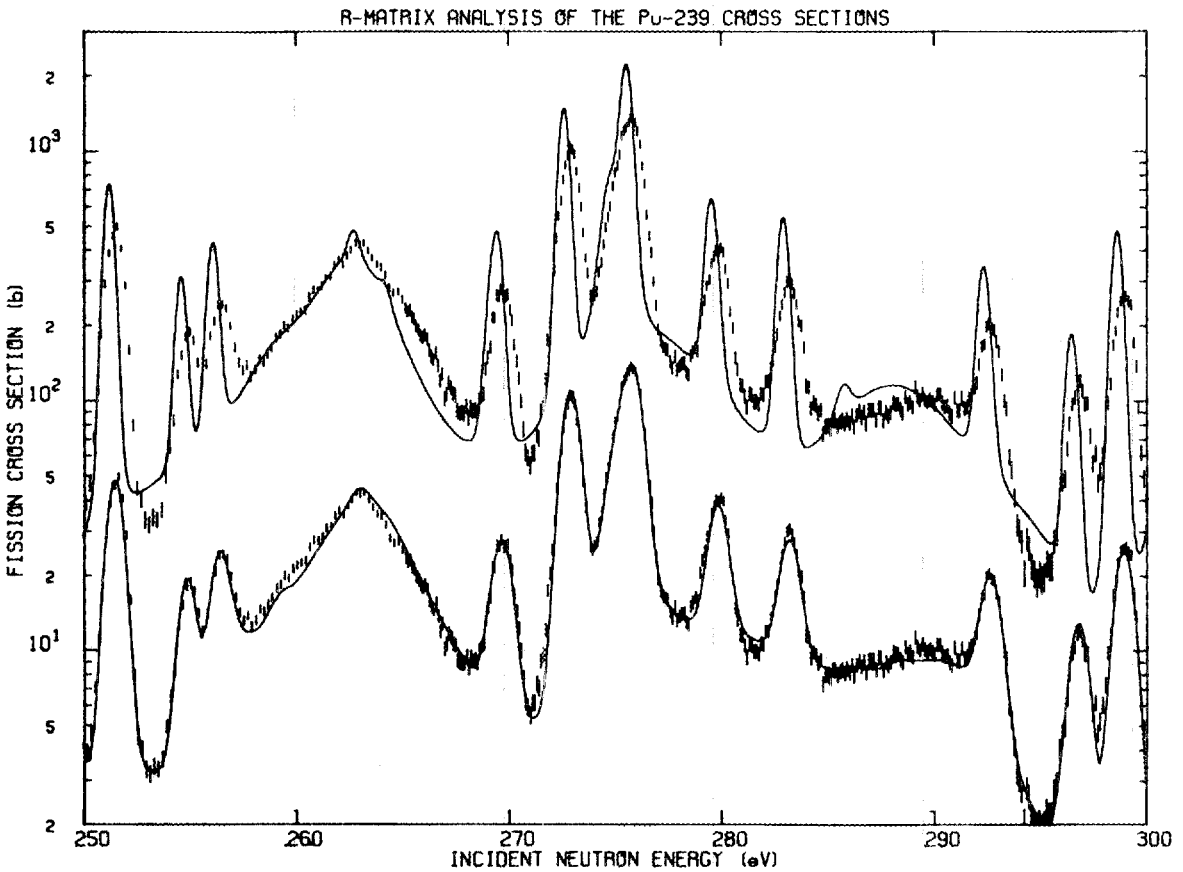

Fig. 24. Comparison of the fission cross sections computed with our resonance parameters, lower solid line, and with ENDF/B-V, upper solid line, with the data from Weston and Todd (1984), over the incident neutron energy range from 250 to 300 eV. The ENDF/B-V calculation and corresponding set of data were displaced up by one decade for clarity.

ORNL-DWG 86-11934

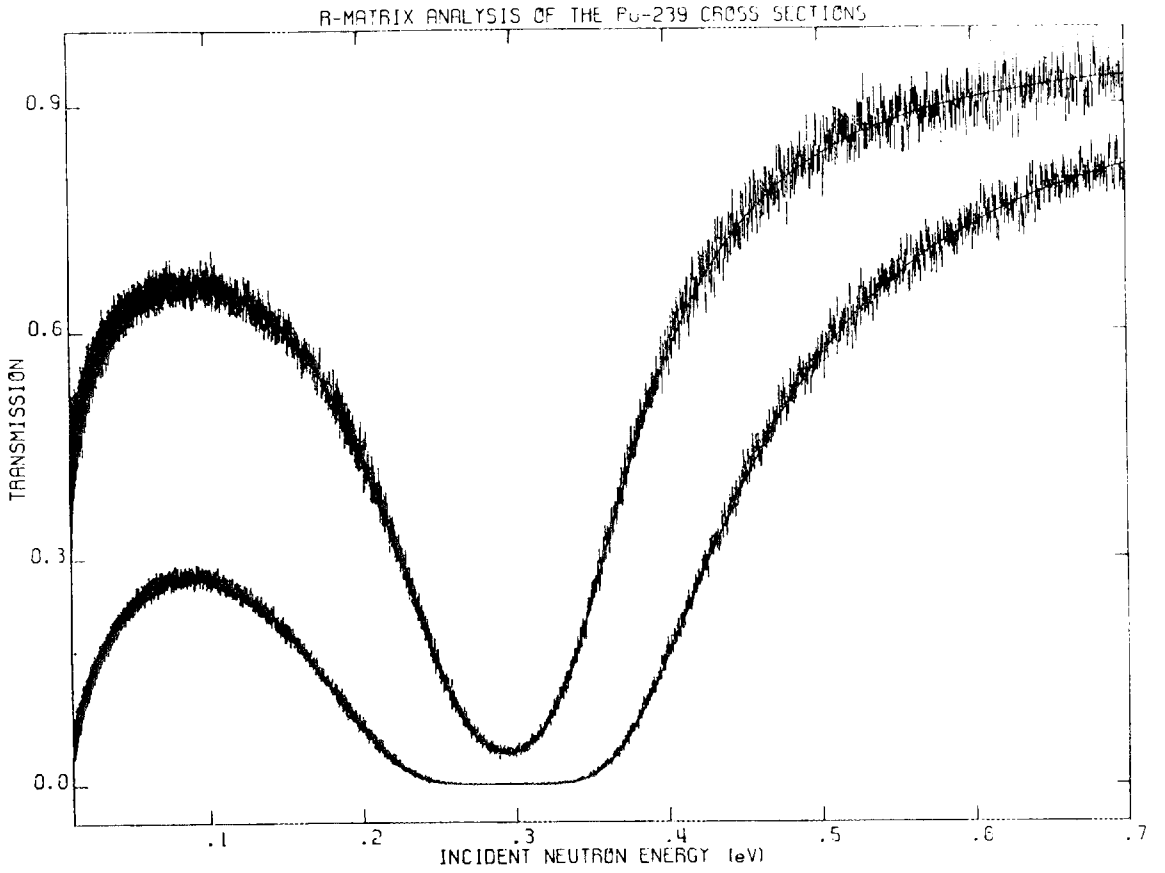

Fig. 25. Comparison of transmission ratios as computed with our resonance parameters, solid line, and as measured by Spencer *et al.* (1984), for thicknesses of 0.00180 and 0.00058 at/b, respectively, over the incident neutron energy region from 0.01 to 0.7 eV.

ORNL-DWG 86-11935

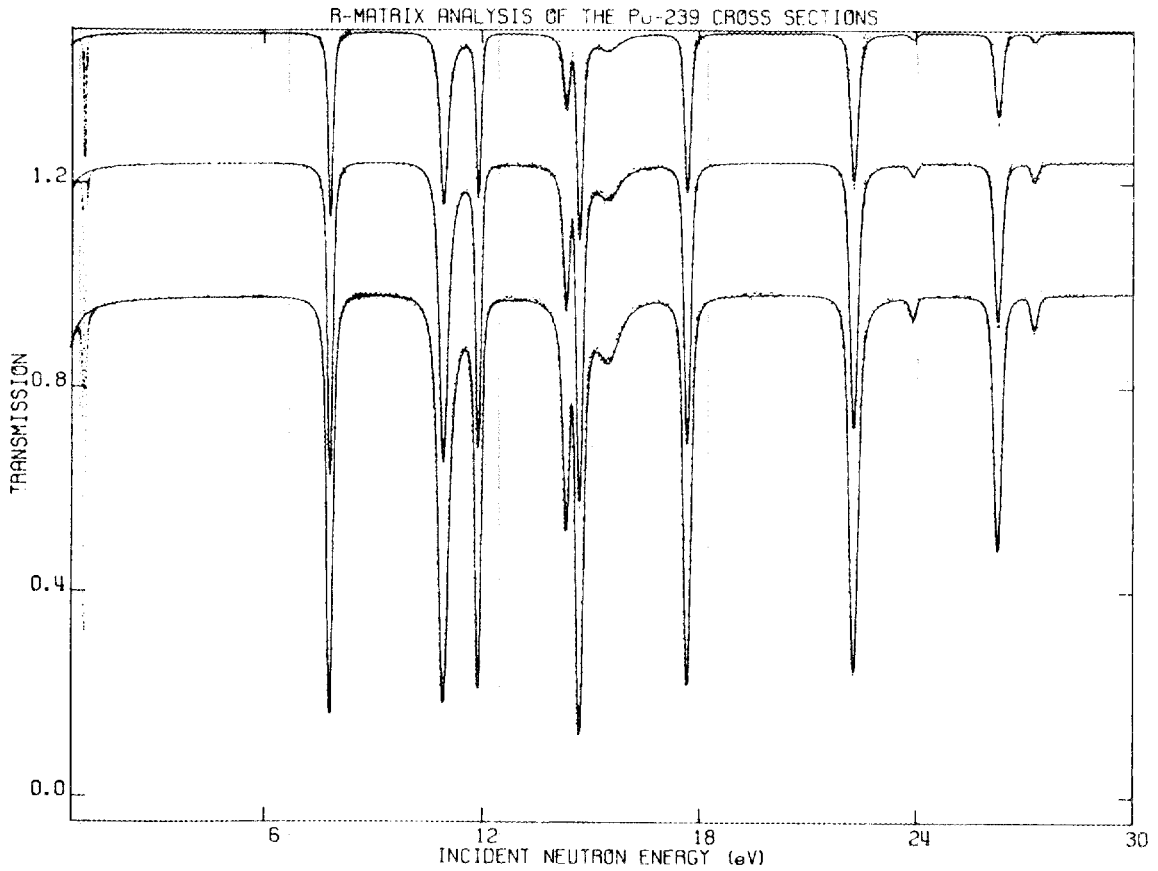

Fig. 26. Comparison of transmission ratios as computed with our resonance parameters, solid lines, and as measured by Spencer *et al.* (1984), for thicknesses of 0.001167, 0.000616, and 0.000291 atom/b, over the incident neutron energy region from 0.7 to 30 eV. The transmission ratios for the two thinner samples have been displaced up by 0.25 and 0.5, respectively for clarity of display. The resonance at 1.056 eV seen in the data but not in the calculation is due to a ^{240}Pu isotopic impurity.

ORNL-DWG 86-11936

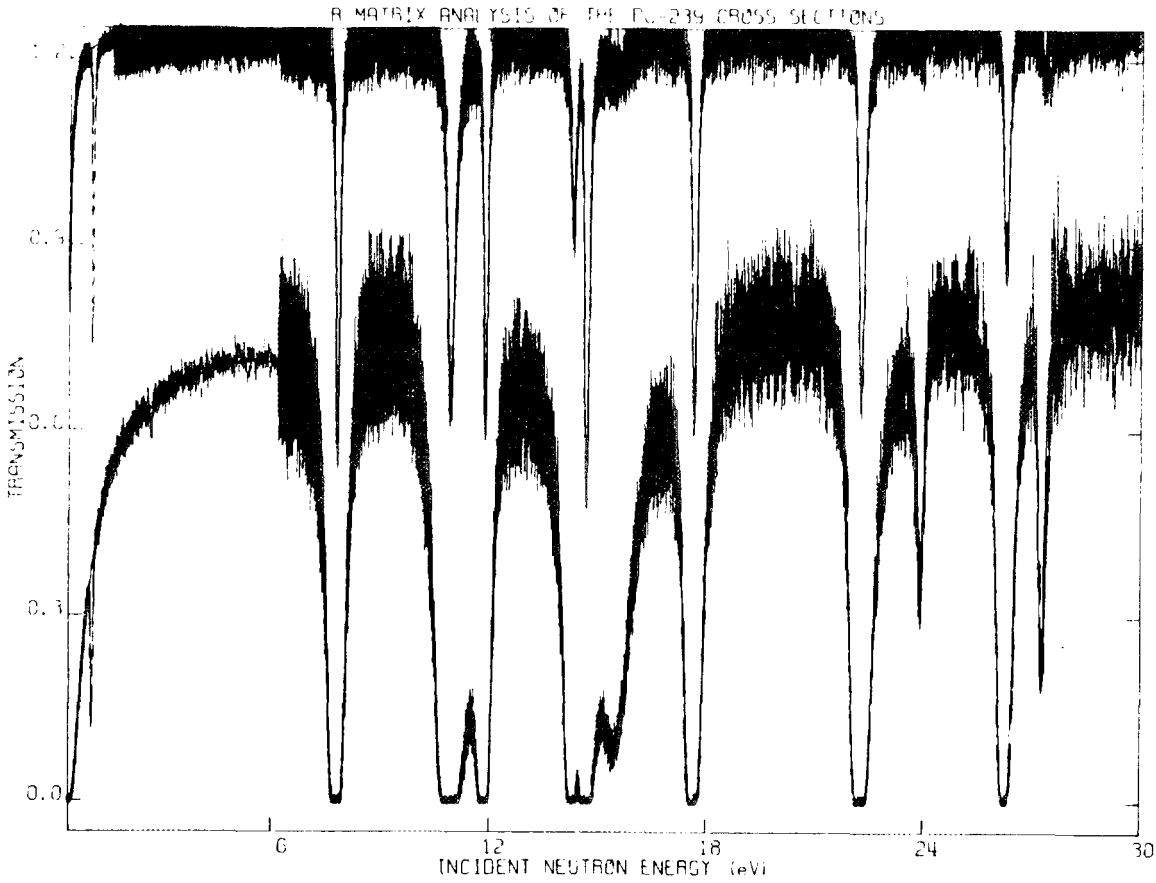

Fig. 27. Comparison of transmission ratios as computed with our resonance parameters, solid lines, and as measured by Harvey *et al.* (1984), on an 18 m flight path, with samples at liquid nitrogen temperature of 0.01802 and 0.00058 atom/b, over the incident neutron energy range from 0.7 to 30 eV. The transmission ratios for the thinner sample have been displaced up by 0.25 for clarity of display. Small resonances near 1.056 and 2.676 eV are due to ^{240}Pu and ^{242}Pu isotopic impurities.

ORNL-DWG 86-11937

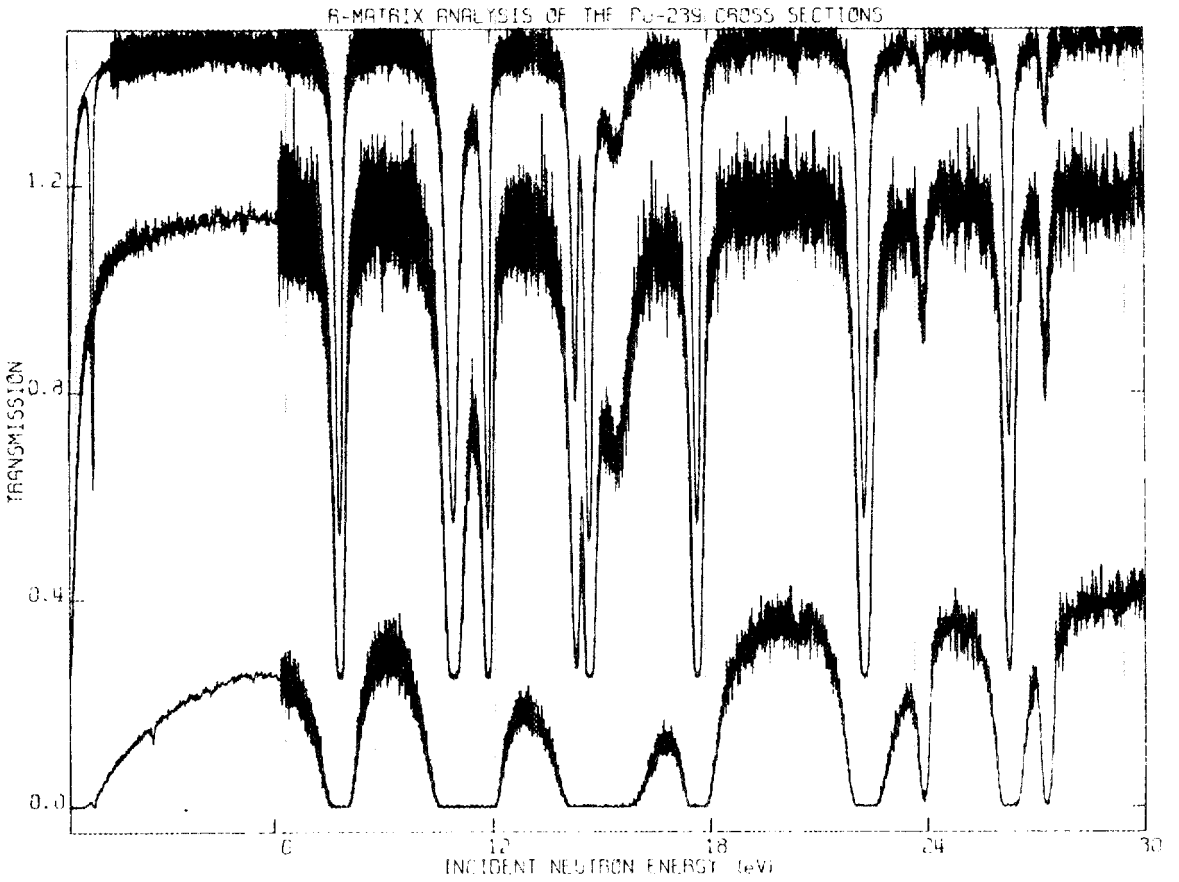

Fig. 28. Comparison of transmission ratios as computed with our resonance parameters, solid lines, and as measured by Harvey *et al.* (1984) on an 18 m flight path, with samples at liquid nitrogen temperature, of 0.07375, 0.00638, and 0.001815 atom/b, over the incident neutron energy range from 0.7 to 30 eV. The transmission ratio for the two thinner samples have been displaced up by 0.25 and 0.5, respectively, for clarity of display. Small resonances near 1.056 and 2.676 eV are due to ^{240}Pu and ^{242}Pu isotopic impurities.

ORNL-DWG 86-11938

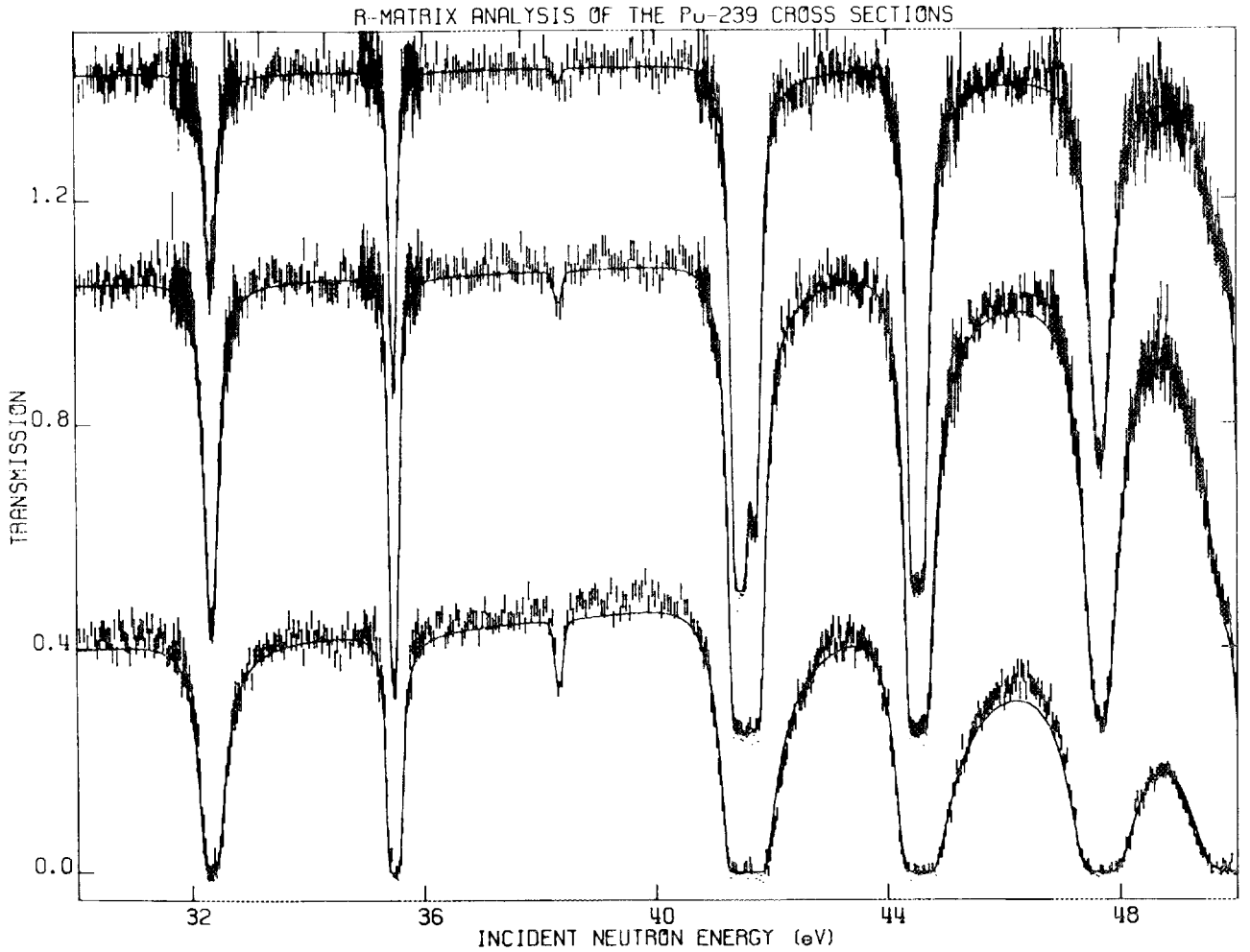

Fig. 29. Comparison of transmission ratios as computed with our resonance parameters, solid lines, and as measured by Harvey *et al.* (1984) on an 80 m flight path, with samples at liquid nitrogen temperature, of 0.0737, 0.0180, and 0.0064 atom/b, over the incident neutron energy range from 30 to 50 eV. The transmission ratio for the 0.0180 at/b was displaced up by 0.25, that of the 0.0064 at/b sample was displaced up by 0.5 for clarity of display. The small level at 38.82 eV is due to a ^{240}Pu impurity and has been included in the calculation.

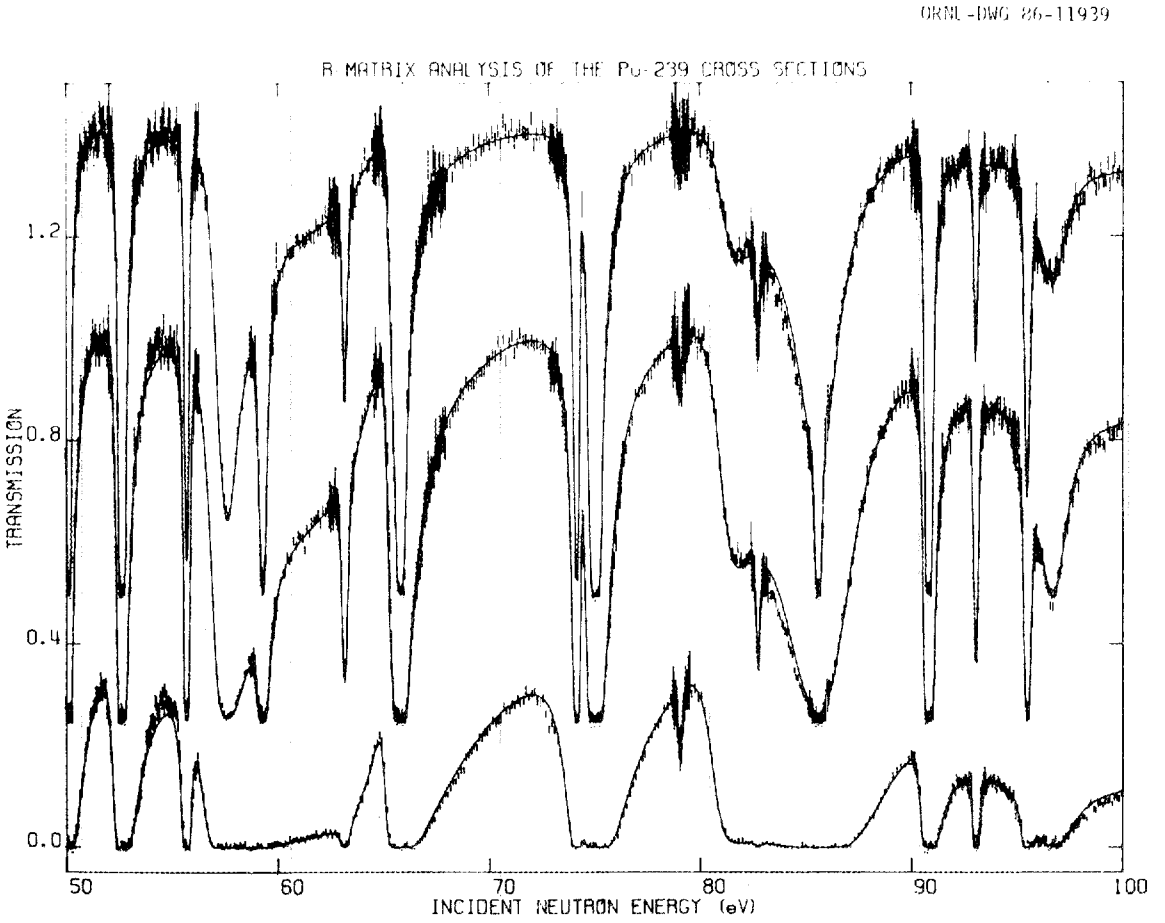

Fig. 30. Comparison of transmission ratios as computed with our resonance parameters, solid lines, and as measured by Harvey *et al.* (1984) on an 80 m flight path, with samples at liquid nitrogen temperature, of 0.0737, 0.0180, and 0.0064 atom/b, over the incident neutron energy range from 50 to 100 eV. The transmission ratio for the 0.0180 atom/b was displaced up by 0.25, that of the 0.0064 atom/b sample was displaced up by 0.5 for clarity of display.

ORNL-DWG 86-11940

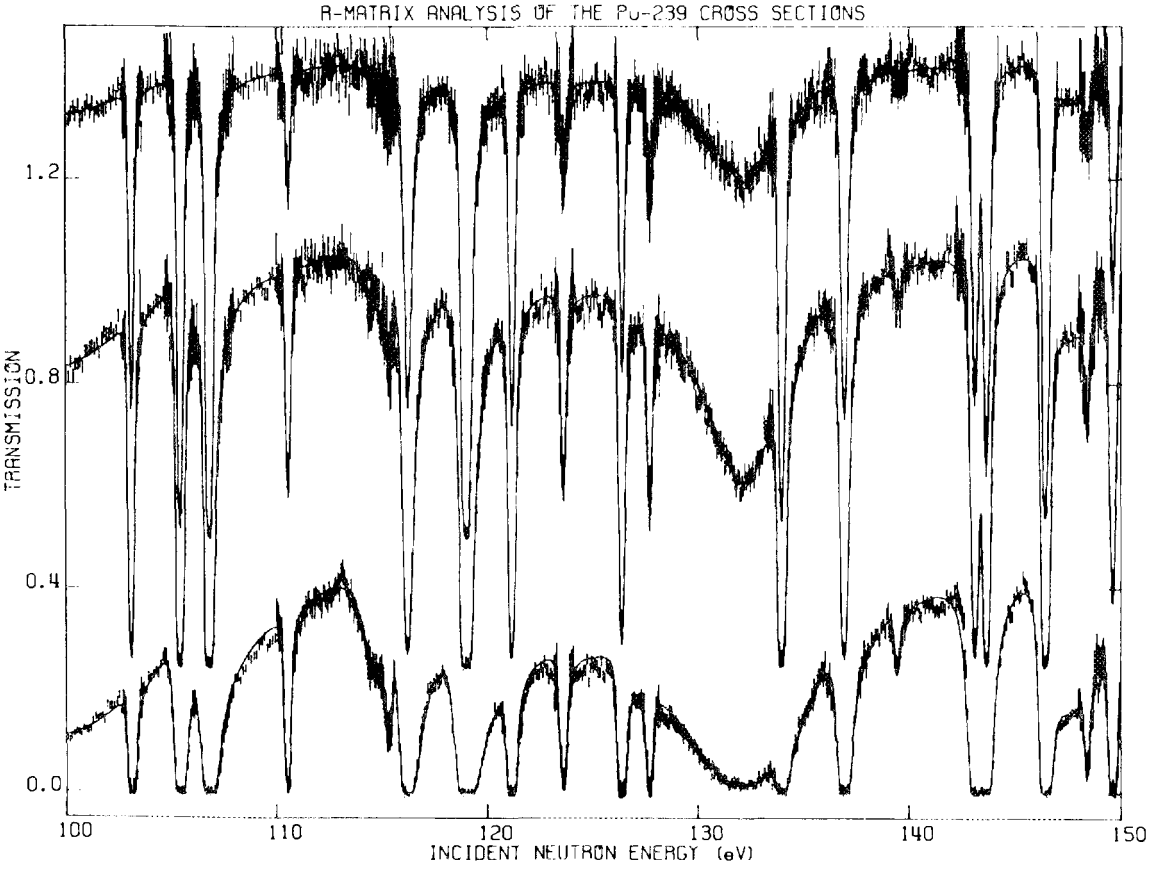

Fig. 31. Comparison of transmission ratios as computed with our resonance parameters, solid lines, and as measured by Harvey *et al.* (1984) on an 80 m flight path, with samples at liquid nitrogen temperature, of 0.0737, 0.0180, and 0.0064 atom/b, over the incident neutron energy range from 100 to 150 eV. The transmission ratio for the 0.0180 atom/b was displaced up by 0.25, that of the 0.0064 atom/b sample was displaced up by 0.5 for clarity of display.

ORNL-DWG 86-11941

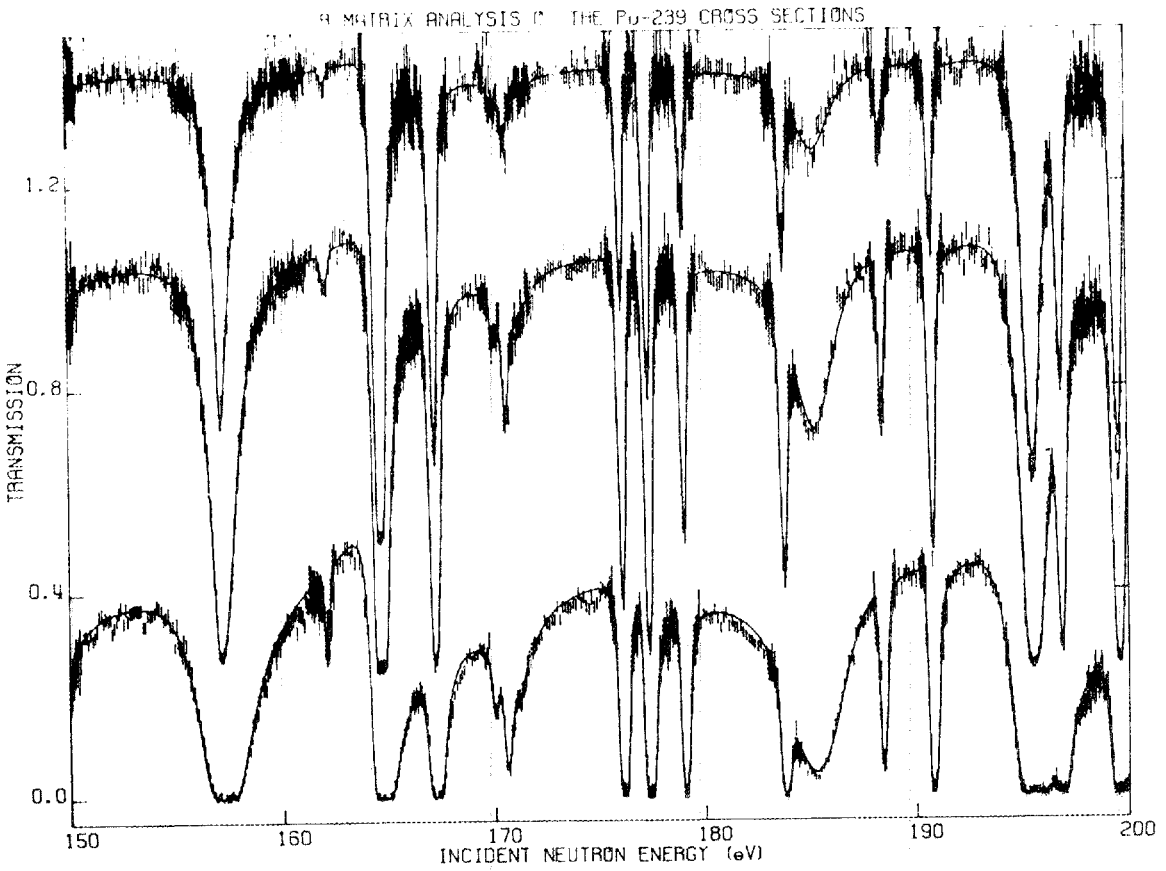

Fig. 32. Comparison of transmission ratios as computed with our resonance parameters, solid lines, and as measured by Harvey *et al.* (1984) on an 80 m flight path, with samples at liquid nitrogen temperature, of 0.0737, 0.0180, and 0.0064 atom/b, over the incident neutron energy range from 150 to 200 eV. The transmission ratio for the 0.0180 atom/b was displaced up by 0.25, that of the 0.0064 atom/b sample was displaced up by 0.5 for clarity of display.

ORNL-DWG 86-11942

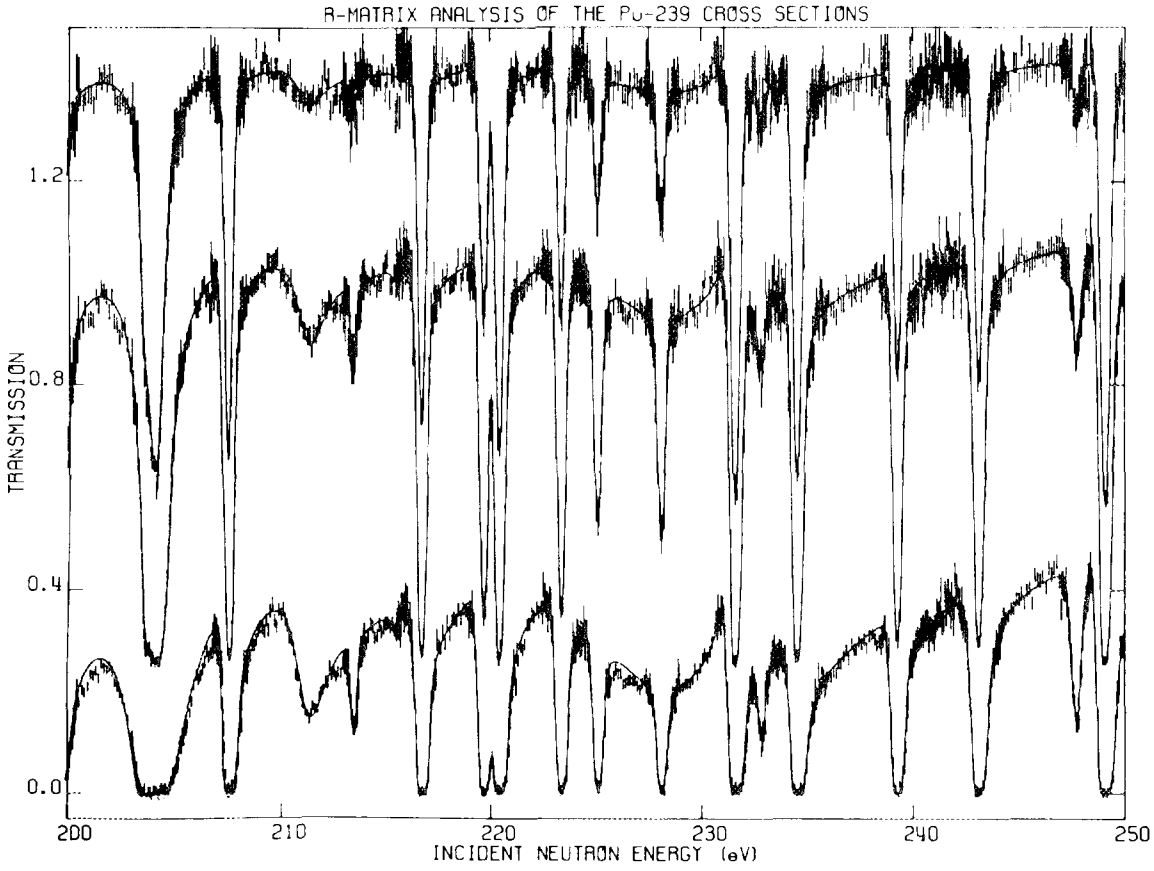

Fig. 33. Comparison of transmission ratios as computed with our resonance parameters, solid lines, and as measured by Harvey *et al.* (1984) on an 80 m flight path, with samples at liquid nitrogen temperature, of 0.0737, 0.0180, and 0.0064 atom/b, over the incident neutron energy range from 200 to 250 eV. The transmission ratio for the 0.0180 atom/b was displaced up by 0.25, that of the 0.0064 atom/b sample was displaced up by 0.5 for clarity of display.

ORNL-DWG 86-11943

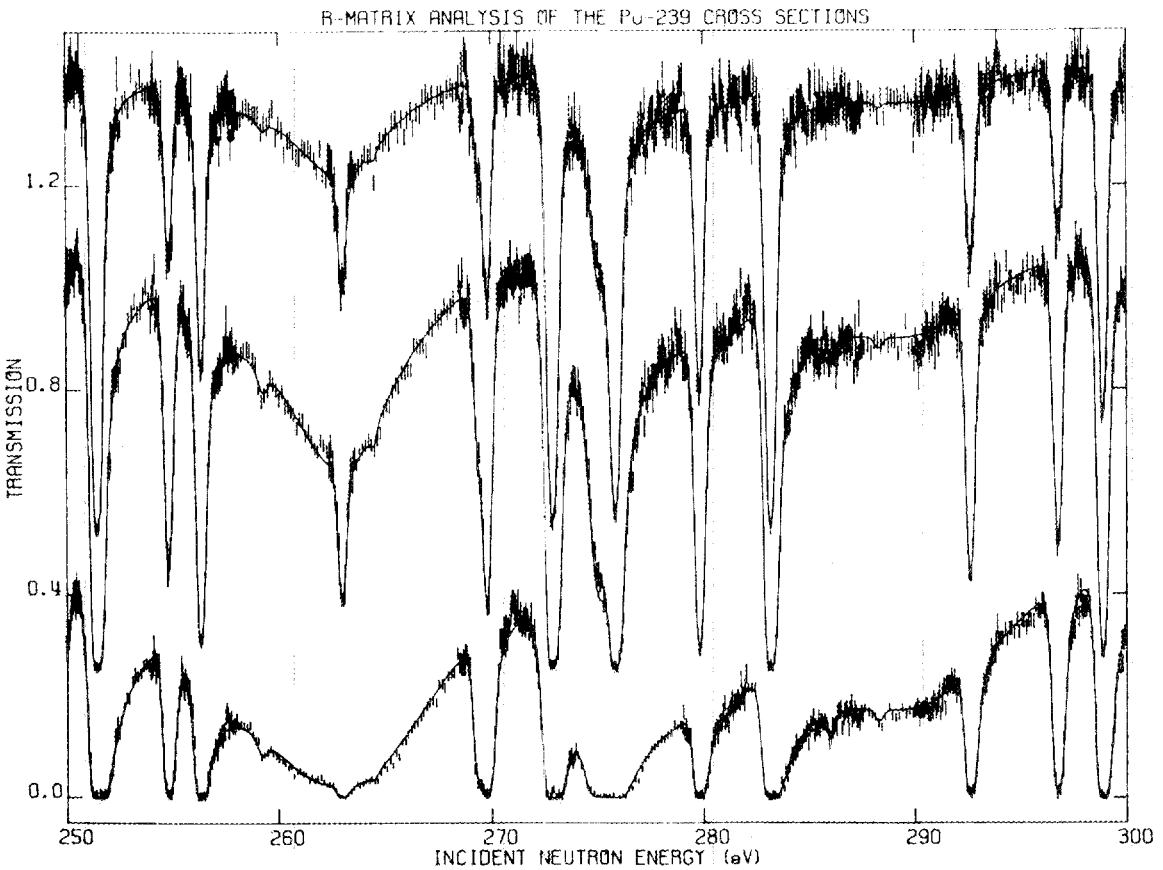

Fig. 34. Comparison of transmission ratios as computed with our resonance parameters, solid lines, and as measured by Harvey *et al.* (1984) on an 80 m flight path, with samples at liquid nitrogen temperature, of 0.0737, 0.0180, and 0.0064 atom/b, over the incident neutron energy range from 250 to 300 eV. The transmission ratio for the 0.0180 atom/b was displaced up by 0.25, that of the 0.0064 atom/b sample was displaced up by 0.5 for clarity of display.

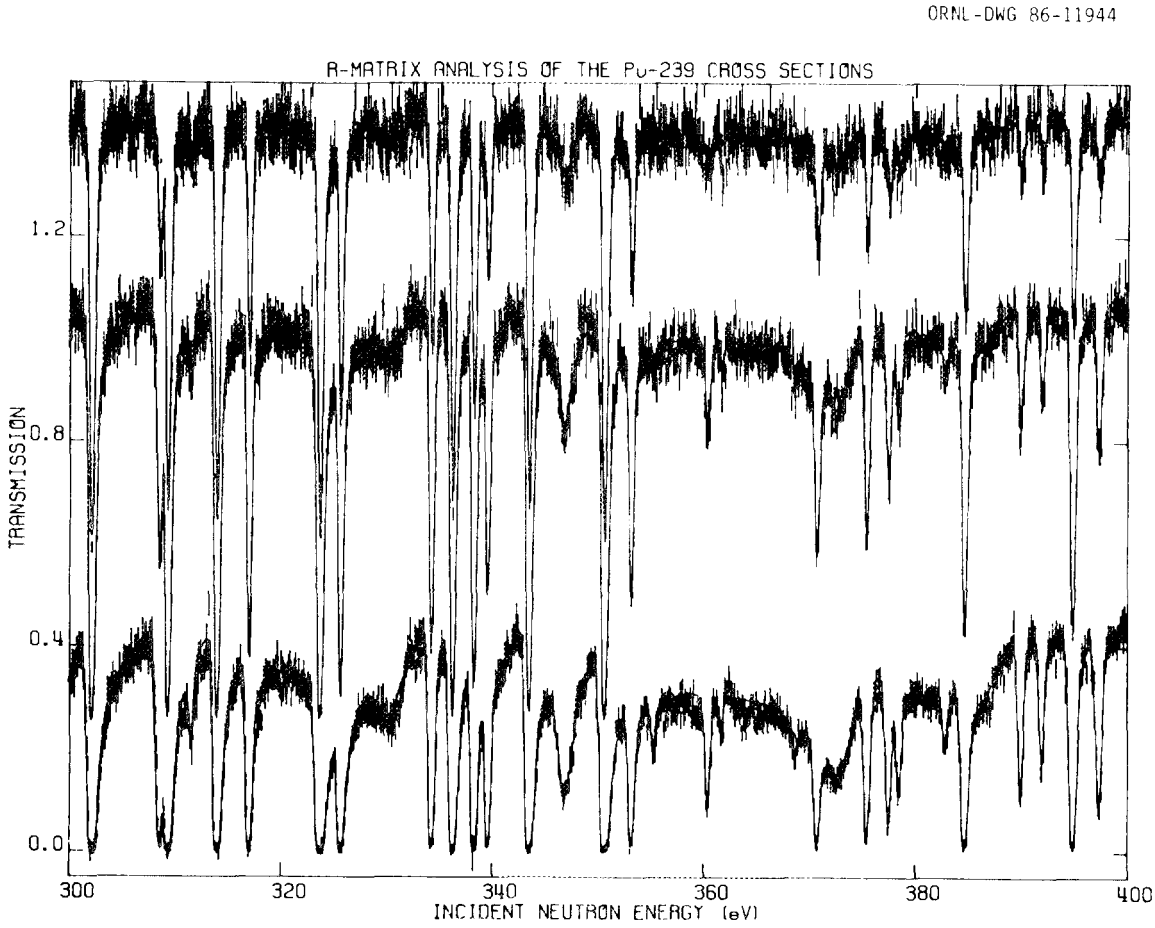

Fig. 35. Comparison of transmission ratios as computed with our resonance parameters, solid lines, and as measured by Harvey *et al.* (1984) on an 80 m flight path, with samples at liquid nitrogen temperature, of 0.0737, 0.0180, and 0.0064 atom/b, over the incident neutron energy range from 300 to 400 eV. The transmission ratio for the 0.0180 atom/b was displaced up by 0.25, that of the 0.0064 atom/b sample was displaced up by 0.5 for clarity of display.

ORNL-DWG 86-11945

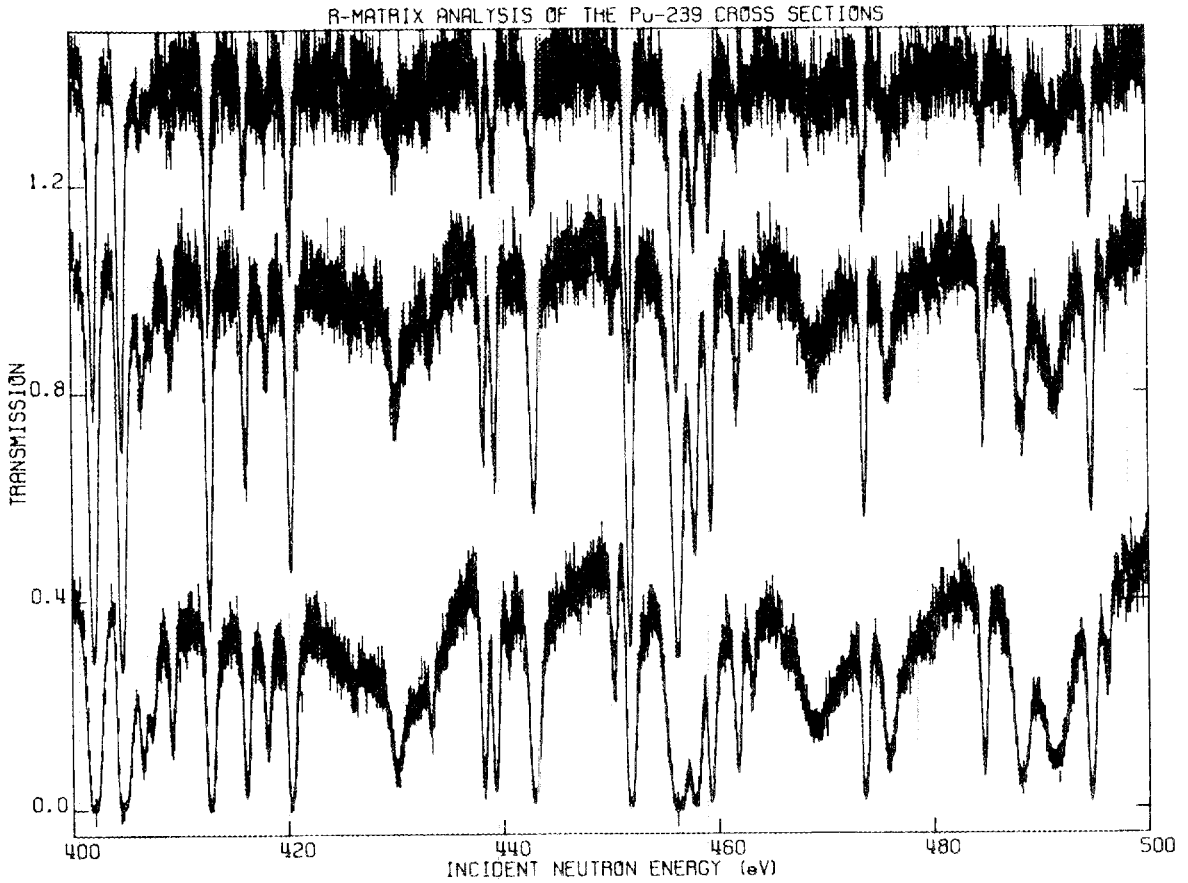

Fig. 36. Comparison of transmission ratios as computed with our resonance parameters, solid lines, and as measured by Harvey *et al.* (1984) on an 80 m flight path, with samples at liquid nitrogen temperature, of 0.0737, 0.0180, and 0.0064 atom/b, over the incident neutron energy range from 400 to 500 eV. The transmission ratio for the 0.0180 atom/b was displaced up by 0.25, that of the 0.0064 atom/b sample was displaced up by 0.5 for clarity of display.

ORNL-DWG 86-11946

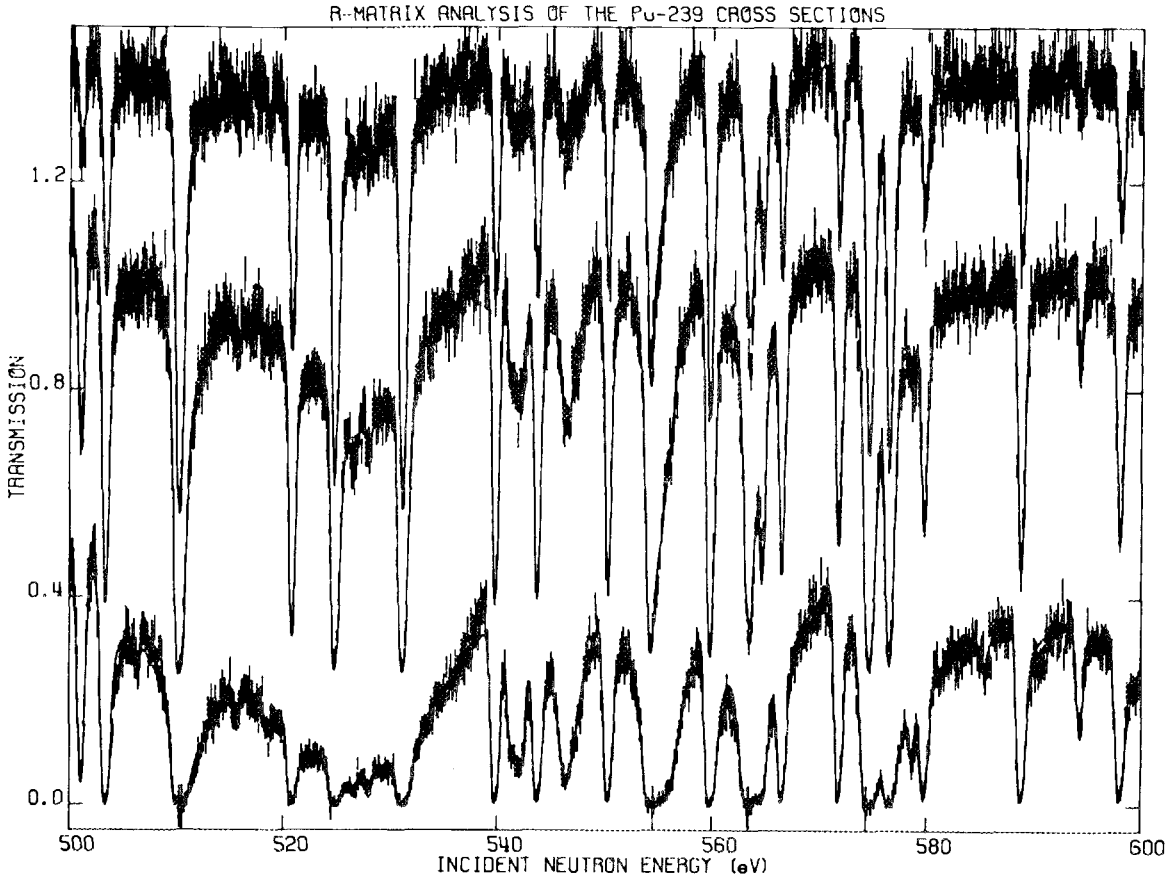

Fig. 37. Comparison of transmission ratios as computed with our resonance parameters, solid lines, and as measured by Harvey *et al.* (1984) on an 80 m flight path, with samples at liquid nitrogen temperature, of 0.0737, 0.0180, and 0.0064 atom/b, over the incident neutron energy range from 500 to 600 eV. The transmission ratio for the 0.0180 atom/b was displaced up by 0.25, that of the 0.0064 atom/b sample was displaced up by 0.5 for clarity of display.

ORNL-DWG 86-11947

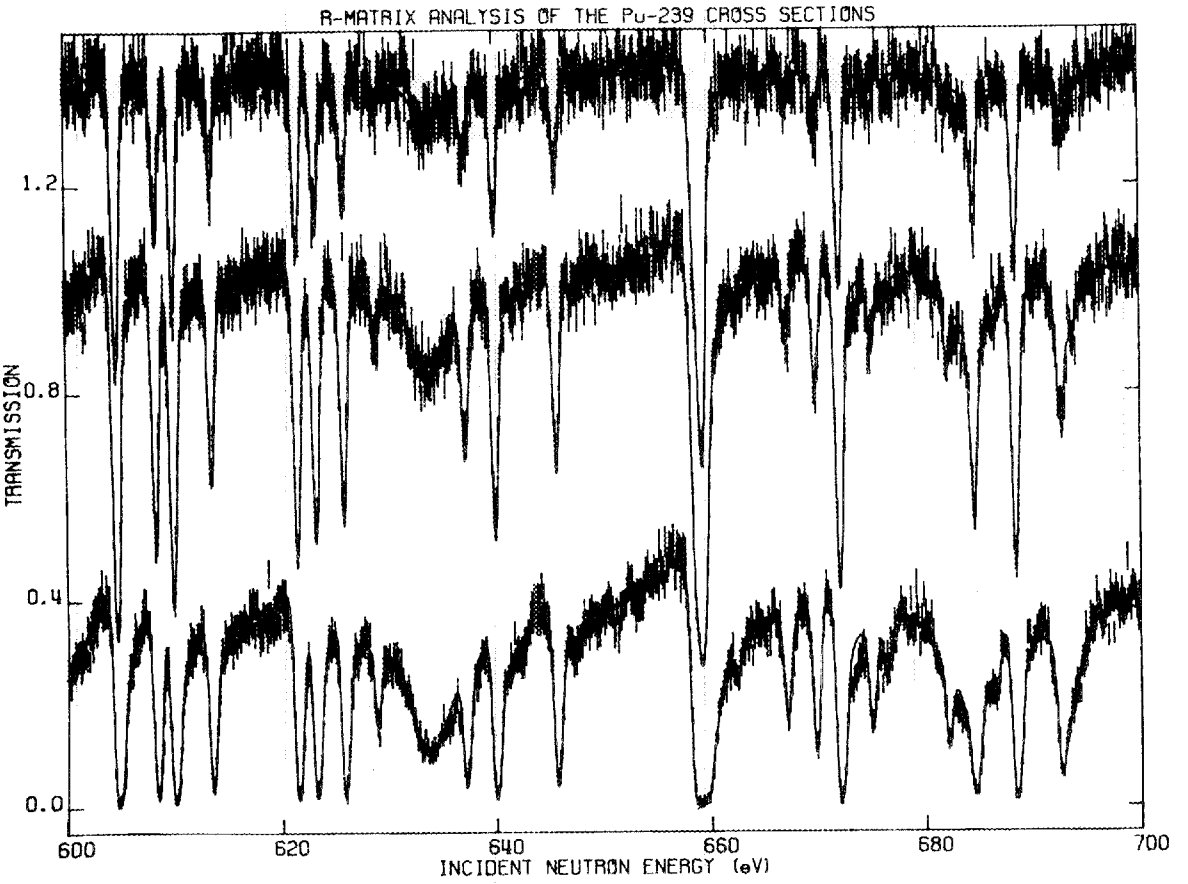

Fig. 38. Comparison of transmission ratios as computed with our resonance parameters, solid lines, and as measured by Harvey *et al.* (1984) on an 80 m flight path, with samples at liquid nitrogen temperature, of 0.0737, 0.0180, and 0.0064 atom/b, over the incident neutron energy range from 600 to 700 eV. The transmission ratio for the 0.0180 atom/b was displaced up by 0.25, that of the 0.0064 atom/b sample was displaced up by 0.5 for clarity of display.

ORNL-DWG 86-11948

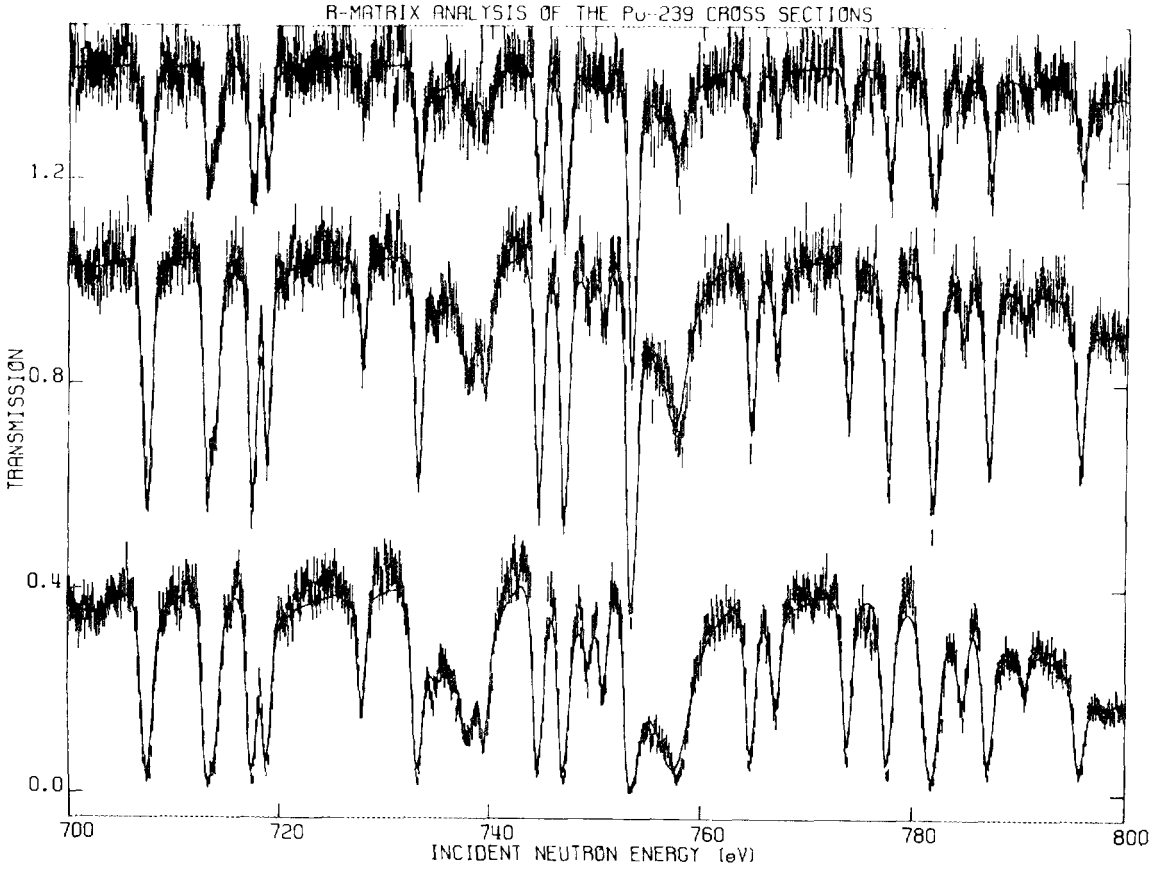

Fig. 39. Comparison of transmission ratios as computed with our resonance parameters, solid lines, and as measured by Harvey *et al.* (1984) on an 80 m flight path, with samples at liquid nitrogen temperature, of 0.0737, 0.0180, and 0.0064 atom/b, over the incident neutron energy range from 700 to 800 eV. The transmission ratio for the 0.0180 atom/b was displaced up by 0.25, that of the 0.0064 atom/b sample was displaced up by 0.5 for clarity of display.

ORNL-DWG 86-11949

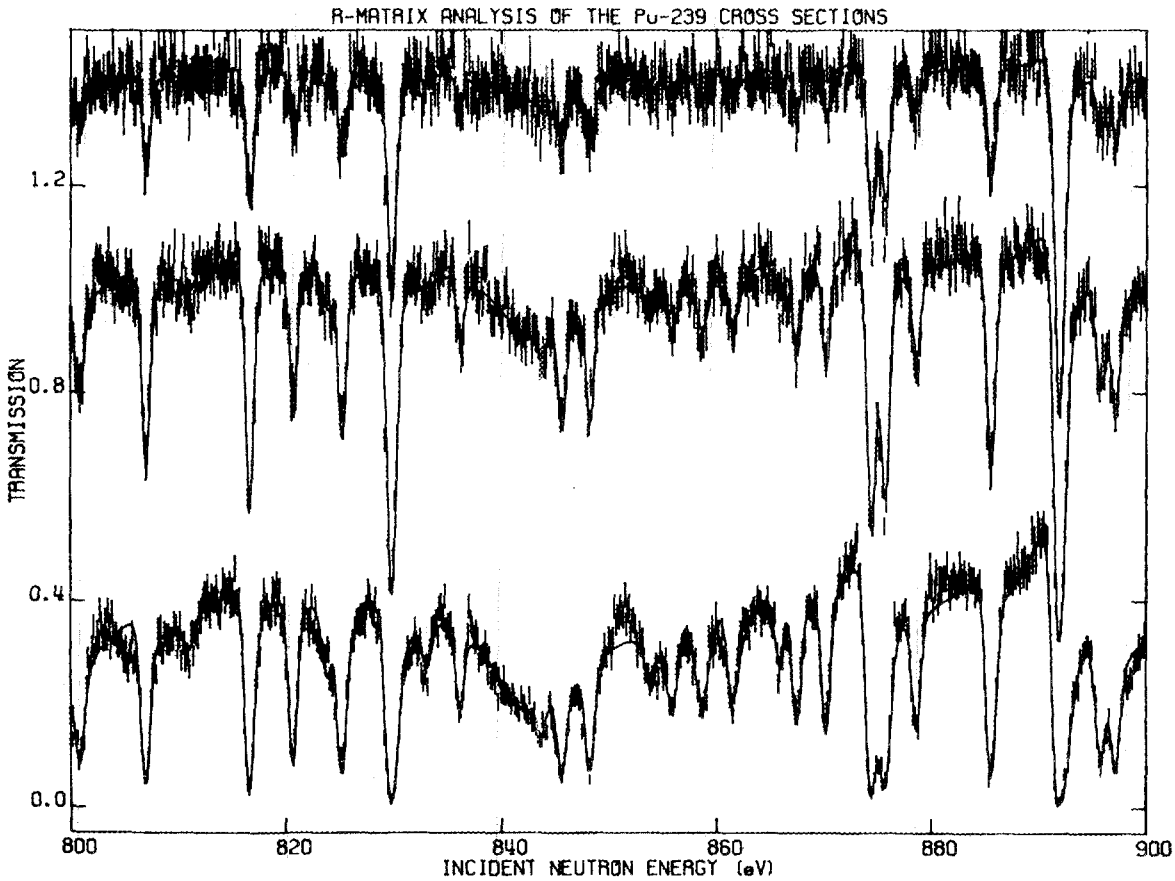

Fig. 40. Comparison of transmission ratios as computed with our resonance parameters, solid lines, and as measured by Harvey *et al.* (1984) on an 80 m flight path, with samples at liquid nitrogen temperature, of 0.0737, 0.0180, and 0.0064 atom/b, over the incident neutron energy range from 800 to 900 eV. The transmission ratio for the 0.0180 atom/b was displaced up by 0.25, that of the 0.0064 atom/b sample was displaced up by 0.5 for clarity of display.

ORNL-DWG 86-11950

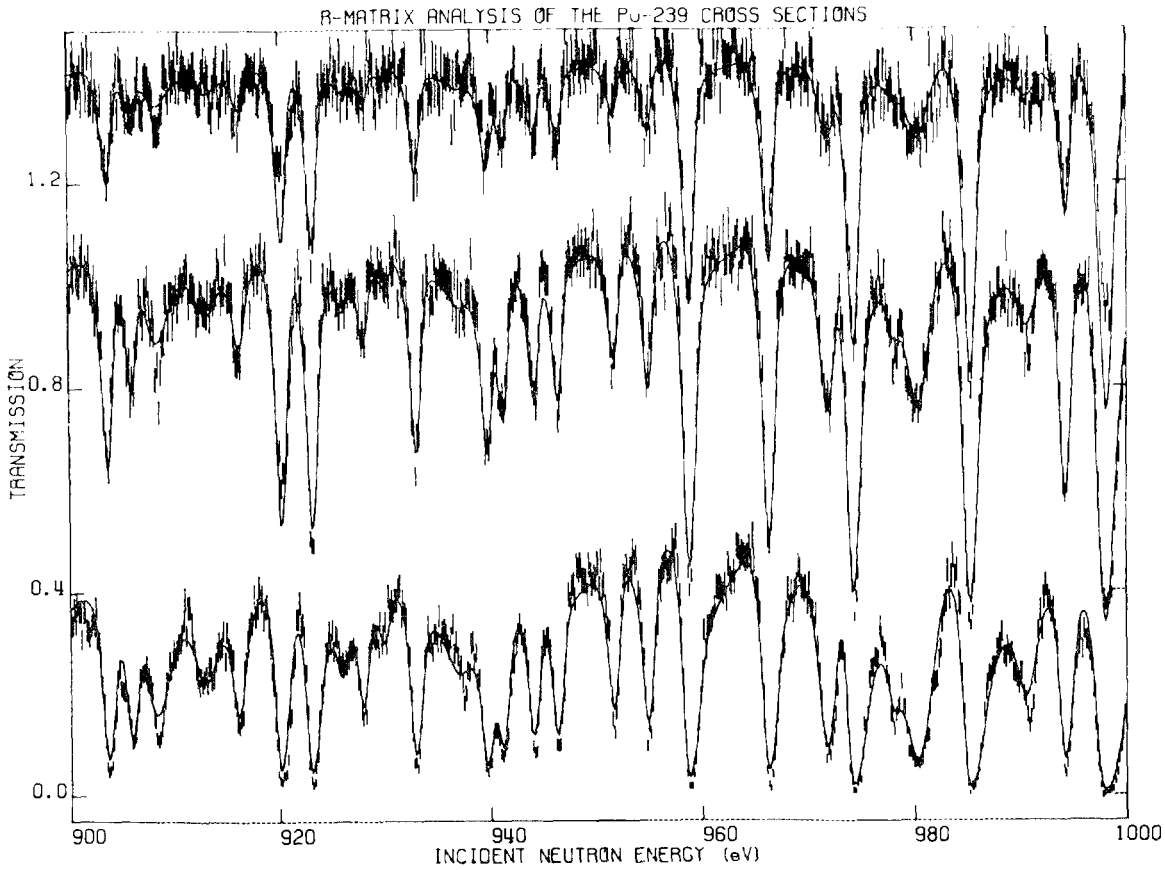

Fig. 41. Comparison of transmission ratios as computed with our resonance parameters, solid lines, and as measured by Harvey *et al.* (1984) on an 80 m flight path, with samples at liquid nitrogen temperature, of 0.0737, 0.0180, and 0.0064 atom/b, over the incident neutron energy range from 900 to 1000 eV. The transmission ratio for the 0.0180 atom/b was displaced up by 0.25, that of the 0.0064 atom/b sample was displaced up by 0.5 for clarity of display.

ORNL-DWG 86-11951

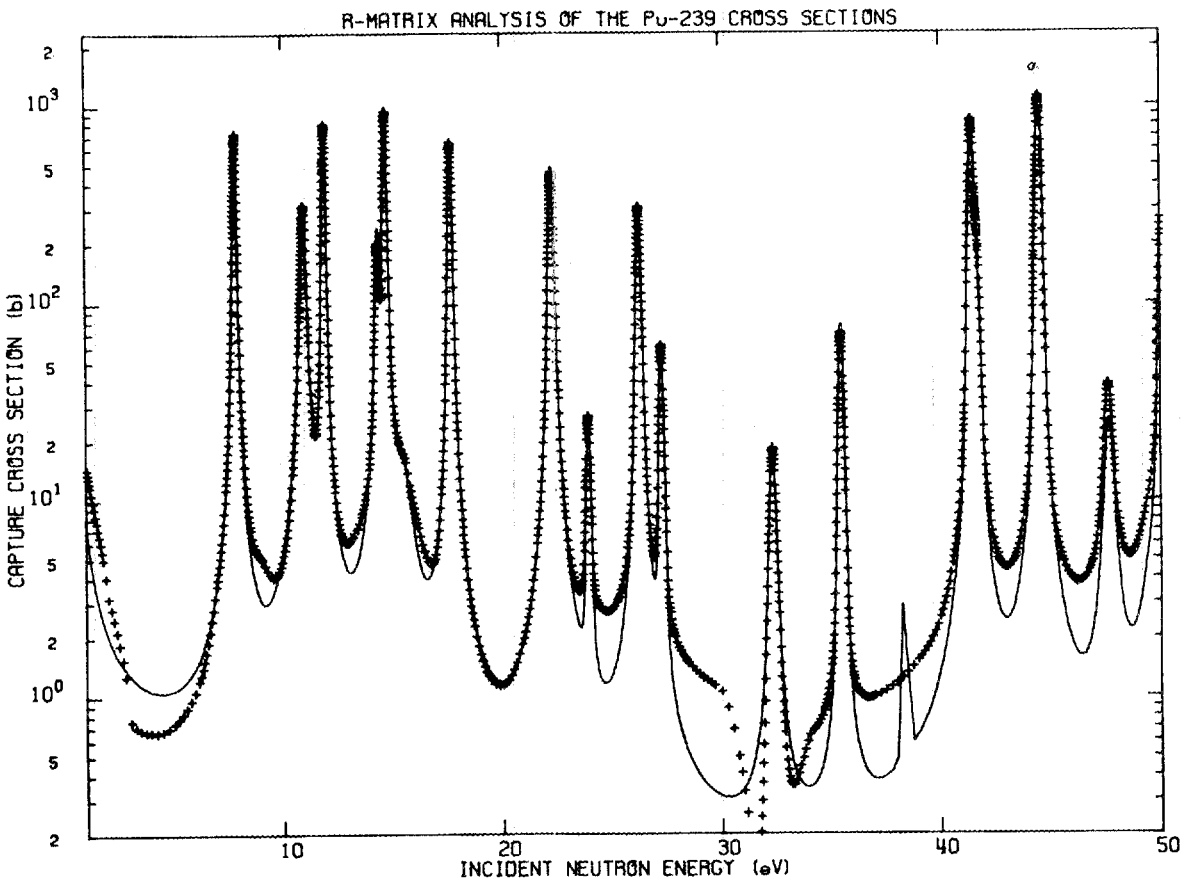

Fig. 42. Comparison of the capture cross section computed with our resonance parameters, solid line, with ENDF/B-V, crosses, over the neutron energy range 0 to 50 eV.

ORNL-DWG 86-11952

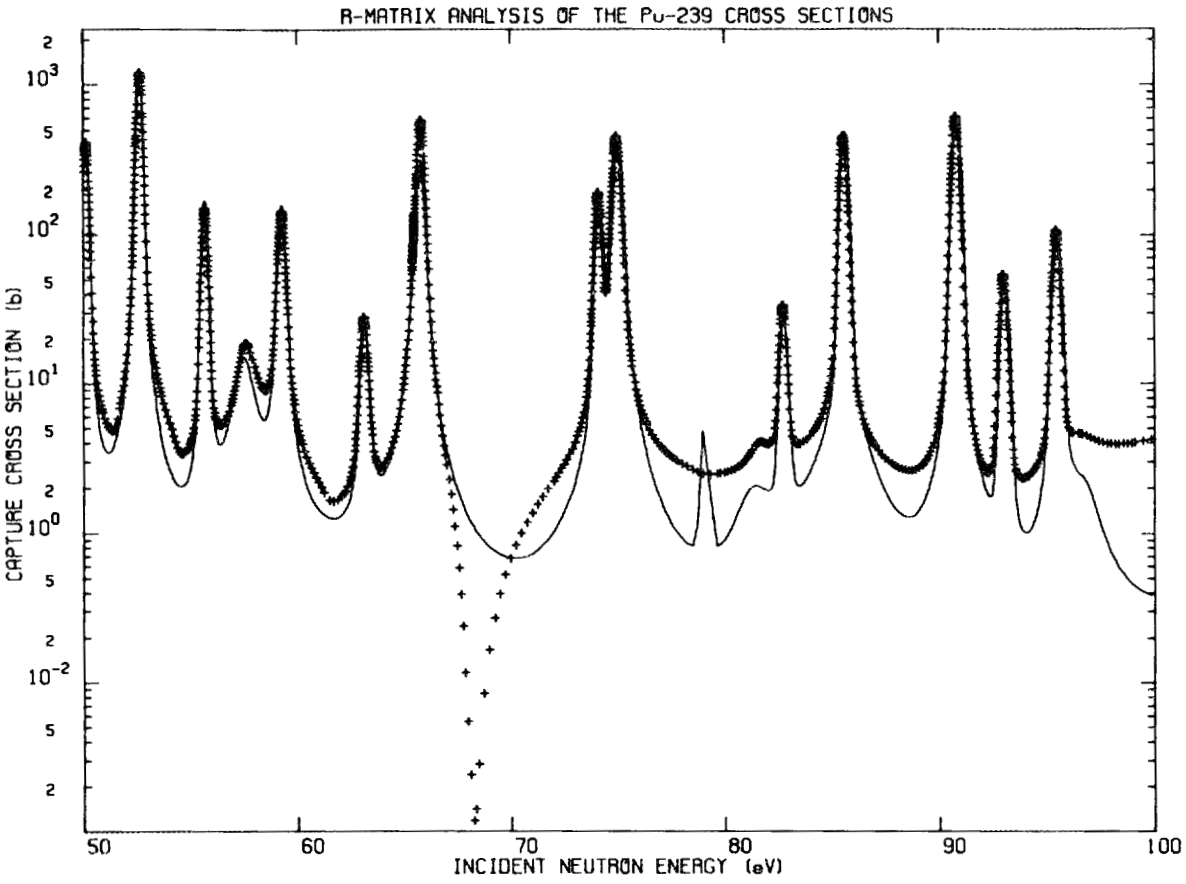

Fig. 43. Comparison of the capture cross section computed with our resonance parameters, solid line, with ENDF/B-V, crosses, over the neutron energy range 50 to 100 eV.

Table 5. Comparison of average fission cross section values over the 10- to 1000-eV energy range

E_L, Low limit of energy band (eV)	$\frac{1}{E_H-E_L}\int_{E_L}^{E_H}\sigma_f(E)dE$ (b)						
	This work	ENDF/B-V	Weston[a] and Todd (1984)	Blons (1973)	Gwin *et al.*[b]	Wagemans *et al.* (1980)	Shunk *et al.* (1966)
10	98.761	104.148	100.620	–	105.13	103.79	–
20	31.398	32.496	31.525 ± 0.160	–	31.59	32.23	42.07
30	3.094	3.421	3.053 ± 0.040	–	3.09	2.58	2.16
40	24.717	25.883	25.617 ± 0.100	28.61	25.67	25.36	24.62
50	71.978	72.968	72.757 ± 0.220	76.81	71.05	73.45	72.32
60	54.718	52.990	53.711 ± 0.210	56.41	55.71	56.28	54.92
70	62.485	62.083	61.565 ± 0.350	64.67	62.88	63.92	59.54
80	64.822	65.844	65.589 ± 0.200	68.04	64.6	67.39	61.49
90	28.149	30.386	29.148 ± 0.100	31.28	28.54	30.28	26.10
100	17.953	18.375	17.976 ± 0.030	18.93	17.96	18.31	17.82
200	17.367	17.651	17.231 ± 0.040	17.79	17.90	17.67	18.26
300	7.912	8.298	8.064 ± 0.022	8.91	8.48	8.56	8.35
400	9.192	9.407	9.254 ± 0.028	9.71	9.40	9.60	9.11
500	15.003	15.373	15.037 ± 0.040	15.51	15.46	15.14	14.65
600	4.105	4.569	4.138 ± 0.017	4.63	4.55	4.26	3.94
700	5.190	5.351	5.386 ± 0.021	5.94	5.34	5.50	5.19
800	4.614	5.073	4.690 ± 0.020	5.11	5.1	4.76	4.37
900	8.069	7.818	8.175 ± 0.032	8.57	7.83	8.14	8.28
40-1000	12.510	12.805	12.582	13.30	12.80	12.88	12.49

[a]Statistical uncertainty only. The normalization uncertainty is 1.9%
[b]Gwin *et al.* (1984) for $10 \leqslant E \leqslant 100$; Gwin *et al.* (1976) for $100 \leqslant E \leqslant 1000$ eV.

Table 6. Comparison of energy integrals of the ^{239}Pu fission cross section over the energy range 0.01 to 30 eV

Energy interval (eV)	$\int_{E_1}^{E_2} \sigma_f(E)dE$ (b·eV)						
	Present analysis	ENDF/B-V	Gwin *et al.*[a] (1984)	Weston and Todd (1984)	Wagemans *et al.* (1980)	Gwin *et al.* (1976)	Gwin *et al.* (1971)
0.01 – 0.02	9.68	9.66	9.70 ± 0.08				
0.02 – 0.03	7.56	7.52	7.53 ± 0.04				7.49
0.03 – 0.04	6.49	6.43	6.45 ± 0.04		6.46		6.44
0.04 – 0.05	5.83	5.77	5.78 ± 0.04		5.79		5.80
0.05 – 0.1	24.99	24.79	24.89 ± 0.07		25.08		24.90
0.1 – 0.2	57.63	58.34	58.29 ± 0.23		59.92		57.87
0.2 – 0.3	199.9	198.9	199.5 ± 1.18		205.97		197.0
0.3 – 0.4	168.6	168.0	168.4 ± 1.08		173.7		174.2
0.4 – 0.5	35.55	35.78	35.08 ± 0.5		36.03		36.4
0.5 – 1.	39.90	38.21	38.13 ± 0.5		39.29		38.93
1. – 6.	59.35	63.67	60.28 ± 2.66		66.83	68.90	65.18
6. – 9.	174.2	182.7	178.7 ± 1.79		181.7	181.7	181.7
9. – 12.6	476.3	503.4	504.4 ± 4.69		498.1	497.9	495.2
12.6 – 20.	516.0	547.3	552.8 ± 5.03	530.4	546.	543.2	547.2
20. – 24.7	216.7	224.3	217.1 ± 2.91	219.7	223.3	222.9	225.1
24.7 – 30.	98.12	100.7	98.78 ± 1.87	96.97	99.18	100.6	100.8
Thermal value (b)	748.4	741.7		741.7	741.9	741.6	741.6

[a]Normalized to 25.15 b·eV over the interval 0.02001 to 0.06001 eV.

Table 7. Comparison of energy integrals of the ^{239}Pu capture cross section over the energy range 0.01 to 30 eV

Energy Interval (eV)	$\int_{E_1}^{E_2} \sigma_{n\gamma}(E)dE$ (b·eV) Present Analysis	ENDF/B-V	Gwin *et al.* (1971)
0.01 – 0.02	3.34	3.32	—
0.02 – 0.1	18.59	18.4	18.9
0.1 – 0.5	299.50	302.	301.
0.5 – 0.8	11.5	12.9	12.7
0.8 – 7.0	13.22	17.4	–[a]
7.0 – 16.0	722.0	694.	710.
16.0 – 30.0	415.0	416.	–[a]

[a]Intervals from 0.8 to 7.0 eV and from 16.0 to 30.0 eV are obscured by chemical and isotopic contaminants.

In Figs. 29 to 41 we compare the high resolution transmission measurements of Harvey *et al.*[39] with corresponding computed transmissions, in the range 30 to 1000 eV. The transmissions were measured on a flight path of 80 m, with samples at the effective temperature of 97 K, and with three thicknesses: 0.0737, 0.0180, and 0.0064 atom/b, respectively. The data of the last two samples were displaced by 0.25 and 0.5, respectively to improve the clarity of the figures.

Because of the poor statistical accuracy, large statistical uncertainties and contamination by chemical and isotopic impurities of the direct capture measurements, the best estimate of the structure of the capture cross section can probably be obtained from a calculation based on the resonance parameters of a consistent analysis of fission and transmission measurements. In Figs. 42 to 47 we compare the capture cross section obtained with our resonance parameters with ENDF/B-V. The two calculations are usually consistent near the peak of the resonances, where the single level Breit-Wigner formalism is a good approximation to the capture cross section. In the valleys between resonances there are large differences between the two calculations; the ENDF/B-V representation often results in an unphysical structure (near 30 or 70 eV) as would be expected because of the nonphysical formalism used: between resonances the cross sections are mostly determined by the "smooth background" File 3.[1]

Table 8. Average absorption cross section and alpha values for ^{239}Pu over the 7.3 to 100 eV energy range

E_L, low limit of energy band (eV)	$\frac{1}{E_H-E_L}\int_{E_L}^{E_H}\sigma_a(E)dE$ (b)				$\langle\sigma_c\rangle/\langle\sigma_f\rangle$			
			Gwin (1971)				Gwin (1971)	
	This work	ENDF/B-V	11-g foil	Ionization chamber	This work	ENDF/B-V	11-g foil	Ionization chamber
7.3	196.1	199.7	209.0 ± 13	207.0 ± 9.0	0.73	0.66	0.76 ± 0.1	0.73 ± 0.07
16.0	44.7	45.5	46.5 ± 3.0	61.2 ± (a)	0.86	0.84	0.89 ± 0.11	–
37.5	72.0	76.8	80.5 ± 5.2	85.8 ± 4.8	2.57	2.66	2.82 ± 0.21	3.1 ± 0.19
50	90.3	93.2	93.4 ± 6.0	94.3 ± 4.3	0.60	0.64	0.64 ± 0.1	0.68 ± 0.10
100	34.13	35.5	35.4 ± 2.3	36.4 ± 1.8	0.90	0.93	0.96 ± 0.12	1.0 ± 0.15
200	35.19	35.2	35.3 ± 2.3	35.6 ± 1.8	1.03	0.99	1.06 ± 0.12	1.05 ± 0.15
300	18.44	17.6	18.6 ± 1.2	18.7 ± 1.3	1.33	1.12	1.34 ± 0.14	1.25 ± 0.18
400	13.9	13.54	13.95 ± 0.9	14.4 ± 1.3	0.51	0.44	0.48 ± 0.09	0.52 ± 0.10
500	27.5	26.5	27.6 ± 1.8	27.3 ± 1.7	0.83	0.72	0.78 ± 0.11	0.78 ± 0.13
600	11.9	11.6	11.8 ± 0.76	12.9 ± 1.4	1.90	1.53	1.87 ± 0.18	1.93 ± 0.24
700	11.9	10.6	11.2 ± 0.72	12.3 ± 1.8	1.30	0.98	1.00 ± 0.12	1.16 ± 0.17
800	10.1	9.25	9.61 ± 0.62	10.4 ± 1.3	1.18	0.82	1.07 ± 0.14	1.06 ± 0.16
900	15.5	13.3	14.5 ± 0.93	16.0 ± 1.4	0.92	0.70	0.77 ± 0.1	0.88 ± 0.14

[a]Not corrected for the contribution of the tungsten to the neutron capture cross section.

ORNL-DWG 86-11953

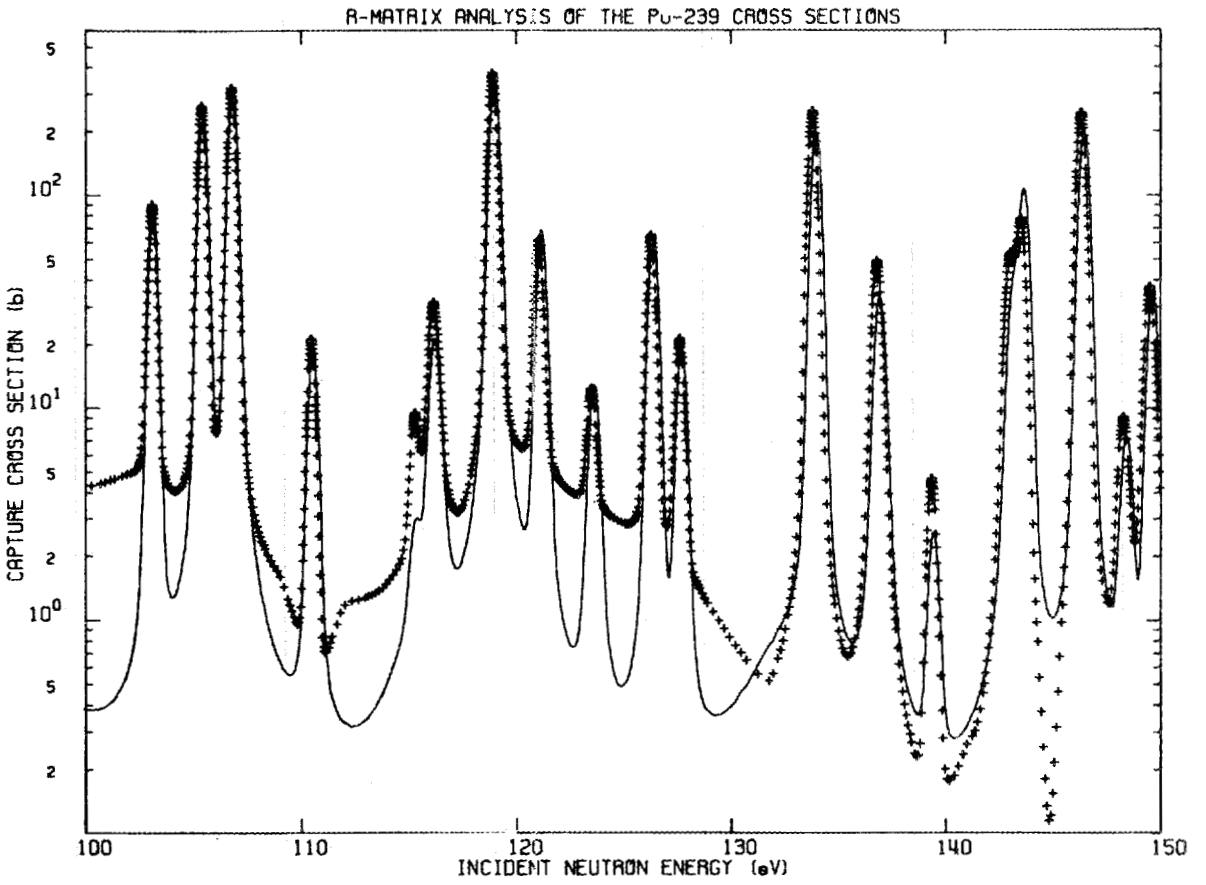

Fig. 44. Comparison of the capture cross section computed with our resonance parameters, solid line, with ENDF/B-V, crosses, over the neutron energy range 100 to 150 eV.

ORNL-DWG 86-11954

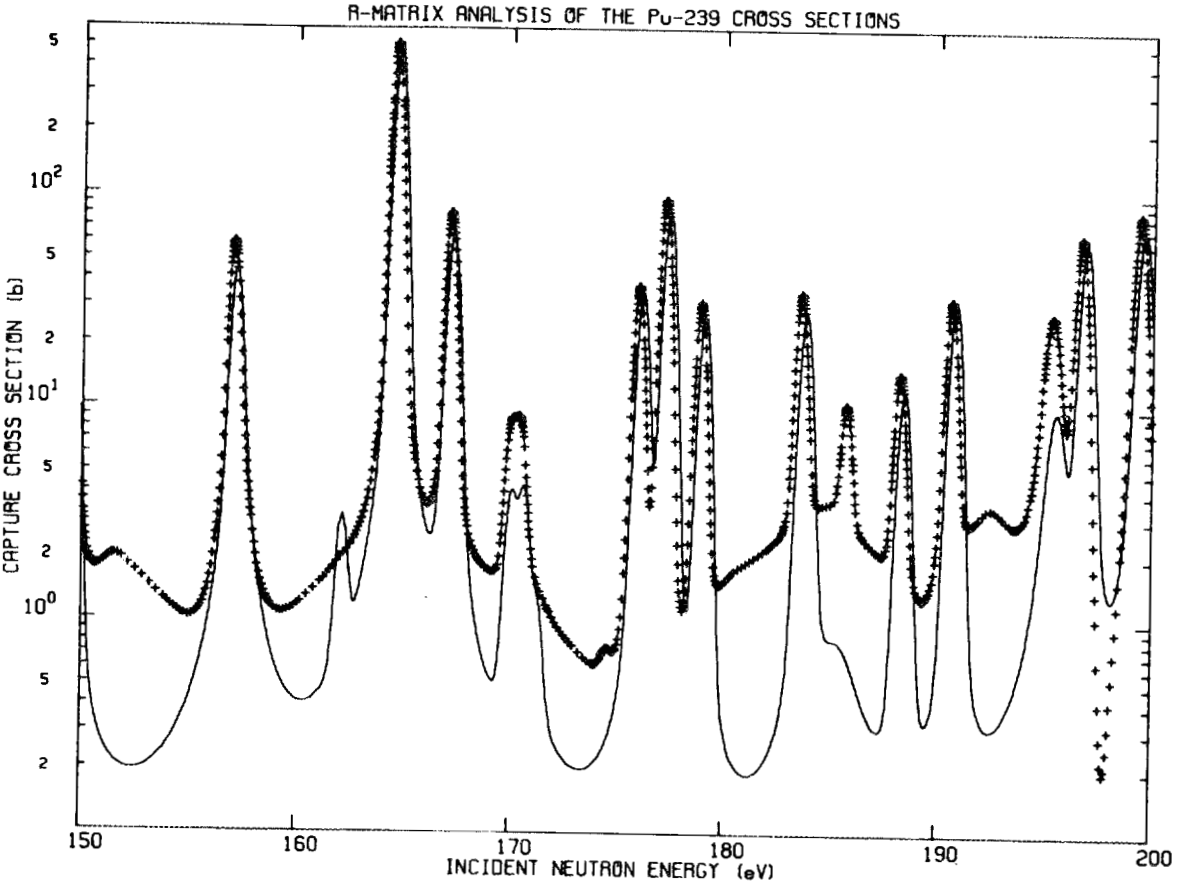

Fig. 45. Comparison of the capture cross section computed with our resonance parameters, solid line, with ENDF/B-V, crosses, over the neutron energy range 150 to 200 eV.

ORNL-DWG 86-11955

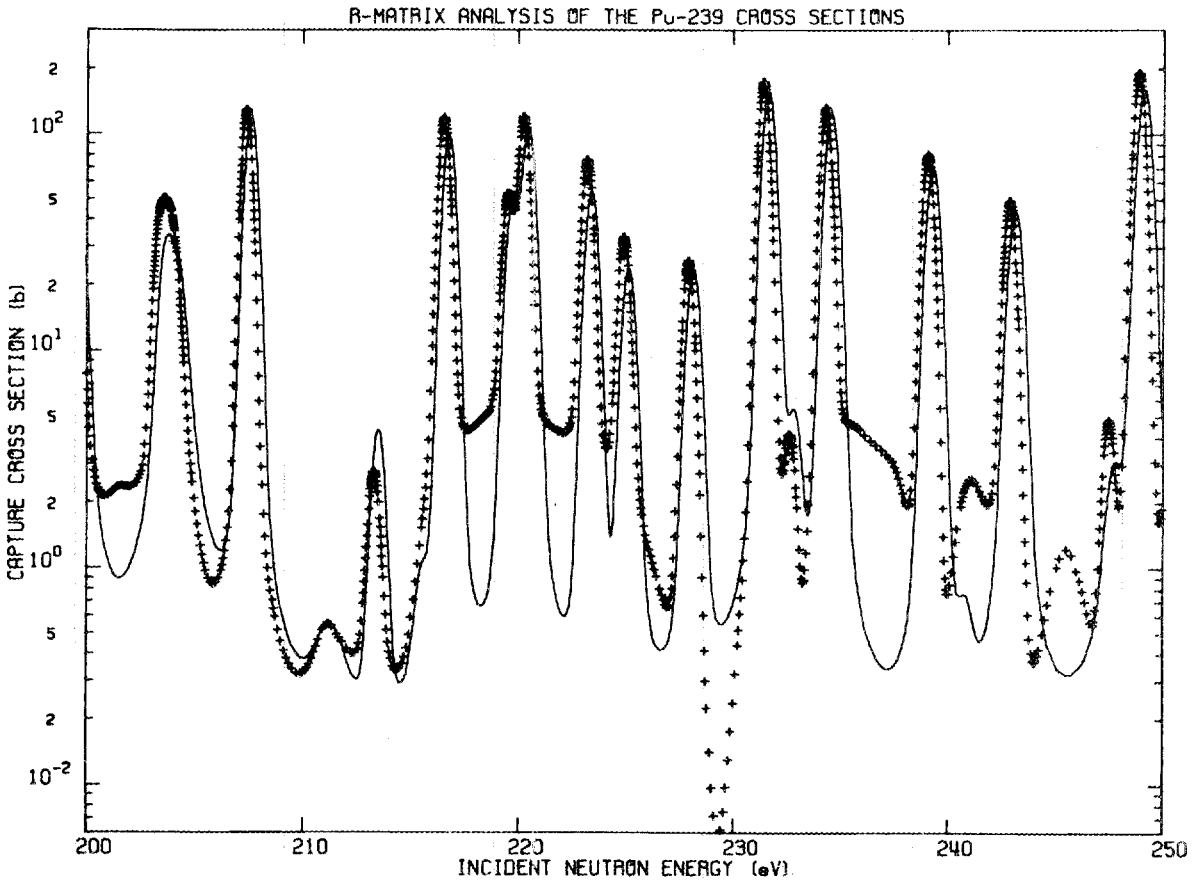

Fig. 46. Comparison of the capture cross section computed with our resonance parameters, solid line, with ENDF/B-V, crosses, over the neutron energy range 200 to 250 eV.

ORNL-DWG 86-11956

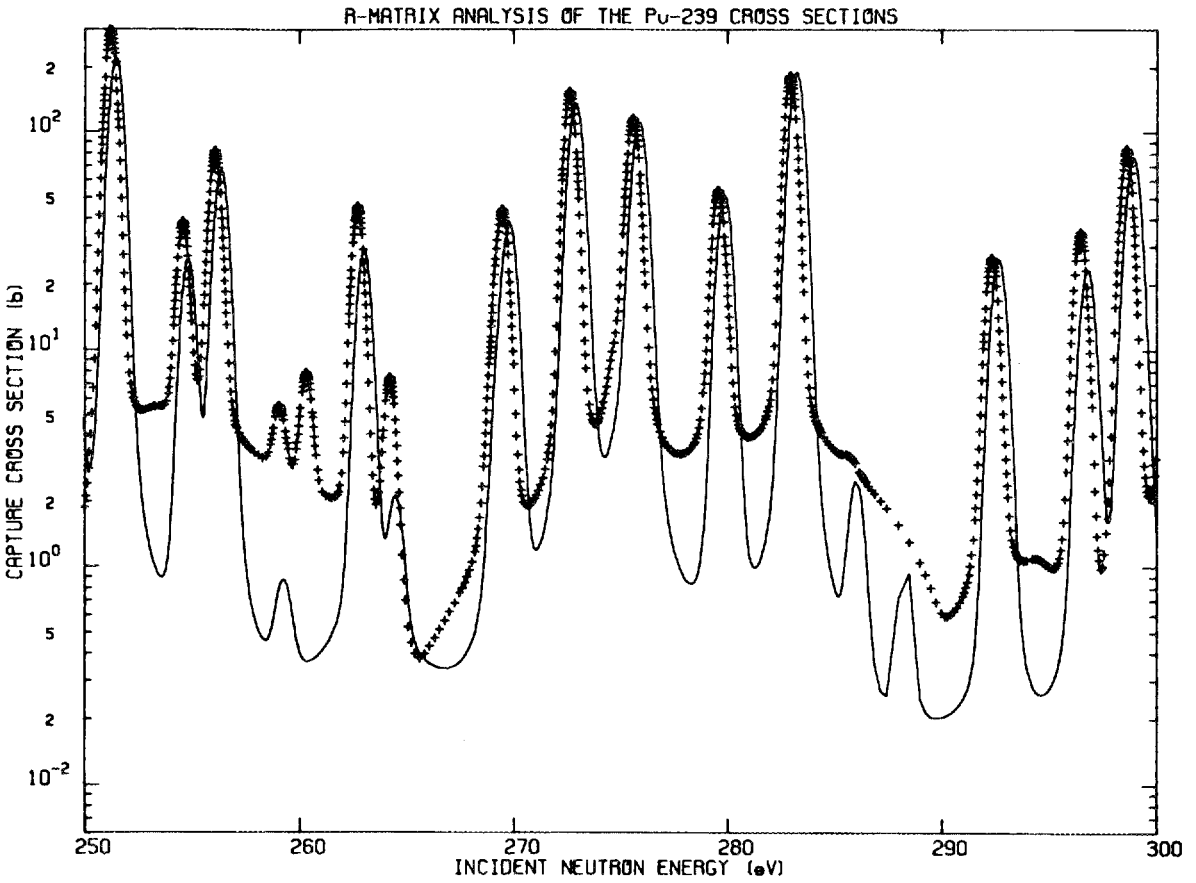

Fig. 47. Comparison of the capture cross section computed with our resonance parameters, solid line, with ENDF/B-V, crosses, over the neutron energy range 250 to 300 eV.

Below 0.5 eV, the R-matrix analysis is mostly constrained by the transmission measurements of Spencer *et al.*[38] (Fig. 25), by the 1971 capture measurement of Gwin *et al.*,[20] renormalized to the thermal value of 269.3 b, and by the 1984 fission measurement of Gwin *et al.*,[36] normalized to the thermal value of 748.1 b (Fig. 1). From 0.5 to 30 eV the analysis is mostly constrained by the "low resolution" transmission data of Harvey *et al.*[39] (Figs. 27 and 28), and by the high accuracy fission data of Gwin *et al.*[36] (Fig. 5), and Weston and Todd[37] (Fig. 6). Above 50 eV the analysis is mostly constrained by the high resolution transmission data of Harvey *et al.*[39] (Figs. 29 to 41), and the high accuracy fission data of Weston and Todd[37] (Figs. 7 to 18). The structure of the fission cross sections from the measurements of Blons,[28] and of Weston and Todd,[37] are quite consistent; however, there are 5% to 10% systematic differences in magnitude of the average fission cross section between the two measurements, as can be seen in Table 5. The difference between the fission of Blons and that of Weston and Todd varies smoothly from about 3 b near 50 eV to 0.4 b near 1 keV, suggesting an error in estimation of the background per unit time in one of the measurements. Since the measurement of Weston and Todd has much better statistical accuracy and appears to have less background, it was given most of the weight in the analysis.

Fission cross sections averaged over decimal intervals, from 10 to 1000 eV, from several measurements and evaluations are compared in Table 5. The fission cross section computed with our resonance parameters is generally consistent to within 2% with that of Weston and Todd.[37] The measurements of Blons,[28] Wagemans *et al.*,[45] and above 300 eV of Gwin *et al.*,[46] are generally 2% to 5% higher than Weston and Todd and our evaluation. We believe these differences to be partly due to a remaining background component in these measurements.

Fission integrals over selected small energy intervals below 30 eV are compared in Table 6. In the important region below 0.5 eV both our evaluation and ENDF/B-V are consistent with the recent measurement of Gwin *et al.*,[36] within the experimental errors of the measurement. Above 1.0 eV our evaluation yields fission integrals a few percent lower than ENDF/B-V but agrees well with the more recent experimental data.

The capture cross sections obtained from our analysis, from ENDF/B-V and from the 1971 Oak Ridge National Laboratory/Rensselaer Polytechnic Institute measurement[20] are compared in Table 7. Several energy regions of the measurements are obscured by the large ^{240}Pu resonance at 1.056 eV and by resonances in the tungsten chemical impurity of the sample (see Fig. 4). Both evaluations are reasonably consistent with the measurement.

Average absorption cross sections from our analysis, from ENDF/B-V, and from the 1976 measurement of Gwin *et al.*[46] are compared in Table 8 over the energy range 7.3 to 1000 eV. The calculations from our resonance parameters and from ENDF/B-V are generally consistent with the experimental values. Ratios of the average capture to the average fission are also compared in Table 8. Again, both our values and ENDF/B-V are generally consistent with the experimental data.

SUMMARY AND CONCLUSIONS

Several sets of ^{239}Pu neutron cross-section data, both recent and old, have been analyzed using R-matrix theory combined with Bayesian equations, a technique which provides a powerful tool for cross-section evaluation procedures. This analysis provides a consistent and precise description of various sets of fission, capture, and transmission data. The evaluation also provides an accurate method for cross-section interpolation at the valleys between resonances where the capture and fission cross sections are exceedingly small, making accurate measurements difficult, and where the single-level formalisms grossly misrepresent the data. In some energy regions the representation of the cross sections could probably be further improved by the addition of more levels and by refitting. The analysis could also be extended to higher energies. The excellent resolution of the transmission ratios measured by Harvey *et al.,* permit the identification of the most important levels to several keV.

As it stands the present analysis is a great improvement over previous evaluations in that it provides a good and consistent representation of the high resolution transmission ratios of Harvey *et al.* and the high accuracy recent fission measurement of Weston and Todd and Gwin *et al.* It also extends the resolved energy region well above previous evaluations.

ACKNOWLEDGEMENTS

We received many helpful suggestions from F. G. Perey and C. M. Perey concerning the Bayesian methodology for cross-section analysis. We are indebted to R. Gwin, J. A. Harvey, R. R. Spencer, and L. W. Weston for letting us use their data prior to publication and for a careful description of the experimental conditions of the measurements. G. L. Tweed contributed to the transmission-ratio data reduction. R. Q. Wright performed all the ENDF/B-V calculations. We are grateful to S. A. Raby for guiding the preparation of the manuscript through its numerous drafts. Two of the authors (R. B. Perez and R. L. Macklin) were also sponsored by DOE grant DE-FG05-85ER40188.

REFERENCES

1. R. Kinsey, Editor, "ENDF-102 Data Formats and Procedures for the Evaluated Nuclear Data File, ENDF," revised, BNL-NCS-50496, Brookhaven National Laboratory (October 1979).
2. G. de Saussure and R. B. Perez, *Ann. Nucl. Energy* **9**, 79 (1982).
3. M. Salvatores, Topical Meeting of the NEANDC, Aix-en-Provence, April 1981.
4. R. N. Hwang, in *Proc. of the Second Jackson Hole Colloquium on Fast Reactor Physics,* June 27-29, 1983, Teton Village, Wyoming.
5. "ENDF/B-V Data File for ^{239}Pu (Mat 1399)," evaluated by E. Kujawski, L. Stewart *et al.* (ENDF/B-V), R. Kinsey, Editor, available from Brookhaven National Laboratory (July 1979).
6. H. Derrien *et al., Proc. of the 1984 IAEA Upsala Conference,* IAEA-336, 449 (to be published).
7. T. Nakagawa *et al., Evaluation of Resonance Parameters of ^{233}U, ^{235}U, ^{238}U, ^{239}Pu, ^{240}Pu, ^{241}Pu, and ^{242}Pu,* Japan Atomic Energy Energy Research Institute Report JAERI-M 9823 (November 1981).
8. B. Goel and F. Weller, *Evaluations for the German Nuclear Data Library KEDAK-3, Part 2: Fissile and Fertile Materials,* KFK-2386/III (March 1977) and private communication from F. Froehner (1981).
9. G. V. Antsipov *et al.,* "Nuclear Data Evaluation for ^{239}Pu in the Energy Region 10^{-5} eV-15 MeV," INDC(CCP)-166/GHJ, International Nuclear Data Committee (1981).
10. E. D. Arthur *et al., Nucl. Sci. Eng.* **88**, 56-70 (1984).
11. M. Divadeenam and J. R. Stehn, *Ann. Nucl. Energy* **11**, 357 (1984).
12. N. M. Larson and F. G. Perey, *Users Guide for SAMMY: A Computer Model for Multilevel R-Matrix Fits to Neutron Data Using Bayes' Equations,* ORNL/TM-7485, Oak Ridge National Laboratory, 1980; see also N. M. Larson, *Updated Users' Guide for SAMMY,* ORNL/TM-9179, Oak Ridge National Laboratory, 1984 and ORNL/TM-9719/R1, 1985.
13. C. W. Reich and M. S. Moore, *Phys. Rev.* **111**, 929 (1958).
14. M. S. Moore, "Measurements on Fissile Nuclides," *Experimental Neutron Resonance Spectroscopy*, Chap. 5, J. A. Harvey, Editor, Academic Press, New York (1970).
15. H. Derrien, "Plutonium-239 Resonance Parameters," *Proc. Specialists' Meeting Resonance Parameters of Fertile Nuclei and ^{239}Pu,* Saclay, May 20-22, 1974, NEANDC(E)163U, P. Ribon, Editor (January 1975).
16. E. Vogt, *Phys. Rev.* **118**, 724 (1960).
17. P. Ribon and G. LeCoq, CEA-N-1484, EANDC(E)138 "A1," Commissariat a l'Energie Atomique (1971).

18. G. D. James and G. de Saussure, "Measurement of Fission Cross-Sections," *Nuclear Fission and Neutron Induced Fission Cross Sections*, Chap. 4, A. Michandon, Editor, Pergamon Press, New York (1981).

19. D. B. Adler and F. T. Adler, "Multilevel Analysis of the ^{239}Pu Cross Sections Below 40 eV," COO-1546-7, University of Illinois, Department of Physics (1967).

20. R. Gwin *et al., Nucl. Sci. Eng.* **45**, 25 (1971).

21. V. V. Kolesov and A. A. Luk'yanov, *Nucl. Constants* **2**, 46, 3 (1982); INDC(CCP)-211/L, International Atomic Energy Agency (1983) (English translation).

22. V. V. Kolesov *et al.*, "Multilevel Analysis of ^{239}Pu Neutron Cross Sections in the Resolved Resonance Region," Nuclear Data for Basic and Applied Science, Santa Fe, NM, May 13-17, 1985, Proceedings to be published someday.

23. G. de Saussure and R. B. Perez, "POLLA, A Fortran Program to Convert R-Matrix-Type Multilevel Resonance Parameters for Fissile Nuclei into Equivalent Kapur-Peierls-Type Parameters," ORNL/TM-2599, Oak Ridge National Laboratory (June 1969).

24. G. F. Auchampaugh, *Nucl. Phys.* **A175**, 65 (1971); see also D. B. Adler and F. T. Adler, *Phys. Rev.* **C6**, 985 (1972).

25. J. A. Farrell, *Phys. Rev.* **165**, 1371 (1968).

26. H. Derrien, "Etude des Sections Efficaces de Reaction des Neutrons de Resonance Avec ^{239}Pu," Thesis, Orsay, Serie A, No. 1172 (1973).

27. E. R. Shunk, W. Brown, and R. LaBauve, *Proc. Conf. Neutron Cross Sections and Technology*, CONF-660303, Vol. II, p. 979, Washington (1966).

28. J. Blons, *Nucl. Sci. Eng.* **51**, 130 (1973).

29. O. D. Simpson and F. B. Simpson, "Evaluation of the Pu-239 Cross Sections in the Resonance Region for the ENDF/B-III Data File," ANCR-1045, Aerojet Nuclear Company (1971).

30. H. Derrien, "Quelques Remarques sur l'Evaluaton des Sections Efficaces Neutroniques de ^{239}Pu Dans le Domaine des Resonances," CEA-N-1638, Commissariat a l'Energie Atomique (1973).

31. M. S. Moore, G. de Saussure, and J. Richard Smith, *Proc. IAEA Consultant Meeting Uranium and Plutonium Isotope Resonance Parameters,* Vienna, Austria, September 28-October 20, 1981, INDC(NDC)-129/GJ, D. E. Cullen, Editor, International Atomic Energy Agency, Nuclear Data Section, Vienna (1982).

32. R. B. Perez *et al., Nucl. Sci. Eng.* **93**, 31-42 (1986).

33. G. F. Auchampauch, *MULTI: A Fortran Code for Least-Squares Shape Fitting of Neutron Cross-Section Data Using the Reich-Moore Multilevel Formalism,* LA-5473-MS, Los Alamos National Laboratory (1974).

34. "CSISRS: Cross-Section Information Standard Retrieval System," available from the Nuclear Data Centers. (CSISRS tape was obtained from Brookhaven National Laboratory in September 1983.)

35. "CINDA: The Index to Literature and Computer Files on Microscopic Neutron Data," International Atomic Energy Agency, Vienna (May 1985).

36. R. Gwin *et al., Nucl. Sci. Eng.* **88**, 37 (1984).

37. L. W. Weston and J. H. Todd, *Nucl. Sci. Eng.* **88**, 567 (1984).

38. R. R. Spencer, J. A. Harvey, N. W. Hill, and L. W. Weston, Oak Ridge National Laboratory, private communication (1985).

39. J. A. Harvey *et al.*, to be published; private communication, ORNL (1985).

40. D. C. Larson, N. M. Larson, and J. A. Harvey, *ORELA Flight Path 1: Determination of its Effective Length vs Energy, Experimental Energies, and Energy Resolution Function and Their Uncertainties,* ORNL/TM-8880,. 1984; also D. C. Larson, N. M. Larson *et al., Laser Measurements of Distances from ORELA Neutron Target to Experiment Stations Along Flight Path 1 and 6,* ORNL/TM-9097 (1985).

41. S. A. R. Wynchank and W. W. Havens, *Nucl. Sci. Eng.* **28**, 458 (1967).

42. J. Trochon, "Etude des Proprietes de la Fission Dans les Resonances de ^{239}Pu Induites Par Neutrons Lents," Thesis, Orsay (1978).

43. S. Weinstein, R. Reed, and R. C. Block, "Neutron Multiplicity Measurements for ^{233}U, ^{235}U, and ^{239}Pu Resonance Fission," p. 477 in *Proc. 2nd IAEA Symp. Physics and Chemistry of Fission,* International Atomic Energy Agency, Vienna (1969).

44. I. V. Kirpichnikov, I. V. Ignatev, and S. I. Sukhoruchkin, *At. Energy* **15**, 211 (1964).

45. C. Wagemans *et al., Ann. Nucl. Energy* **7**, 495 (1980).

46. R.Gwin *et al., Nucl. Sci. Eng.* **59**, 79 (1976).

47. E. J. Axton, *Ann. Nucl. Energy*, submitted for publication (1986); preprint by private communication from R. W. Peelle.

INTERNAL DISTRIBUTION

1. L. S. Abbott
2. H. P. Carter
3–7. G. de Saussure
8. J. K. Dickens
9. G. F. Flanagan
10. R. Gwin
11. J. A. Harvey
12. D. M. Hetrick
13. N. W. Hill
14. C. H. Johnson
15. D. C. Larson
16–20. N. M. Larson
21. R. L. Macklin
22–26. Roger L. Macklin
27. F. C. Maienschein
28. R. W. Peelle
29. C. M. Perey
30. F. G. Perey
31–35. R. B. Perez
36. R. R. Spencer
37. G. L. Tweed
38. L. W. Weston
39. R. Q. Wright
40. A. Zucker
41. P. W. Dickson, Jr. (Consultant)
42. G. H. Golub (Consultant)
43. R. M. Haralick (Consultant)
44. D. Steiner (Consultant)
45. Central Research Library
46. Y-12 Document Ref. Section
47. Laboratory Records ORNL, RC
48. ORNL Patent Office

EXTERNAL DISTRIBUTION

49. Director, Division of Reactor Research and Technology, DOE, Washington, D.C. 20545.
50. Office of the Assistant Manager for Energy Research and Development, DOE-ORO, Oak Ridge, TN 37831.
51. Dr. W. P. Poenitz, Argonne National Laboratory, 9700 South Cass Ave., Argonne, IL 60439
52. Mr. Philip B. Hemmig, Chief, Physics Branch, Reactor Research and Technology, Office of Energy Technology, U.S. Department of Energy, Washington, DC 20545
53. Dr. R. C. Block, Department of Nuclear Engineering, Rensselaer Polytechnic Institute, Troy, NY 12181
54. Dr. Donald L. Smith, Building 314, Applied Physics Division, Argonne National Laboratory, 9700 South Cass Ave., Argonne, IL 60439
55. Dr. S. L. Whetstone, Division of Nuclear Physics, Office of Energy Research, U.S. Department of Energy, Room G-315, Washington, D.C. 20545
56. Dr. M. R. Bhat, Building 197D, National Nuclear Data Center, Brookhaven National Laboratory, Upton, NY 11973
57. Dr. G. F. Auchampaugh, Los Alamos Scientific Laboratory, MS 442, P-3, Los Alamos, NM 87545
58. Dr. R. F. Carlton, Middle Tennessee State University, Physics Department, Box 407, Murfreesboro, TN 37132
59. Dr. E. C. Lynn, Nuclear Physics Division, Atomic Energy Research Establishment Harwell, Didcot, Oxon, OX11, ORA, United Kingdom

60. Dr. M. G. Sowerby, Nuclear Physics Division, Bldg. 418, Atomic Energy Research Establishment, Harwell, Didcot, Oxon, OX11, ORA, United Kingdom
61. Dr. Roger White, Lawrence Livermore National Laboratory, P.O. Box 808, Livermore, CA 94550
62. Dr. R. R. Winters, Physics Department, Denison University, Granville, Ohio 43023
63. Dr. Herman Weigmann, Central Bureau for Nuclear Measurements, Steenweg naar Retie, B-2400, Geel, Belgium
64. Dr. G. L. Morgan, Los Alamos National Laboratory, P.O. Box 1663, Group P-15, MS D406, Los Alamos, NM 87545
65. Dr. C. Coceva, ENEA Comitato Nazionale, Centro Richerche Energie, Ezio Clemental, via G. Maxxini, 2, 40138, Bologna, Italy
66. Dr. O. A. Wasson, RADP-B119, National Bureau of Standards, Washington, DC 20234
67. Dr. M. S. Moore, Los Alamos Scientific Laboratory, P.O. Box 1663, MS-442, Los Alamos, NM 87545
68. Dr. P. G. Young, Los Alamos Scientific Laboratory, P.O. Box 1663, MS-B243, Group T-2, Los Alamos, NM 87545
69. E. D. Arthur, Los Alamos Scientific Laboratory, P.O. Box 1663, Group T-2, MS-243, Los Alamos, NM 87545
70. D. G. Madland, Los Alamos Scientific Laboratory, P.O. Box 1663, Los Alamos, NM 87545
71. R. E. MacFarlane, Los Alamos Scientific Laboratory, P.O. Box 1663, Los Alamos, NM 87545
72. L. S. Stewart, Los Alamos Scientific Laboratory, P.O. Box 1663, Los Alamos, NM 87545
73. M. Salvatores, Commissariat a l'Energie Atomique, Centre d'Etudes Nucleaires de Cadarache, Boite Postale No. 1, 13115 Saint-Paul-Lez-Durance, France
74. R. N. Hwang, Argonne National Laboratory, Applied Physics Division, Argonne, IL 60439
75. T. Nakagawa, Japan Atomic Energy Research Institute, Tokai Research Establishment Linac Laboratory, Tokai-Mura, Naka-Gun, Ibaraki-Ken, Japan
76. Dr. F. H. Froehner, Institut fur Neutronenphysik, und Reaktortechnik, Kernforschungszentrum Karlsruhe, Postfach 3640, 7500 Karlsruhe, Federal Republic of Germany
77. S. Pearlstein, Brookhaven National Laboratory, Building 197D, National Nuclear Data Center, Upton, NY 11973
78. J. Blons, C.E.N. Saclay, Departement de Physique Nucleaire, BP 2, 91190 Gif-sur-Yvette, France

79–83. H. Derrien, Commissariat a l'Energie Atomique, Centre d'Etudes Nucleaires de Cadarache, Boite Postale No. 1, 13115 Saint-Paul-Lez-Durance, France

84–110. Technical Information Center